DISSERTATION

submitted to the

Combined Faculties for the Natural Sciences

and for Mathematics

of the

Ruperto-Carola University of

Heidelberg, Germany

for the degree of

Doctor of Natural Sciences

presented by:

Siddharth Nanguneri, M.Sc. in Biotechnology

born in: Hyderabad, India

Oral Examination:……

Localization of Subcellular Structures with Super Resolution Light Microscopy on Thin Sections of Nervous Tissue

Referees: Prof. Dr. Thomas Kuner

Prof. Dr. Stephan Frings

Acknowledgements

First of all, I would like to thank Prof. Dr. Thomas Kuner for the topic and freedom he gave me to pursue it. I would like to thank Prof. Dr. Mike Heilemann for the support he provided with super-resolution light microscopy. I would also like to thank Heinz Horstmann for giving me the time for discussions.

A special thanks to my lab members. In a sense, work in the lab was fun mainly because of the presence of my lab members who were supportive with ideas and discussions. I also thank Michaela Kaiser and Claudia Kocksch for the necessary technical help I needed for my project.

Last but not least, I would like to thank my parents for their support and for giving me the freedom to do what I desire.

Summary

Release of synaptic vesicles (SV) is a process that is orchestrated by proteins present in the presynaptic terminus called the active zone (AZ). Knowledge of the placement of proteins is necessary to understand how SV release occurs. There is limited information on the location of the AZ proteins from studies of biochemical assays or immuno-electron microscope.

Developments in fluorescence light microscopy are capable of reaching sub-nanometer resolution and therefore can be used to image multiple proteins of the AZ. For instance, a technique called *direct* Stochastic Optical Reconstruction Microscopy (*d*STORM) can reach a resolution of 20 nm in the x-y plane, which is an order of magnitude greater than conventional light microscope. This work is devoted to developing techniques, which enables the use of *d*STORM on thick brain tissue samples. In this respect, two thick tissue handling techniques have been explored, namely *tomo*STORM and Tokuyasu's ultracryotomy. Using *tomo*STORM, we could construct a super-resolution 3D structure of the calyx of Held synapse. In addition, we also demonstrate multicolor capability by being able to localize the abundantly distributed mitochondria to the synaptic compartment of the calyx of Held. Due to antibody staining limitations, Tokuyasu's ultracryotomy was explored. Using this approach we gathered dual-color super-resolution data in the calyx of Held on the distribution of Bassoon with respect to Piccolo. In agreement with the standard-resolution microscopy, overview image of Bassoon and Piccolo show that both proteins exist together in the majority of the AZs. In addition we can show at the nanoscopic level in a given AZ that the two proteins not only exist as separate entities but are also found to be colocalized. We also gathered data on the distribution of Septin 5 and Piccolo and found that at P7 Septin 5 and Piccolo colocalize while at P17 they do not colocalize. This observation is consistent with the finding that Septin 5 may cluster voltage gated calcium channels at P7 at the AZ.

In addition, as *d*STORM is limited to photoswitching of 2 dyes, efforts were made to extend this. To this extent, we show efficient photoswitching of phalloidin conjugated to ATTO 488, TRITC and BODIPY 650.

In summary, this thesis is focused on adapting *d*STORM to thick tissue samples and developing multicolor photoswitching probes to explore multiple protein distribution in the synaptic compartments of mammalian brain tissue.

Zusammenfassung

Die Freisetzung synaptischer Vesikel (SV) ist ein Prozess, der durch Proteine im präsynaptischen Terminus, auch aktive Zone (AZ) genannt, vermittelt wird. Kenntnis der Proteinverteilung ist zum Verständnis des Mechanismus der Vesikelfreisetzung notwendig.

Biochemische Analysen oder immunoelektronische Mikroskopiestudien haben bisher nur wenig Aufschluss über die Lokalisation von Proteinen in der aktiven Zone liefern können.

Durch die Entwicklungen in der Fluoreszenzmikroskopie sind Auflösungen im Nanometer-Bereich und darunter erreichbar, die zur Auflösung von Proteinen der aktiven Zone fähig sind. Die *d*STORM-Methode (*direct* Stochastic Optical Reconstruction Microscopy; dt.: *direkt* stochastische optische Rekonstruktionsmikroskopie) erreicht etwa eine Auflösung von 20nm in der XY-Achse, und liegt damit um den Faktor 10 unter der Auflösung konventioneller Lichtmikroskopie.

Diese Arbeit befasst sich mit der Entwicklung von Methoden, die den Gebrauch von *d*STORM mit dicken Gewebeschnitten aus dem Säugetierhirn. In diesem Kontext wurden 2 Methoden zur Verarbeitung dicker Proben untersucht, *tomo*STORM und Tokuyasu´s Ultracryotomie.

Durch *tomo*STORM konnte eine hochauflösende 3D Struktur der Calyx von Held Synapse konstruiert werden. Zusätzlich konnte die Fähigkeit, mehrere Farben zu verarbeiten, durch die Lokalisation stark verteilter Mitochondrien im synaptischen Bereich der Calyx von Held gezeigt werden. Mit diesem Ansatz konnten zweifarbige, hochauflösende Daten der Calyx von Held im Bezug auf die Verteilung von Bassoon im Verhältnis zu Piccolo gesammelt werden. Übereinstimmend mit normalauflösender Mikroskopie zeigen die Daten eine Coexistenz von Bassoon und Piccolo in der Mehrheit der AZs. Zusätzlich konnte auf nanoskopischem Level gezeigt werden, dass beide Proteine nicht nur als separate Einheiten existieren sondern auch kolokalisieren.

Daten zur Kolokalisation von Septin 5 und Piccolo haben gezeigt, dass Septin 5 und Piccolo bei P7 kolokalisieren, während dies bei P17 nicht der Fall ist. Diese

Beobachtung bestätigt die Erkenntnis, dass Septin 5 essentiell für die räumliche Ansammlung spannungsabhängiger Kalziumkanäle in der ektiven Zone bei P7 ist.
Zusätzlich wurde versucht, die Kapazität von *d*STORM zu erhöhen, die derzeit bei 2 Farbstoffen liegt. Effizientes Auflösen von Phalloidinkonjugaten mit ATTO488, TRITC und BODIPY 650 konnte gezeigt werden.

Zusammenfassend konzentriert sich diese Arbeit auf die Anpassung von *d*STORM auf dicke Gewebeschnitte und die Entwicklung von mehrfarbigen Photoswitching Proben um die Verteilung von mehreren Proteinen in den synaptischen Bereichen des Säugetiergehirns zu untersuchen.

1 Introduction

Sensory information such as the smell of an odor perceived at the periphery is processed by higher areas of the brain leading to the formation of a percept, which may further be translated into an appropriate muscle action such as avoidance of an object. This form of information processing that occurs in the nervous system of organisms is mediated by synaptic transmission. Information is passed on from one neuron to another neuron at special sites of contact called synapses. Synapses are specialized junctions where one neuron contacts and communicates with another neuron or cell type. The first neuron is said to be presynaptic and the second neuron is said to be postsynaptic. There are two types of synaptic contacts found in the nervous system, namely electrical synapses and chemical synapses. Electrical synapses occur at gap junctions where the membranes from the presynaptic and postsynaptic neurons are separated by a gap of 3 nm. Most synaptic transmission in the central nervous system (CNS) is, however, chemical in nature. The presynaptic and postsynaptic neurons at the chemical synapse are separated by a synaptic cleft, which is 20-50 nm wide. The cleft is filled with a matrix of fibrous extracellular protein. The presynaptic side also known as the axon terminal contains synaptic vesicles that store neurotransmitters.

The chemical synapse is characterized by dense protein accumulations that make it electron dense within membranes on either side of the cleft (Figure 1.1). Neurotransmitters, once released, bind to membrane receptors at the postsynaptic density (PSD). These receptors convert the chemical signal into an electrical signal

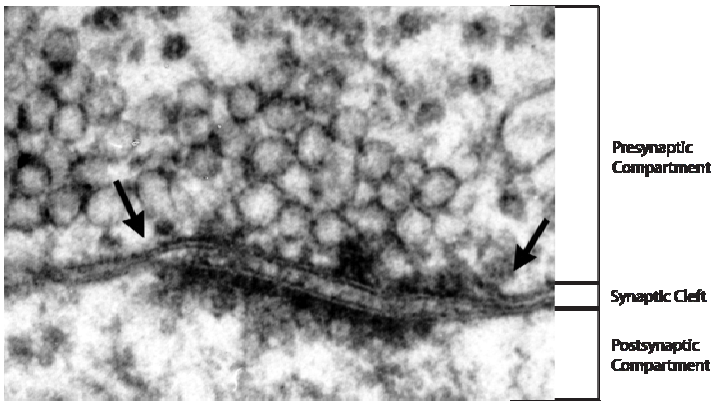

Figure 1.1: Electron micrograph showing a synaptic junction, which is characterized by an electron dense accumulation marking the active zone and a postsynaptic black smear marking the post synaptic density with vesicles in close proximity to the active zone. The presynaptic density and the post synaptic density are separated by the synaptic cleft. Courtesy: Heinz Horstmann

The basic requirements of chemical synaptic transmission comprises the following:

1) synthesis of neurotransmitter
2) packing it into synaptic vesicles
3) a mechanism to make synaptic vesicles fuse with the plasma membrane to release its contents into the cleft in response to an action potential
4) a mechanism for producing a postsynaptic current
5) a mechanism for removing neurotransmitter from the synaptic cleft
6) to be useful for sensation, perception and control of movement they should occur rapidly

Neurotransmitter release into the synaptic cleft is triggered by an action potential in the axon terminal. Voltage gated calcium channels, which are present at the site of release open upon depolarization in the active zone. Alteration of protein conformation makes the plasma membrane fuse releasing the contents of vesicles.

An understanding of the synaptic vesicle (SV) release process requires the characterization of synaptic proteins requires the characterization of the synaptic protein organization. The investigation on molecular scale necessitates the use of tools that provide nanometer scale resolution. Tools such as gold-EM, EM tomography and super-resolution light microscopy have the power to address this issue. Each technique has its advantages and disadvantages. EM for instance offers

the superior resolution and provides morphological information. However, it is cumbersome and limited in field of view. Super-resolution light microscopy has a plenty of molecular information but has no morphological information. However, super-resolution light microscope provides larger fields of view and therefore makes investigation of a population of synapses feasible. In this thesis, methods are developed to study the distribution of active zone protein organization

1.1 The Presynaptic Cytomatrix of the Active Zone

The synaptic protein architecture has been characterized by a combination of complementary methods that allowed for the construction of an average model of the placement of various proteins. Super-resolution light microscopy, where used, has revealed differences in active zone protein organization thereby underlining its use.

The active zone is a detergent insoluble protein matrix that is composed of evolutionarily conserved proteins such as Septins, RIM, Munc13, RIM-BP, α-liprin and ELKS. Moreover, in vertebrate synapses there are two additional cytomatrix proteins called Bassoon and Piccolo (Südhof, 2012).

The active zone has at least 4 important functions: First, it docks and primes synaptic vesicle for its release. Second, the active zone proteins recruit calcium channels to the presynaptic membrane so that the calcium influx happens as close to the synaptic vesicle as possible. Third, presence of cell adhesion molecules enables the positioning of presynaptic and postsynaptic protein machinery opposite each other. Lastly, presynaptic proteins mediate short and longterm plasticity that is observed in synapses (Südhof, 2012).

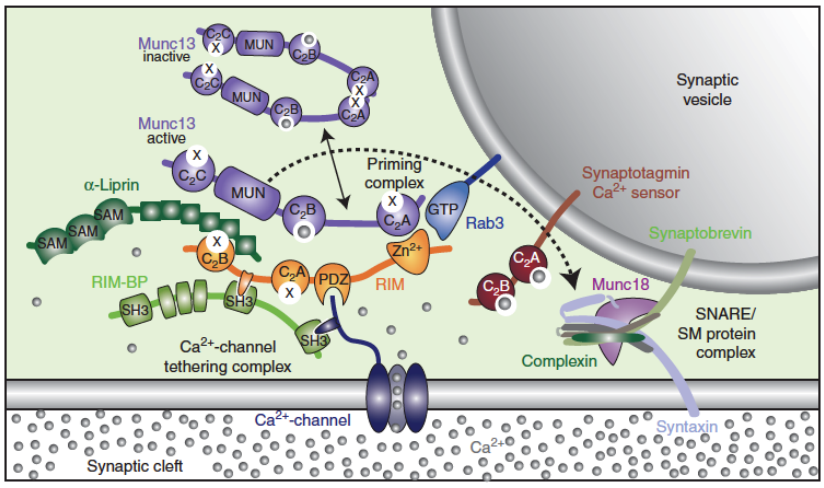

Figure 1.2: A schematic showing all the components that are needed at the active zone to mediate the release of a synaptic vesicle. Adapted from Südhof and Rizo, 2011

1.1.1 Molecular components of the AZ

Electron micrographs of presynaptic structures appear as cone-shaped particles, which are interconnected by a meshwork of filamentous structures that extend into the cytoplasm (Bloom and Aghajnian 1968; Phillips et al. 2001). In addition, electron microscope tomography of the frog neuromuscular junction reveals a highly ordered presynaptic structure composed of “pegs”, “ribs” and “beams”. “Pegs” are the putative calcium channels, which link to synaptic vesicles and the “rib”. The “ribs” in turn contact “beams” (Harlow et al. 2001). Both the “beams” and the “ribs” are part of the cytomatrix of the active zone.

Most proteins that compose the matrix are multidomain proteins where each domain has its corresponding binding partner (Figure 1.2). This renders them to perform multiple functions. RIM, for instance, is a protein, which is needed for vesicle docking and priming (Koushika et al., 2001; Schoch et al., 2002; Gracheva et al., 2008; Kaeser et al., 2011; Deng et al., 2011; Han et al., 2011).

Munc13 has two functions in the active zone. It enables the SNARE/SM complex fusion machinery for exocytosis (Basu et al., 2005; Stevens et al., 2005) and it is involved in short-term memory formation by regulating this priming activity.

α-liprin keeps the active zone as a cohesive unit (Zhen and Jin, 1999; Dai et al., 2006). This protein was also shown to link trans-synaptic cell-adhesion to presynaptic active zone assembly. This is done via binding of α-liprin to LAR type receptor phosphotyrosine phosphatase (Ackley et al., 2005).

ELKS has multiple binding partners such as RIM, α-liprin, and Rab6. Interestingly, an active zone protein in Drosophila called Bruchpilot is organized in such a way that it is a fusion protein where its N-terminal domain is related to ELKS while its C-terminal is related to plectin. Deletion of Bruchpilot causes a loss of t-bar, which is a characteristic of Drosophila synapses (Wagh et al., 2006).

As proteins of target for this thesis Bassoon, Piccolo, Septin 5 and voltage-gated calcium channels are described in more detail.

1.1.2 The CAZ Proteins Bassoon and Piccolo

Bassoon and Piccolo/Aczonin are active zone proteins and they are known to cluster synaptic vesicles as partial deletion of both of them disrupts vesicle clusters (Mukherjee et al. 2010). They are the largest active zone proteins identified so far weighing 420 and 530 kDa respectively (tom Dieck et al., 1998; Cases-Langhoff et al., 1996; Fenster et al., 2000; Wang et al., 1999). Both proteins have 10 regions in common called the Piccolo Bassoon homology (PBH) domains (Figure 1.3). The first 2 regions have 2 zinc finger domains. Regions 4, 6, 8 of the PBH domain have CC regions. The C-terminal region of Piccolo is composed of a PDZ-domain and 2 C2-domains (C2A and C2B), which are structurally related to those found in RIMs and the N-terminus is composed of a proline-rich Q-domain.

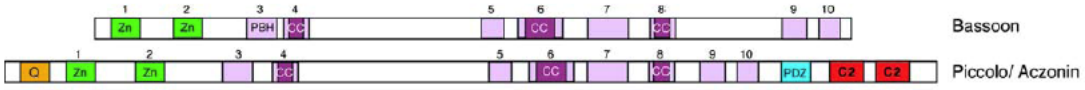

Figure 1.3: Bassoon and Piccolo are highly homologous and share between them many domains namely: Zinc finger domain, coiled-coil domains and Piccolo-Bassoon-Homology sequence. Adapted from Schoch S et al. 2006

Mutant mice with truncated Bassoon (weighing 180 kD), which lacks the central region had been generated. Electrophysiology on hippocampal cultures reveal that a significant fraction of glutamatergic synapses are inactive but active synapses have normal release probability when compared to wild type synapses. At the ultrastructure level inactive synapse has a comparable appearance to wild type synapses. These mutant mice, however, undergo epileptic seizures. In photoreceptors and inner ear hair cells, a truncated version of Bassoon causes the synaptic ribbons to float and thus impairs neurotransmission. Therefore, Bassoon plays a role in anchoring synaptic ribbons (Altrock et al., 2003; Dick et al., 2003; Dresbach et al., 2003).

In addition, Bassoon knockout mice show severe deficits in vesicle replenishment and voltage-gated calcium channel clustering. For instance, in cerebellar mossy fiber to granule cell synapses, it was found that short-term depression was enhanced in the absence of Bassoon. Further analysis revealed that vesicle-reloading rate was halved at these synapses (Hallermann, S. et al, 2010). In ribbon synapses, Bassoon in conjunction with synaptic ribbon was found to create release-sites by organizing voltage-gated calcium channels and the synaptic vesicles. Lack of Bassoon in these synapses interfered with vesicle replenishment (Frank T. et al 2010). In another similar study, Bassoon localizes voltage-gated calcium channels to the active zone via molecular interaction with the RIM-binding proteins (Davydova D et al, 2014).

Lastly, the importance of both Bassoon and Piccolo in the active zone is underscored by the fact that their leads to degradation of synapses (Waites et al. 2013).

1.1.3 Septins and the Voltage-Gated Calcium Channels

Septins are a conserved family of GTP/GDP binding proteins encoded by 14 genes. They are associated with secretion, phagocytosis, cytokinesis, sperm motility and neurological diseases like Parkinsons and Schizophrenia (Ihara et al., 2003; Barral and Kinoshita, 2008; Weirich et al., 2008; Suzuki et al., 2009). These filamentous proteins have been implicated in docking or priming of vesicles for release in secretory cells (Hirokawa et al., 1989, Beites et al., 2005). They are 8.25 nm in diameter and are multiples of 25 nm in length (Hsu et al., 1998). They function by

braking release by binding to syntaxin of the t-SNARE complex in secretory cells (Beites et al., 1995, 2005).

From the time of onset of hearing at P8-P12 till completion of development at P17-P19 the nature of coupling between synaptic vesicles and voltage gated calcium channels (VGCCs) changes from a microdomain configuration where there is loose coupling so that a single vesicle is released by a cluster of VGCCs to a nanodomain configuration where there is tight coupling so that a single vesicle is released by one VGCC (Fedchyshyn and Wang, 2005). (Figure 1.4)

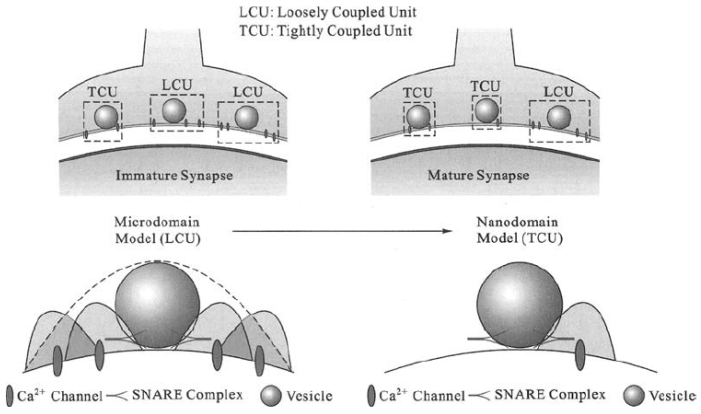

Figure 1.4: Left is a schematic of an immature synapse where predominantly loose coupling between the calcium channels and the vesicles exist. Vesicles sense an overlapping cloud of calcium from a microdomain of calcium channels. Vesicles in this configuration are on average farther than 10 nm from the plasma membrane. Right is a schematic of a mature synapse where predominantly tight coupling between the calcium channels and the vesicles exist. Vesicles sense a calcium cloud from a single channel. Vesicles in this configuration are as close as 5 nm to the plasma membrane. Adapted from Lu-Yang Wang, 2007

These findings suggest that microdomain and nanodomain configurations are distinct physical modalities and Septin 5 could play a possible role in determining the configurations (Figure 1.5). Septin 5 antibody, for instance, colocalizes with vGlut1 at the release plate of immature synapse (P8-P12) and does not colocalize with vGlut1 in mature synapse at P16-P19. Moreover, Bassoon antibody colocalizes with vGlut1 at all age levels. Therefore, Septin 5 plays a role in SV organization near active zone (Yi-Mei Yang et al., 2010).

In mature synapses 22 % of SVs are docked versus 10.5 % in immature synapses are within 5 nm of release plate. Between 5 nm and 20 nm from the active zone more SVs in immature synapse are found than in mature synapse. In Septin 5 knockout animals the above-discussed parameters are similar across all developmental stages and they are similar to those found in mature synapses. Evoked EPSCs are larger in septin 5 knockout immature synapses than in wild type immature synapses. No difference, however, was found in mature synapses between the 2 genotypes. EGTA binds calcium ions and attenuates release when SVs and VGCCs are further apart as occurs under microdomain conditions and is hardly effective when SVs and VGCCs are tightly coupled under nanodomain conditions. In Septin 5 knockout animals however, EGTA is has no effect suggesting tight coupling (Yi-Mei Yang et al., 2010).

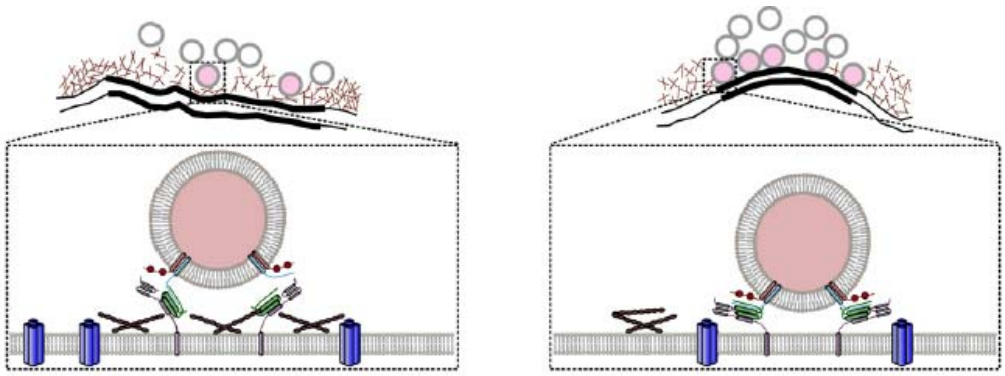

Figure 1.5: Schematic of a vesicle, which is primed for release. Septin 5 is present at P-8 as shown in the left panel. It interacts with syntaxin motif of the SNARE protein to brake the release of the vesicle. At P17 there is no Septin 5 interacting with SNAREs and therefore the vesicle is closer to the plasma membrane. Adapted from Yi-Mei Yang et al, 2010

1.2 The calyx of Held as a model synapse

The calyx of Held is an excitatory gigantic axosomatic terminal in the auditory brainstem that attracted physiologists because of the ease to perform patch-clamp recording simultaneously from the pre- and post-synaptic cell (Borst JGG. et al., 1995). The calyx of Held is formed by axons originating from the globular bushy cells (GBCs) of AVCN (Thompson AM, Schofield BR, 2000) (Figure 1.6). Almost all cells of MNTB are excited by contralateral sounds. The heavily myelinated axons of GBC allows for fast transmission of nerve signal. Due to large number of vesicles present at

the release site a single input can trigger a spike without failure. From a developmental perspective the calyx is needed for the survival of the principal cell (Jean-Baptiste M., Morest DK., 1975).

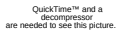

Figure 1.6: A) A dorso-ventral section of the brain-stem showing the auditory pathway which begins with the hair cell contacting the cochlear spiral ganglion which provide input to the globular bushy cells whose terminals end in the MNTB as the calyx of Held B) A schematic of the calyx of Held and its postsynaptic partner. The calyx of Held contains multiple active zones acting in parallel. Adapted from von Gersdorff, H. and Borst, JGG, 2002

The calyx of Held allows the principal cell to provide well-timed and sustained inhibition to other auditory nuclei. This is made possible by special adaptation found in the calyx of Held which include a large number of release sites with release probability, a large readily releasable pool, fast presynaptic calcium clearance, a large quantal size and fast AMPA-type glutamate receptors. Because there are so many active zones acting in parallel per principal cell, the calyceal currents are dominant. The number of active zones is estimated to be between 300 and 700 and about 100 vesicles on average are released with a single action potential (Borst J. G. G.; van Hoeve J. S. 2012). Synaptotagmin 2 is involved in the rapid release of vesicles at the calyceal terminal. In the principal cell, the AMPA and NMDA glutamate receptors mediate the current. AMPA receptors show fast gating due to abundance of flop variant of GluA4 subunit.

Due to the ease of recording, the calyx of Held has been the model synapse for the electrophysiological analysis of mammalian synaptic transmission. Moreover, as the soma of the neuron containing the calyx of Held is located much further apart, it is

also a convenient system for genetic manipulation. In other words injection of recombinant virus into the soma does not damage the calyx itself. In addition to all this, the calyx of Held has lent itself well to developmental analysis. For instance, starting at the onset of hearing the synapse develops from a cup shaped structure into a highly fenestrated structure. This developmental change is also accompanied by changes in the protein levels and hence the electrical properties of the synapse. Given the convenience of investigation and that a wealth of information about this synapse has been harnessed we chose to investigate protein distribution with super-resolution light microscopy in the calyx of Held. The calyx of Held has been chosen as standard synapse for the synaptic protein distribution investigation so that data gathered can be correlated with the existing information to enrich our understanding of the workings of calyx of Held.

1.3 Imaging technologies for tissue imaging

In the section below, various imaging techniques are described that have the potential to reach nanoscopic resolution. Techniques, which have the ability to reach nanoscopic resolution are important for the molecular characterization of synaptic proteins present in the active zone.

1.3.1 Characterization of Molecules by Electron Microscopy

Despite advances made from biochemical and molecular biological investigations, there is still a need for the molecules to be visualized as where they are located with respect to a substructure of a cell. Electron microscope is well suited for visualizing the various components of cells at a very high resolution (1 nm). It is from EM studies the average vesicle size is determined to be 40 nm at the synaptic terminus. Though conventional EM provides morphological information, it lacks molecular information. In order to obtain molecular information, one performs immunogold-labeling using gold nanoparticles which exist in different sizes like 10 nm, 20 nm, etc. A gold nanoparticle is easily visualized in EM as a dark particle as it is an electron rich metal. Under practical considerations, use of immunogold-labeling allows one to look at one molecule at a time.

EM tomography offers another way to unravel the identity molecules in biological sample in native conditions (Medalia O, et al., 2002). Conventional EM on chemically fixed biological material uses heavy metal staining to provide contrast. EM tomography on thick biological specimen is limited by the lack of contrast in the specimen and therefore cannot be used to determine the organization of molecules inside a cellular compartment in tissue (Fernández-Busnadiego R, et al., 2013).

1.3.2 Characterization of Molecules by Light Microscopy

Fluorescence light microscope offers an option to deal with the ability to simultaneously label multiple proteins.

In 1873 Ernst Abbe discovered that microscopic things when examined under a lens-based optical microscope if present as close as a half the wavelength of light cannot be discerned. A point source of light when focused through lens based system forms a diffraction limited spot with a full width at half maximum of $\lambda/(2n\sin^2\theta)$. All fluorophores within this spot emit at the same time and therefore cannot be separated from each other (Hell, S. W., 2007). As a result, molecules mediating vesicle release when stained with fluorescent markers and viewed with fluorescent microscope which is diffraction limited appear as a blur prohibiting one to precisely localize them with subnanometer precision – a prerequisite to understanding their function (Figure 1.7)

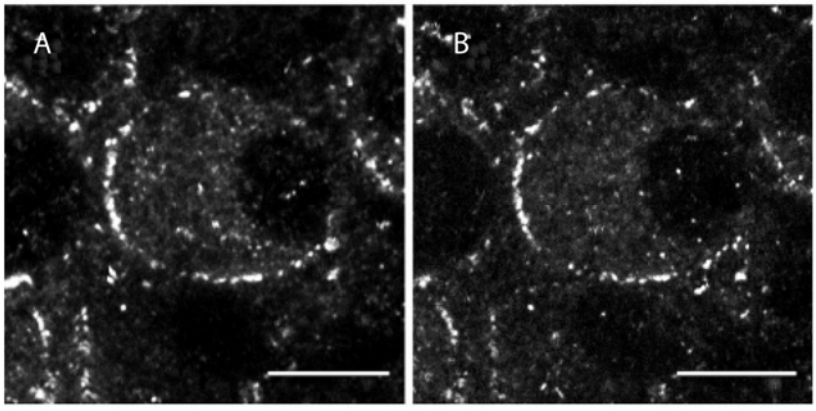

Figure 1.7: A calyx of Held is labeled for active zone scaffold proteins Bassoon and piccolo and viewed in the conventional fluorescence microscope. Due to diffractional limitation of the conventional

microscope, synaptic proteins appear blurred and therefore lack exact positional information. Dondzillo, A. et al., 2010

1.3.3 Diffraction-Unlimited Light Microscopy

Entering the scene is an array of next generation light microscopy techniques which are famous for circumventing the diffraction barrier of conventional light microscope with the ability to reach resolutions of 20 -50 nm in the x-y plane which can resolve protein aggregates that compose macromolecular structures such as viruses (Muranyi W, et al., 2013) and nuclear pore complex (Szymborska A, et al., 2013) (Figure 1.8).

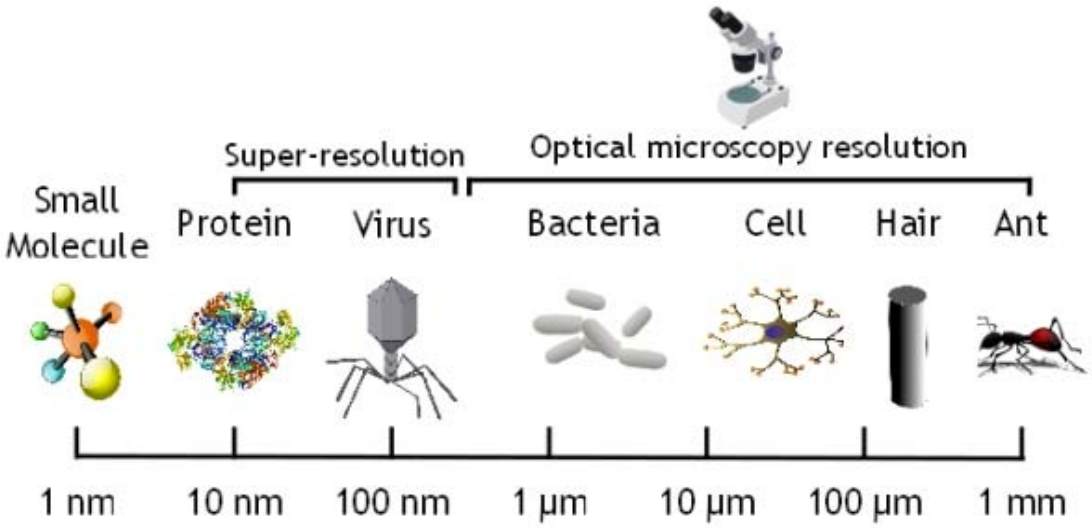

Figure 1.8: The above schematic illustrates dimensions of objects probed by optical microscope. Conventional optical microscopes can visualize objects down to the size of a bacterium. Protein aggregates and viral particles can be visualized or resolved with the aid of super-resolution light microscopy. Molecules down to the size of a small molecule requires X-ray diffraction. Adapted from http://www.npl.co.uk/biotechnology/research/super-resolution-imaging/

There are two general schemes in which this is accomplished: one is done deterministically like Stimulated Emission Depletion (STED) (Hell, S. W., Wichman, J., 1994; Hell, S. W., Kroug, M., 1995) while the other is done stochastically (Rust, M. J. et al., 2006; Betzig, E. et al., 2006; Heilemann et al., 2008) such as stochastic optical reconstruction microscopy (STORM).

STED

In the 1990s an idea arose which harnessed the molecular states of fluorophores for a subdiffraction imaging microscope called Stimulated Emission Depletion (STED) (Hell, S. W., Wichman, J., 1994; Hell, S. W., Kroug, M., 1995). Typically fluorescence involves exciting an electron by light from ground state (S_0) to an excited state (S_1).

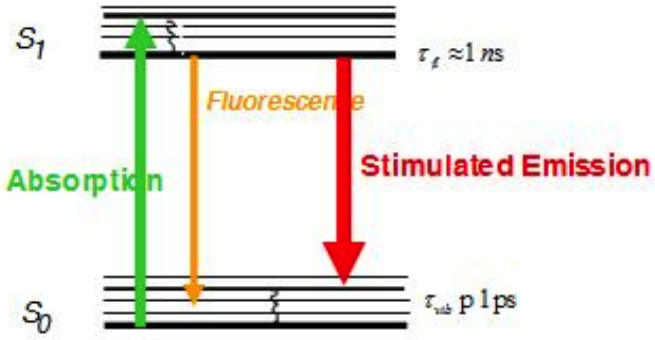

Figure 1.9: Electrons in a fluorescent dye are excited from ground state (S_0) to excited state (S_1) by absorption of photons (green arrow = higher energy). Both S_0 and S_1 are made of vibrational states. Relaxation of electrons to ground state causes emission of photons as fluorescence (yellow arrow = lower energy). In stimulated emission (red arrow) electrons are forced to relax onto higher vibrational states of the ground state thereby emitting photons with energy lower than conventional fluorescence.

The electron falls back to the ground state by releasing a photon of higher wavelength. Recording of this fluorescence by a conventional microscope leads to the diffraction blurring of the point source of fluorescence. As the purpose of super-resolution microscopy is to discriminate point sources within the diffraction limited spot, in STED, a second beam in the shape of a donut called the depletion beam (Figure 1.9), is used to quench the fluorescence around a given point source giving rise to a superior resolution of 20 nm. This is accomplished by making sure that the electrons from the molecules outside the point source of interest fall back to a higher vibrational state of the ground state (Figure 1.10). As a result, less energy is required to give away thereby emitting a photon in the higher wavelength region than photons emitted by the fluorophores present in the point source of interest.

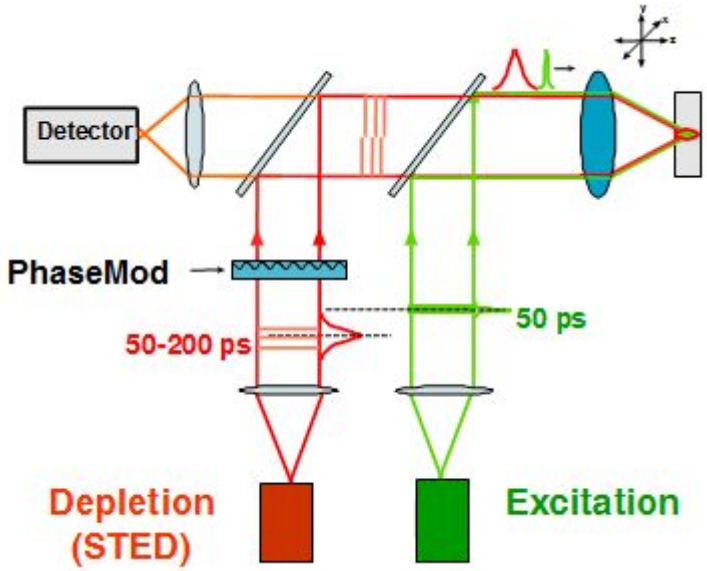

Figure 1.10: A schematic of STED microscope. A depletion beam is overlaid on an excitation beam that results in fluorescence image, which is diffraction-unlimited.

Repeating this process by scanning across the entire sample gives rise to super-resolution image. STED is an ensemble technique, as it cannot discriminate between individual fluorescent molecules composing the point source. Moreover, it is deterministic in that each point of sample is scanned sequentially analogous to a scanning confocal microscope.

*d*STORM

Single molecule detection offers another way to overcome the diffraction barrier of light microscope. In single molecule detection the accuracy of the position of the fluorophore depends on the number of photons collected (Gelles, J. et al., 1988). Based on this principle, fluorescence imaging with one-nanometer accuracy (FIONA) has been demonstrated to study the mechanism of movement on actin and tubulin filaments (Yildiz, A. et al., 2003). However, FIONA in itself does not lend to overcoming the diffraction barrier, due to the presence of multiple emitters in close proximity.

Therefore, a method called stochastic optical reconstruction microscopy (STORM) was introduced where fluorophores from a densely labeled sample are switched on and off stochastically (Rust, M. J. et al., 2006; Betzig, E. et al., 2006; Heilemann et al., 2008). A typical STORM imaging consists of acquisition of several thousand frames where each frame comprises a fraction of fluorophores that are switched on so that each fluorophore is sparsely distributed and thus optically resolvable. As a result, the position of each fluorophore can be determined with a high accuracy. Repeating this procedure on all frames allows the determination of the position of all fluorophores and an image is reconstructed. The resolution obtained from this process is about 20 nm. (Figure 1.11)

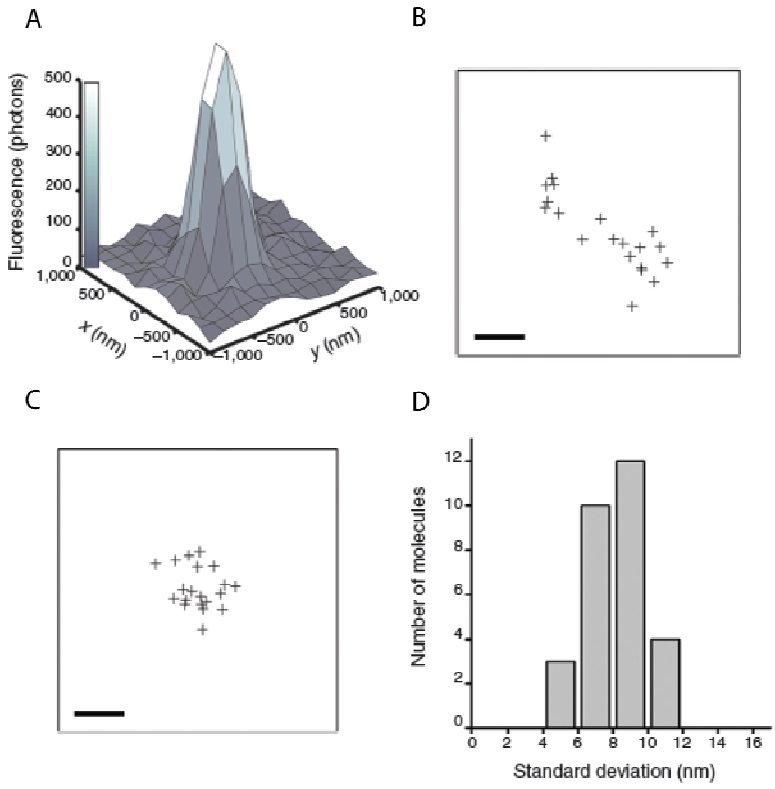

Figure 1.11: (A) This graph depicts a fluorescent spot – the x-y plane shows the extent of spread of the fluorescent spot and the z-axis depicts the number of photons gathered. (B) A spot from each frame is fitted to a 2D gaussian and its center localized forming a collection of spots. (C) the collection of spots is drift corrected and (D) the standard deviation is calculated which is the precision of localization. Adapted from Rust, M.J. et al 2006

The resolution of the image depends on the accuracy with which a given fluorophore has been localized as it undergoes a number of switching events. Summation of all the

localizations of a given fluorophore would give a point-spread function as the one depicted in (Figure 1.11). This is fitted to a Gaussian to calculate the standard deviation. The standard deviation calculated from a drift corrected positions gives on average 8 nm. This value corresponds to the uncertainty in the localization of single switch per imaging cycle. Full-width half maximum of such a distribution translates to 18 nm. Therefore, when an image is reconstructed under the above mentioned localization uncertainity two photoswitches, which are 20 nm apart can be resolved (Rust, M. J. et al., 2006).

Direct STORM uses Cy5 directly as a photoswitch (Figure 1.12). The authors report switching on and off of Cy5 but reactivation of Cy5 requires a high power of 532 nm laser (Heilemann, M. et al., 2008). In a typical *d*STORM imaging session, a densely labeled structure is irradiated with 633 nm laser to which switches Cy5 on and then off. Activation of Cy5 is made possible by shining 532 nm laser. The fluorophore turns on and then turns off with a rate constant Koff that linearly scales with the power of red laser while rate constant Kon linearly scales with the power of green laser. Linear dependence of rate constants enables the experimentator to adjust the density of probes populating an imaging cycle by adjust the intensity of red and green laser (Heilemann, M. et al., 2008).

*d*STORM can be used in combination with SNAP-tag technology. Moreover, probes, which are smaller in size than a conventional antibody can afford to be conjugated with only one fluorophore molecule thereby bringing the dye as close to the target as possible. Hence, *d*STORM is well suited for subdiffraction measurements of samples labeled with small nano-probes.

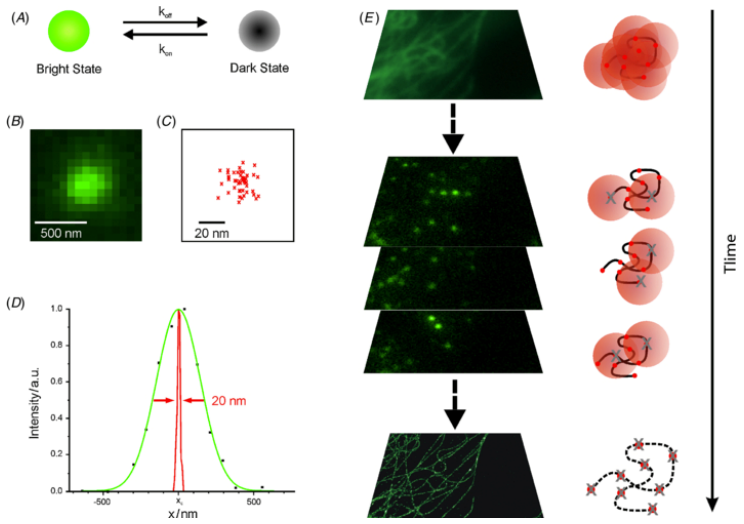

Figure 1.12: In the *d*STORM scheme, the fluorophore is turned from a light state to dark state in presence of reducing agents like MEA (A). Each spot is detected (B) and fitted to a Gaussian (D) to localize is its center (C). Collection of many localization events (E) produces a super-resolved structure. (Adapted from Heilemann et al, 2008)

There exists an optical trick, which can be performed to better the resolution along the z-axis (Huang B. et al., 2008). This trick, however, is an intrinsic property of STORM. As mentioned before, in STORM there are randomly distributed spots of fluorescence. These spots are spots, which are in the focal volume. A focal volume consists of a focal plane where the fluorescent spot is at its brightest. As the fluorescent spot moves away from the focal plane its brightness diminishes as the point spread function (PSF) of spot increases. This increase in PSF is symmetric meaning just from the increase one cannot say if the spot is below or above the focal plane. One can destroy this symmetry by introducing a cylindrical lens, which introduces an asymmetric PSF. (Figure 1.13)

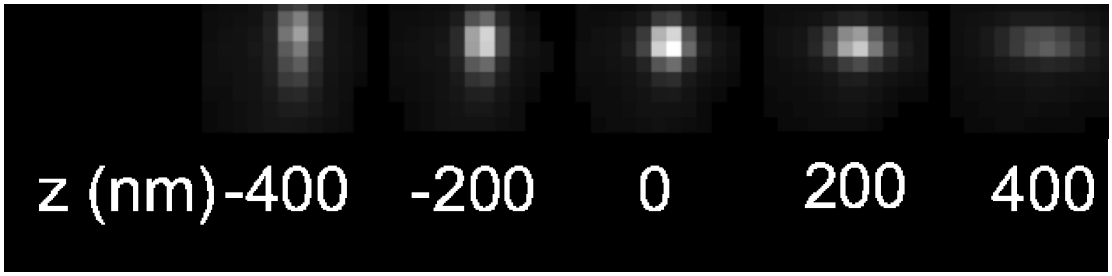

Figure 1.13: Cylindrical-lens-based astigmatism discriminates positions of single fluorophores in the focal volume.

For instance, depending on how the cylindrical lens is installed along the optical path, spots above the focal plane could be horizontally elliptical while spots below the focal plane are vertically elliptical and spots at the focal plane are perfectly round. By engineering the PSF in this fashion people have reported a z resolution along the z-axis of 50 nm (Huang B. et al, 2009). A reconstructed 3D STORM image is typically color-coded, where color is used to code for depth. (Figure 1.14)

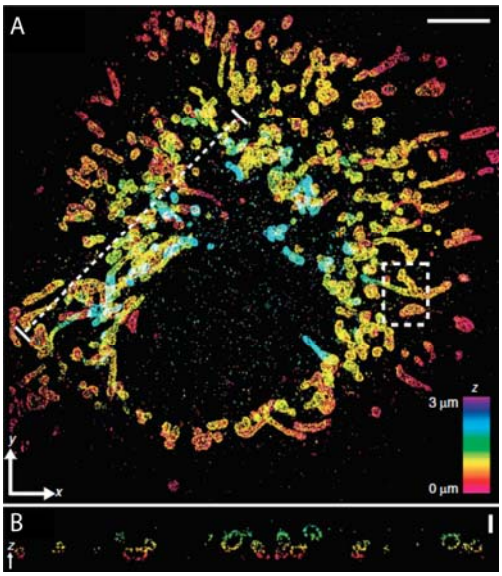

Figure 1.14: (A) 3D STORM reconstruction of mitochondria in a whole cell. The distance in z is color coded. (B) represents optical sections along x-z plane. Adapted from Huang B. et al, 2009

Alternatively, a light microscopic technique called Array Tomography pioneered in Steven Smith's lab accomplishes improvement of the z-resolution by physically sectioning the sample. The resolution here is then dictated by the thickness of the physical section, which can be as low as 40 nm (Micheva, K. and Smith, S. 2007). In Array Tomography, a tissue sample is embedded in a plastic resin. Hydrophilic resins such as LR White when solid can be cut using a diamond knife into sections as thin as 40 nm. And subsequently they can be immunolabeled with fluorescent antibodies for light microscope. Serial sections forming a ribbon can be collected, imaged and overlaid on top of eachother to form 3 D structures with a voxel size of 200 nm x 200 nm x 70 nm. (Figure 1.15)

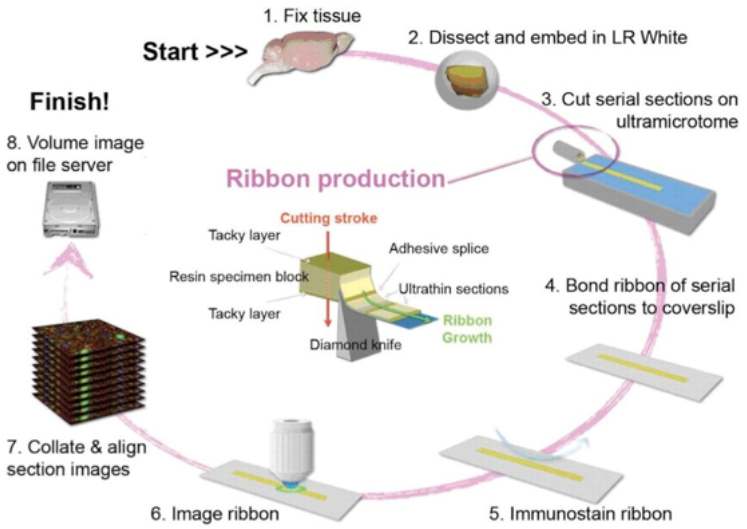

Figure 1.15: A schematic of Array Tomography. Adapted from Micheva and Smith 2007

This technique can be combined with *d*STORM to obtain the 2 dimensional super-resolution images on thin sections and subsequently arriving at a voxel size of 20 nm x 20 nm x *k* nm, where *k* is limited by the thickness to which the plastic resin section can be made.

For the work of presynaptic protein investigation in this thesis, *d*STORM is preferred to STED due not only to the fact that single molecule localization microscopy allows for the possibility of superior z-resolution but also to the convenience in setting up a STORM microscope.

1.3.4 Alternative Photoswitches for Multicolor *d*STORM

Lastly, as the active zone is a multi-protein complex, it is important to develop switching strategies, which enable switching of multiple fluorophores in one buffer condition. Due to redox potential considerations, a maximum of two fluorophores, namely Alexa 532 and Alexa 647, can be switched on and off in *d*STORM. Therefore, inspired by nature, the switching properties of fluorophores conjugated to phalloidin were explored.

Fluorophores in close proximity to a quencher such as tryptophan undergo quenching by photoinduced electron transfer. In PET electron-transfer from donor to acceptor occurs via nonradiative dissipation of excited state energy. Free-energy of reaction and distance between donor and acceptor determines the electron-transfer. PET quenching can happen through transient molecular collision, which is also called 'dynamic quenching' or by formation of stable molecular complexes in a process called 'static quenching'. It is static quenching that provides the necessary contrast for analysis in single-molecule spectroscopy and fluorescence correlation spectroscopy (PET-FCS). The hetero-dimer complex formation between donor and acceptor in PET results from differences in oxidation and reduction potentials of the interacting compounds undergoing PET.

This form of fluorescence quenching can be used to report on conformational changes in macromolecules. Tryptophan and guanine are compounds among amino-acids and nucleic acids that efficiently quench fluorescence from oxazine and rhodamine fluorophores. Polypeptides with the appropriate fluorophore/quencher pair are used in PET-FCS to study fast conformational changes with nanosecond time resolution. (Figure 1.16)

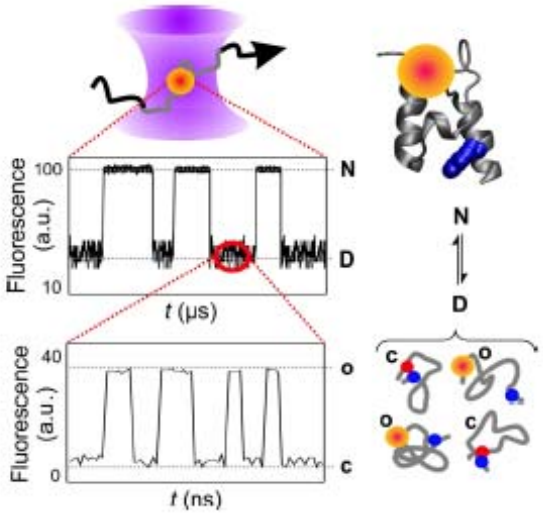

Figure 1.16: The effect of photon-induced-electron transfer combined with fluorescence correlation spectroscopy is exploited in the study of protein folding dynamics. Use of PET-FCS enables detection of folding events with nanosecond temporal resolution. Adapted from Neuweiler et al, 2009

Probes such as phalloidin where fluorophores are in close proximity to a quencher such as tryptophan are predicted to make good photoswitches. Investigation of different phalloidin-fluorophore conjugates could enable expansion of the number of already existing photoswitches to more than two.

1.4 Investigation of neuronal protein assemblies by Single Molecule Localization Microscopy (SMLM)

Super-resolution light microscopy has already been used for studying how proteins in neurons are organized. These studies, as reviewed below, highlight the importance of the use of super-resolution light microscopy for correlating nanoscopic structure with function.

Actin cytoskeleton

STORM has been used to look at actin distribution in axons and dendrites. It was found that actin in axons was organized as rings spaced about 190 nm in distance (Figure 1.17). In dendrites the actin filaments were not rings but filaments. The periodicity of actin rings also determines the periodicity of sodium channels (Xu, K et al., 2012).

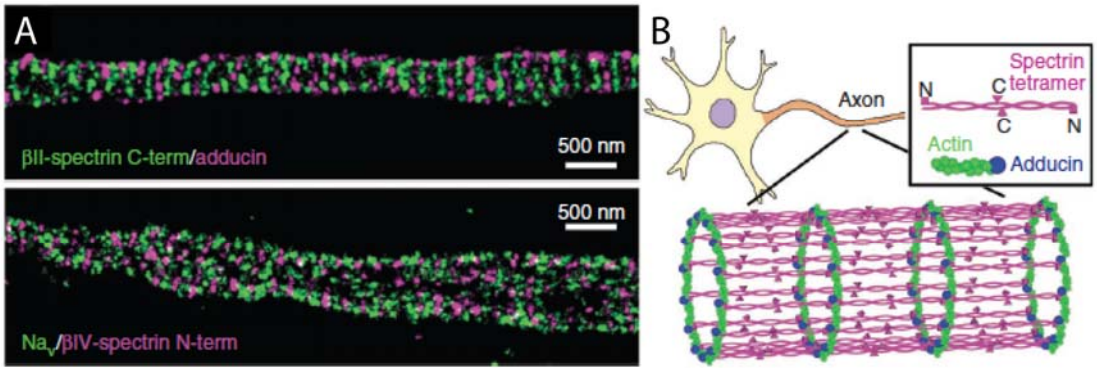

Figure 1.17: Actin in axons do not form continuous filaments but form rings which are spaced about 190 nm. Connecting the rings are spectrin filaments. Adapted from Xu, K. et al 2012

In auditory hair cells Bassoon was shown to cluster calcium channels (Frank, T. et al., 2010). The mammalian brain tissue is challenging. Nevertheless three color STORM performed on brain tissue revealed a highly oriented presynaptic distribution of active zone proteins (Dani, A. et al. 2010). STORM analysis to map the synaptic proteins with respect to each other was limited to those synapses, which were oriented perpendicular to the synaptic plane. This way not only pre- and postsynaptic proteins could be resolved from each other to reveal the synaptic cleft but proteins within one compartment could also be assigned a specific location within the compartment. For instance, calcium channel binding protein RIM1 was found to be closer to the synaptic cleft compared to vesicle organizing scaffold protein Bassoon and piccolo. (Figure 1.18)

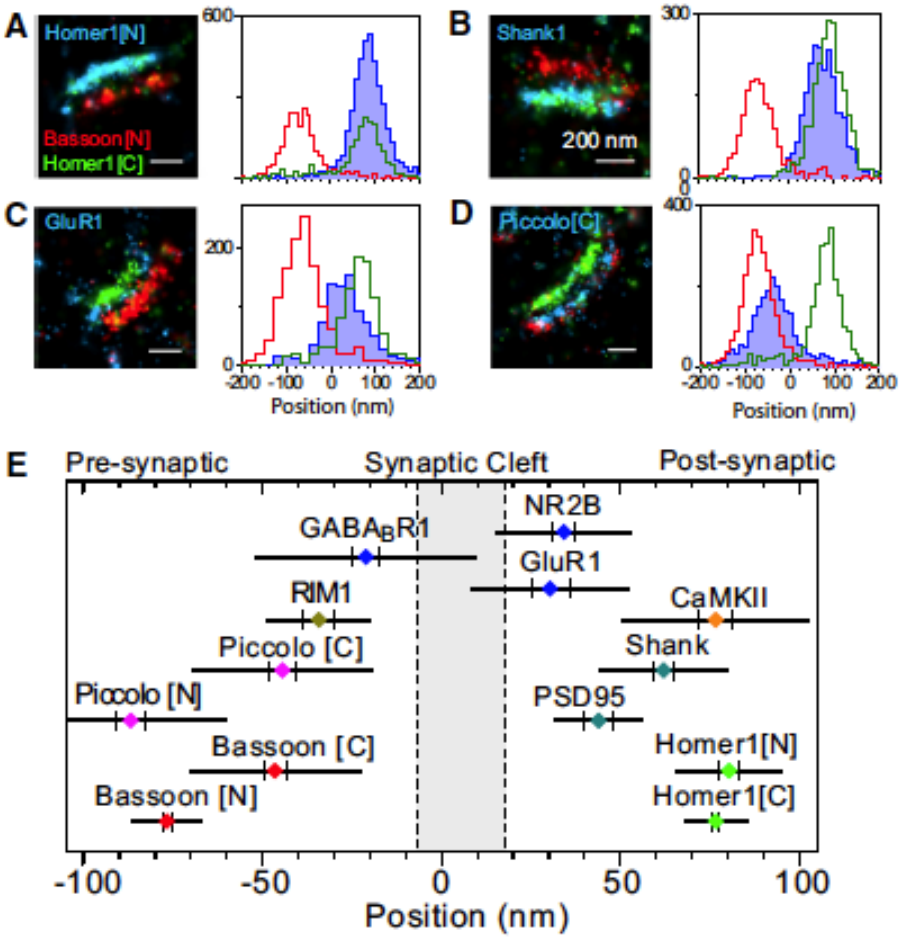

Figure 1.18: STORM imaging of various synaptic proteins in the mammalian brain, when viewed from the side reveals an ordered arrangement of the various pre- and postsynaptic proteins. Adapted from Dani et al 2010

Post synapse: Spine Morphology and Actin dynamics

Actin dynamics was monitored as a way to reveal changes in spine morphology. Actin dynamics was followed using live-PALM with spt (single particle tracking) PALM (Urban, N. T. et al., 2011). This showed actin filament polymerization was toward the center of the spine head from multiple perisynaptic sites of assembly, which is useful for repositioning of glutamate receptors (GluRs).

Quantum dot tracking of AMPARs between synaptic and extrasynaptic compartments showed rapid replacement of desensitized receptors was found (Choquet, D., 2010). FRAP in addition also showed that majority of AMPARs are stable even though the structure of PSD is dynamic.

1.5 Chapter summary and Aims of the thesis:

The multidomain property enables the active zone protein to interact with multiple binding partners thereby rendering cohesion to the active zone cohesion. In addition this multidomain property also allows each protein to play multiple roles as can be seen from individual domain deletion studies.

Though we have an average model of the way proteins are organized, all studies addressed the role of a protein either in isolation or at best looked at the interaction with another partner. Therefore, there still is a need to obtain in one snapshot the placement of many proteins composing the active zone. The mammalian brain tissue is organized in a more complicated manner that requires development of technology to facilitate complete labeling of synaptic proteins.

In this thesis, efforts made in developing tissue processing methods and labeling technologies are described to enable us to perform super-resolution light microscopy on multiple proteins of the active zone so that we can from looking at the way they are organized understand the role of synaptic release that they partake in.

2 Materials and Methods

2.1 Stereotaxic surgery

All experiments were conducted in accordance with the German animal welfare guidelines and approved by the responsible authority (Regierungspräsidium Karlsruhe, Germany). All necessary steps were taken to ameliorate suffering of the rats, including systemic anesthesia (isofluorane) and local wound anesthesia (Lidocaine), post-surgery pain treatment, professional handling, behavioural observation and housing in individually ventilated cages at 21° C and 55% humidity. The stereotaxic injections into the ventral cochlear nucleus (VCN) of two Sprague Dawley rats and tissue processing were done as reported previously (Wimmer V. C. et al., 2004), but using isoflurane inhalation anesthesia (Schwenger D. B. et al., 2010).

Briefly, the VCN of P3 Sprague Dawley rats were injected with rAAV particles in the following manner. Injection capillaries were pulled from micropipettes and collected in a box. A rat pup is anasthesized with 5 % isoflurane (Baxter, Deerfield, IL) in oxygen for approximately 5 min (Vaporizer: Isotec4, Sugivet, Dublin, OH). Approximately, 30 µl of Lidocain is administered into the head (the area of surgery) to alleviate pain. The pup is then mounted on a stereotax (Kopf Instruments, Tujunga, CA). The skin covering the skull is cut to expose the skull. A craniectromy in the occipital lobe is performed using a dental drill to open a window of size 2 x 3 mm. Rat Ringer's solution (in mM: 135 NaCl, 5.4 KCl, 5 HEPES, 1.8 $CaCl_2$, 1 $MgCl_2$) is used from time to time to keep the surgery area from drying. Using an electronic leveler (eLeVeLeR, Sigmann Elektronik, Hüffenhardt, Germany) the head was leveled in such a way that the roof of the skull is parallel to the ground plate of the stereotax.

2.5 µl of virus solution is collected in injection capillaries. The tip of the capillary is placed at the bregma for the zero. The capillary is then lifted to a height of 0.45 mm and moved to positions to inject in the following manner:

X (mm)	Y (mm)	Z (mm)
-6.6	0.7	6.5
-7.0	0.7	6.5
-7.4	0.7	6.5
-6.8	0.9	6.5
-7.2	0.9	6.5
-7.6	0.9	6.5

Table 2.1: Stereotaxic coordinates to inject in the VCN of P3 rat brain

After in vivo protein expression for the time period of 8 days rats were transcardially perfused with 20 ml of isotonic PBS followed immediately with 50 ml of 4% paraformaldehyde in phosphate buffer 0.1 M pH 7.4. The brain was directly removed and stored over night at 4° C in the same fixative. 100 mm sections were cut on a Leica VT1400 vibratome through the MNTB region and further processed as described below.

2.2 Molecular Biology

The gene of interest is amplified with PCR using forward and reverse primers that contain 20-30 bases complementary to the gene of interest. In addition the primers also have sequences of 10-20 bases that specify the digestion site for restriction enzymes.

AAV pAM vector

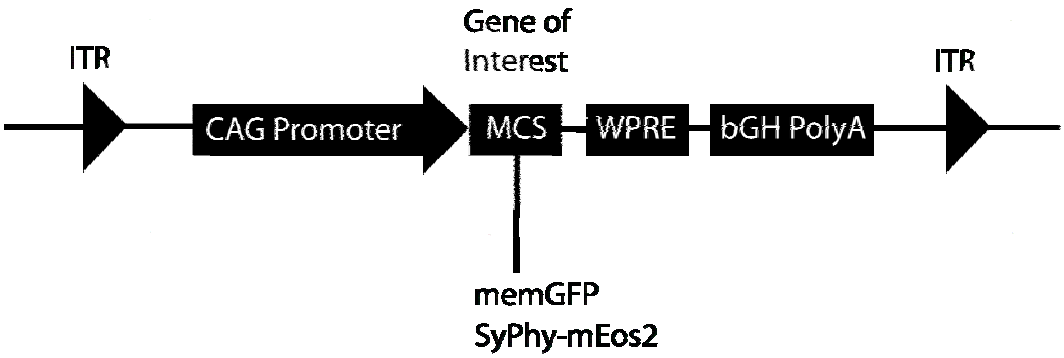

Membrane targeted GFP (memGFP)

memGFP gene was amplified from template DNA pBKS (from Anna Dondzillo's Thesis) by PCR with following restriction sites for subcloning in pAM-vector: BamHI and HindIII

Primer sequence: 5' to 3'
memGFP BamHI Forward:
CATAGCGGATCCATGGGTTGCTGTTTCTCC
memGFP HindIII Reverse:
CATAGCAAGCTTTTACTTGTACAGCTCGTCCAT

mEos2

mEos2 (Addgene) was subcloned to replace eGFP from the pAM vector containing Synaptophysin-eGFP (Wimmer et al., 2004) to generate Synaptophysin-mEos2.

mEos2 was amplified from the template DNA mEos2 vector Addgene by PCR with following restriction sites for subcloning im
pAM-vector: BamHI and SacI

Primer sequence: 5' to 3'
mEos2-Pml-Forward:
GTAGGATCCATGAGTGCGATTAAGCCAGACATGAAGAT
mEos2-SacI-Reverse:
GAGAGCTCTTATCGTCTGGCATTGTCAGGCAATCCAGA

Subclone SyPhy BamHI Fragment from fusion construct pAM-SyPhy-EGFP in pAM-mEos2 to get pAM-SyPhy-mEos2

2.3 Virus Production

AAV production is a 5-day process. On day one cells at a density of $4x10^6$ cells per 14 cm plate in 20 ml DMEM are seeded. Cells, passaged for not more than 12 times, are used. On day two the cells are transfected in the following manner. Equimolar

amounts of pAM and helper constructs are mixed to a weight of 37.5 µg and mixed with $CaCl_2$ in a 50 ml falcon. HeBS (280 mM NaCl, 50 mM HEPES, 1.5 mM Na_2HPO_4, and pH is adjusted with NaOH to 7.05) is added to DNA-$CaCl_2$ solution mixture while vortexing the falcon for 70 seconds. This constitutes the transfection solution, 2 ml of which is added to the cell culture plate. The plates are swirled gently for uniform distribution and transferred to the incubator. On day three the medium is completely removed and replaced with 25 ml fresh DMEM. On day four the cells are harvested in the following manner. Cells are collected in a 50 ml falcon tubes by scraping them off with a cell scraper. The falcon tubes are spun at 1050 rpm at room temperature for 15 min. The supernatant is discarded and 1 ml of lysis buffer per plate is added. The cells are subjected to three rounds of freeze/thaw cycle between dry ice/ ethanol bath and 37° C water bath for 10 min each. For further purification, 50 U of benzonase per plate is added and incubated for 2 h at 37° C. The falcon is spun at 4500 rpm at 4° C 15 min. The supernatant is collected in a syringe and pushed through a 0.45 µm filter into a 15 ml falcon tube. The collected fluid forms the crude lysate. For further purification of crude lysate is done by passing the crude lysate through heparin agarose column attached to Amicon-ULTRA filter.

2.4 Resin Embedding

Resin embedding with LRWhite was done as described by Micheva et al (2007). Briefly, the fixed tissue was further immersion fixed at 4° C overnight. After rinsing with PBS the tissue was dehydrated in a graded series of ethanol until complete dehydration with 100% ethanol. The tissue was then infiltrated with LRWhite resin (three times, 5 mins at 4° C and left overnight), embedded in gelatin capsules and polymerized at 50°C.

For Lowicryl HM20, tissue sections were high pressure frozen as described (Bubeck D et al., 2008). Freeze substitution was performed in a mixture of 3% uranyl acetate and methanol at -85° C for 70 h, followed by 3 washes in methanol at -85° C after which sections were warmed upto -40° C at 5° C/h. Tissue sections were infiltrated and embedded in Lowicry HM20 at -40° C and UV polymerized for 36 h at -40° C after which temperature was raised to room temperature. UV polymerization was

continued for another 24 h.

2.5 Ribbon Making

Ultrathin sections (40 nm) were cut with an ultramicrotome (Ultracut E, Reichert Jung, NY) using the procedure described by Harris et al (2006). The ribbons obtained were mounted on coverslips, which were made hydrophilic by treatment with a mixture of 1:1 sulphuric acid and hydrogen peroxide. The ribbons were then further processed for immunostaining.

2.6 Immunostaining for *tomo*STORM

Following mounting on coverslips, the ribbons were washed in PBS (5 min) and immunostained following established protocols (Tse FW et al. 1997). This was followed by blocking with 5% FCS in PBS. Primary antibodies were diluted in 5% FCS in PBS and applied on the ribbon for 2 hours. Samples were washed 3 times with PBS. The appropriate secondary antibody diluted in 5% FCS in PBS was applied for 30 min followed by washing in PBS for 3 times. The antibodies used for *tomo*STORM are listed below.

Primary Antibodies	Catalog Number	Dilution	Species	Embedding Material
Anti-GFP	Abcam ab6556	1:200	rabbit	HM 20
Anti-cytochrome C oxidase	Sigma C9616	1:500	sheep	HM 20 and LR White
Anti-PSD 95	Neuromab 75-348	1:200	mouse monoclonal	HM 20
Bassoon	Enzo Lifesciences SAP7F407	1:200	mouse monoclonal	HM 20
Anti-GFP	Life technologies A11122	1:200	rabbit	LR White

Table 2.2: Primary antibodies used for immunostaining for *tomo*STORM

Secondary Antibodies	Catalog Number	Dilution	Fluorophore
Anti-rabbit	Life technologies A21236	1:500	Alexa 647
Anti-sheep	Life technologies A21245	1:500	Alexa 647
Anti-mouse	Life technologies A11002	1:500	Alexa 647
Anti-rabbit	Life technologies A11009	1:500	Self-conjugated with ATTO 520 AD 520-31

Table 2.3: Secondary antibodies used for immunostaining for *tomo*STORM

2.7 Tokuyasu's Cryosections

The region of interest (ROI) is cut out and immersed in 2.3 M sucrose. Sucrose acts as a cryoprotectant thereby preventing ice-crystal formation. After overnight immersion a piece is fished out and placed on a sample holder. The piece with the sample holder is then plunged into liquid nitrogen so that the piece becomes solid and ready for cutting thin sections.

The ultracryotome is prepared by bringing the cutting chamber to the desired temperature. For instance, to cut 4 µm thin sections, a chamber temperature of -80° C is desired to make sections of 100 nm – 300 nm thickness. The temperature is lowered by introducing liquid nitrogen into the cutting chamber.

Once, the desired temperature is reached the block is cut into ultrathin sections with a cryo diamond knife (Diatome). The cut sections are picked up with a sucrose loop and placed on a coverslip. These sections are subsequently immunostained for *d*STORM imaging.

2.8 Immunostaining for Tokuyasu Cryosectioning

The section placed on the coverslip is washed until the sucrose is completely dissolved. The section is dismounted and remounted to obtain flat sections. This was followed by blocking with 5% FCS in PBS. Primary antibodies were diluted in 5% FCS in PBS and applied on the ribbon for 2 hours. Samples were washed 3 times with PBS. The appropriate secondary antibody diluted in 5% FCS in PBS was applied for 30 min followed by washing in PBS for 3 times. The antibodies used for staining are listed below.

Primary Antibodies	Catalog Number	Dilution	Species
Anti-Bassoon	Enzo lifesciences SAP7F407	1:200	Mouse monoclonal
Anti-Piccolo	Synaptic Systems	1:200	Guinea pig
Anti-Septin 5	Santa Cruz Biotechnology	1:50	Mouse monoclonal
Anti-vGlut1	Synaptic Systems	1:200	rabbit
GFP nanotrap	Chromotek	1:200	Recombinant probe, origin: Alpaca

Table 2.4: Primary antibodies used for immunostaining on Tokuyasu's cryosections

Secondary Antibodies	Catalog Number	Dilution	Fluorophore
Anti-mouse	Life technologies A21245	1:500	Alexa 647
Anti-rabbit	Life technologies A21448	1:500	Alexa 647
Anti-mouse	Life technologies A21236	1:500	Alexa 532
Anti-rabbit	Life technologies L43000	1:500	Alexa 532

Table 2.5: Secondary antibodies used for immunostaining on Tokuyasu's cryosections

2.9 Dye-antibody Conjugation

40 µl of unconjugated at a concentration of (0.5 -2 mg/ml) was aliquoted in a fresh 1.5 ml Eppendorf tube. 10 µl of 1.5 ml $NaHCO_3$ was added to make the pH to 8.5. 5 µl of dye NHS ester dissolved in methanol or DMSO to a concentration of 1 µg/µl was added to the antibody and $NaHCO_3$ mixture. The entire reaction is allowed take place in the dark for one hour. After one hour a illustra NAP-5 column (GE Healthcare Life Sciences) is prepared by washing the column with 2 ml of PBS. Then, the reaction volume is pipetted onto the surface of the column and allowed to seep into the column. 200 µl of PBS is added initially to ensure formation of a crisp band. This is followed by filling the column with more PBS for separation of free dye from dye-antibody conjugate. The separation process can be tracked by eye. The dye-antibody conjugate, owing to higher molecular weight, elutes out first, which is collected in a fresh 1.5 ml Eppendorf tube. A volume of 300-400 µl of the dye-antibody conjugate should be present.

2.10 Electron Microscopy

LR White

70 nm sections of LR White embedded MNTB were cut with a diamond-knife (Diatome) in an ultramicrotome (Ultracut E, Reichert Jung, NY). The sections are collected on a Formvar-coated copper grid (Plano). Subsequently, for contrast enhancement, sections were treated with Reynold's Pb-citrate (Sigma) and uranlyacetate (Sigma) for 25 min in the dark.

HM 20

70 nm sections of HM 20 embedded MNTB were cut with a diamond-knife in an ultramicrotome. Tissue sections made from HM 20 embedded tissue block already contains uranyl-acetate, which is the contrast enhancement agent. Therefore, no further processing of thin tissue for contrast enhancement is required.

Transmission Electron Microscopy of the sections on the formvar grid were taken using Leo 906 E microscope.

2.11 *d*STORM Imaging

*d*STORM images were recorded on a custom-built microscope using experimental protocols that were described earlier Heilemann et al. 2008. Briefly, a multi-line laser (Innova 70C, Coherent, USA) was coupled into an inverted microscope (IX71, Olympus, Japan), and the fluorescence signal was detected using an electron-multiplying charge-coupled device (EMCCD) (Ixon, Andor, Ireland) and appropriate filters and dichroic mirrors (AHF, Tübingen, Germany). Alexa Fluor 647 was photoswitched in oxygen-free aqueous buffer containing 100 mM mercaptoethylamine and using two illumination wavelengths, 405 nm (0.1–1 kW/cm^2) for activation, 532 nm (1-5 kW/cm^2), 561 nm (1-5 kW/cm^2) and 647 nm (1–5 kW/cm^2) for read-out. Image reconstruction was performed using the *rapid*STORM software package Wolter S et al. 2010. Typically, 8000 frames were recorded to reconstruct a *d*STORM image.

Dual-color *d*STORM imaging for *tomo*STORM

Dual-color *d*STORM imaging was performed by sequentially imaging Alexa Fluor 647. As a first target, cytochrome c oxidase was labeled, imaged and bleached. Successful bleaching was verified in control experiments to exclude that Alexa Fluor 647 was driven into long-lived dark states and recovered to fluorescence. In a next round, the ribbon was stained for anti GFP with Alexa 647 and imaged. For alignment of the *d*STORM images, we recorded wide field images of memGFP distribution in each of these steps. To achieve this in the first step, memGFP was stained and visualized with ATTO520.

Dual-color *d*STORM imaging for Tokuyasu's Cryosections

Dual-color *d*STORM imaging was performed by sequentially imaging Alexa Fluor 647 followed by imaging Alexa Fluor 532.

3D *d*STORM imaging

3D *d*STORM measurements were recorded by installing a 500 mm focal length cylindrical lens (LJ1144RM-A, Thorlabs) in the detection pathway to introduce the necessary astigmatism.

2.12 Image Reconstruction

There are slight variations in the way images acquired using different procedures were reconstructed. This section describes how the reconstruction was done for images acquired through each procedure.

2.12.1 Image Reconstruction for *tomo*STORM

The localization files containing the final super-resolved images were aligned using the MultiStackReg plugin of ImageJ (Micheva et al., 2010). The MultiStackReg plugin works by performing cross-correlations between pairs of adjacent images in the stack. It applies a transformation to one image and adjusts the parameters of the transformation to maximize the cross-correlation between the two adjacent images. To achieve dual color super-resolution imaging, staining of the membrane-bound GFP (memGFP) was carried out using both Alexa Fluor 647 (used for *d*STORM) and ATTO520 (standard-resolution image used as reference image for registering multiple channels). By way of reference images, registration between two distinct (cytochrome c and memGFP) super-resolution channels could be achieved. The aligned and surface rendered image stacks were visualized in 3D using Amira 4.1.2 software (Visage Imaging, Richmond, Victoria, Australia) (see also Figure S1).

Figure 2.1: Image registration procedure for one-color imaging. In a first step (i), the sum-TIRF images of individual sections were registered using MultiStackReg, producing a transformation matrix for consecutive sections. In a second step (ii), the transformation matrix was applied to register the corresponding super-resolution images of consecutive sections. (B) Image registration procedure for two-color imaging. As a reference image, a cellular structure was recorded in a spectrally separate channel for each section and prior to super-resolution imaging (i). The super-resolution image of the same section was recorded on another spectral channel, and after the recording, the fluorophores were photobleached. To image a second structure, the sample was re-stained, and the series of sections was recorded following the same procedure (ii). Registration of each super-resolution stack was performed using the transformation matrix obtained from registering the reference images recorded in each round of imaging (iii). As the same reference structure was used for each recording of a stack of super-resolution images, the different stacks could be overlaid.

The resolution of the *d*STORM image thus gathered was calculated as follows: a localization of a spot of fluorescence was z-projected and fitted to a Gaussian to

calculate its standard deviation. From the standard deviation the full width at half maximum, which is a measure of the resolution was calculated to be 28 nm in the x and y plane Figure 2.2. The resolution along the z-axis is determined by the section thickness, which is 40 nm. Though a resolution of 20 nm is reported in the literature, we obtained a value, which is greater. This can be attributed to the fact that sections carried autofluorescence that increased background levels. As localization precision is a function not only of the number of photons gathered but also to the background count, we observed a worsening of resolution. This could in future be tackled by using buffer conditions, which increase the number photons from the dye. Use of heavy water has an influence on the photon output of fluorophores (Klehs K et al. 2014)

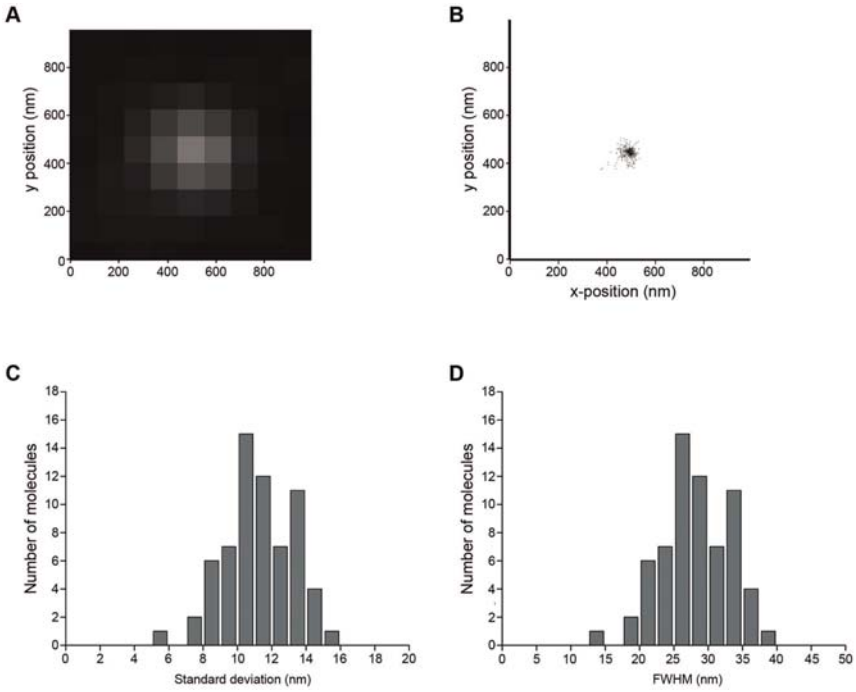

Figure 2.2: Determination of the spatial resolution. (A) point-spread function of a single fluorophore, (B) localization pattern of one single fluorophore that was localized multiple times through reversible photoswitching, (C) histogram of the standard deviation of localizations of 66 single-molecule point-spread functions (average standard deviation 12 nm) and (D) histogram of the full-width half-maximum (FWHM) of 66 single-molecule point-spread functions (average FWHM 28 nm).

2.12.2 Image Reconstruction for Tokuyasu's Cryosections

2D *d*STORM

Reconstruction for 2D *d*STORM was done as described above for *tomo*STORM. The alignment between Alexa 647 channel and Alexa 532 channel was done using autofluorescent spots, which was detected in both channels.

3D *d*STORM

A cylindrical lens with a focal length of 500 mm was placed between the tube lens and the camera of the OlympusIX81 to introduce astigmatism for 3D-*d*STORM. A z-stack of fluorescent microspheres was recorded with 10 nm steps. The corresponding PSF widths in x and y were determined by fitting an elliptical Gaussian function and were plotted against the z-position (Figure 2.3 a). The ratio of the width in x to the width in y at different z-values yielded a calibration curve (Figure 2.3 b). For every detected localization, the z position was determined by fitting an elliptical Gaussian function. The z position was assigned to the respective localization and a 3D-*d*STORM image was reconstructed with axial position color-coded for a range of 600 nm with a localization precision in z of 63.8 nm.

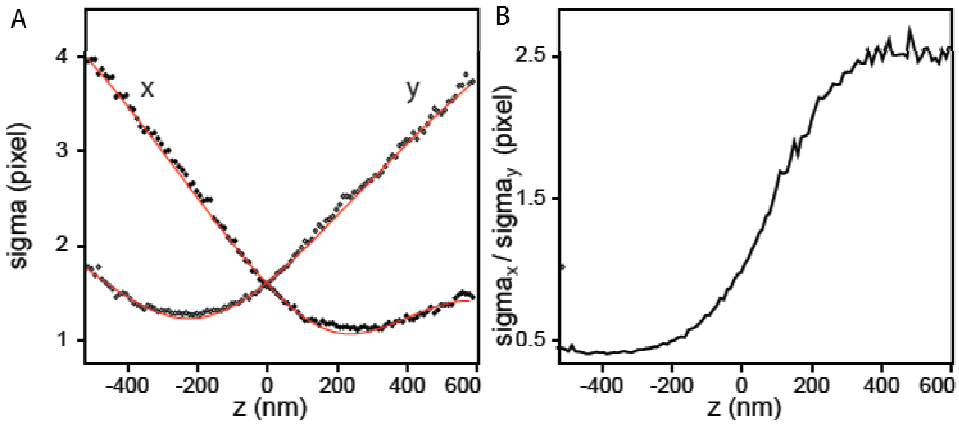

Figure 2.3: 3D-*d*STORM imaging by astigmatism. The PSF width in x and y of fluorescent microspheres are plotted against the z-value (A) and yield a calibration curve for z-position determination (B).

2.13 Transgenic Mouse

GFP-P/Q-Type calcium channel knock-in transgenic mouse (Mark MD et al., 2011) was a kind gift from Stefan Herlitz to Thomas Kuner.

2.14 Primary Cultured Hippocampal Neurons

Primary cultures of rat hippocampal neurons were prepared from E19 rat embryos as described previously (Dresbach et al., 2003). Cells from the embryonic brains were dissociated in calcium- and magnesium-free Hank's balanced salts solution (HBSS) by 20 min incubation with 0.25% trypsin (Sigma). These were plated onto poly-L-lysine-coated coverslips at a density of 60000 cells/cm^2 in Dulbecco's Modified Eagle Medium (DMEM) (Life Technolgies) including 10% fetal calf serum (FCS) (Life Technologies). Antibiotics (100 U/ml penicillin, 100 µg/ml streptomycin) (Life Technologies), and glutamine (2 mM) (Life Technologies). Twenty-four hours after plating, the medium was exchanged for Neurobasal (Life Technologies) including 2% B27 (Life Technologies), antibiotics (Life Technologies), and 0.5 mM glutamine (Life Technologies). Cells were kept in a humidified 95% air, 5% CO_2 incubator and were used for imaging experiments after 12 days in culture.

2.15 Hela Cells

A cell culture stock of Hela cells was washed with PBS (1 mL) (Life Technologies). Trypsin (1.5 mL, Sigma) was added. After 2 minutes of incubation, trypsin was removed from the cells. 5 mL of medium DMEM, 10% FCS, 5% PenStrep (Life Technologies), 5% L-glutamine (Life Technologies) was added. The cells have been diluted to a final concentration of 37.5 cells per µL. 400 µL of this suspension were added into each chamber of an 8-well LabTek (Nunc). Cells have been incubated over night at 37°C and 5% carbon dioxide until 70% confluency.

2.16 Transfection

The transfection of 9-day-old neuronal cultures was done as per the protocol from Invitrogen for Lipofectamine 2000 Transfection Reagent. Briefly, 4 aliquots of

lipofectamine reagent were diluted in Opti-MEM Medium (Life Technologies). DNA for synaptophysin-mEos2 was then diluted in the above mix and incubated for 15 min. The DNA-lipid-complex was subsequently added to cells and incubated for 3 days.

2.17 Fixation and Staining

Both Hela cells and hippocampal neuronal cultures were first washed in 1 X PBS (Crystal PBS Buffer, Bioline) and fixed in 4 % PFA (paraformaldehyde, Sigma) with 0.5% glutaraldehyde (Serva) for 15 min. Cells were then blocked in 0.1 % Triton (Merck) mixed in 5 % FCS (Life Technologies) for 15 min. The cells were then treated for 2 hours at room temperature with 1:200 phalloidin-dye conjugate (phalloidin-ATTO 488, phalloidin-Tetramethylrhodamine B isothiocyanate (TRITC) (Sigma) with initial concentration 10 nmol and phalloidin-BODIPY 650 (Invitrogen) with initial concentration 300 U) in the blocking solution. After 5 min washing with PBS, the cells were imaged in PBS immediately. Samples stained with phalloidin-Alexa 647 were imaged in oxygen-free aqueous buffer containing 100 mM mercaptoethylamine (MEA, Sigma)

2.18 Super-resolution Microscopy for Phalloidin-dye Conjugates

A multi-line argon-krypton laser (Innova 70C; Coherent, USA) was coupled into an inverted microscope (IX71, Olympus, Japan) equipped with a 60x oil immersion objective (PlanApo 60x, NA 1.45, Olympus) and operated in total internal reflection fluorescence (TIRF) mode. Excitation and fluorescent light was separated using a dichroic mirror. Here either FF560/659-Di01 (AHF, Germany) or FF410/504/588/669-Di01 (AHF, Germany) or HC576/661 (AHF, Germany) were used. The fluorescence signal was read out with an electron-multiplying CCD camera (EMCCD; Andor Ixon DU 897, Belfast, Ireland). Illumination intensities were adjusted to 1 – 5 kW/cm² (488 nm and 647 nm) and 5 - 7.5 kW/cm^2 (568 nm). Images were acquired with an integration time of 30 ms and EM gain of 200. Typically, between 10000 and 100000 images were recorded. Images were reconstructed with

rapidSTORM (Wolter et al., 2010) with the following settings: FWHM of 300 nm, pixel size of 20 nm for the reconstructed image.

Super-resolution imaging was performed in PBS. Samples stained with phalloidin-ATTO 488 were irradiated at 488 nm, phalloidin-TRITC at 568 nm and phalloidin-BODIPY 650 at 647 nm. Appropriate emission filters were used (BrightLine HC 550/88, ET Bandpass 610/60 and ET Bandpass 700/75; AHF Analysentechnik, Germany). Alexa Fluor 647 was imaged both in PBS as well as in the presence of 100 mM MEA in oxygen-depleted PBS at pH 7.4 according to the *d*STORM protocol (Heilemann et al., 2008).

Dual-color super-resolution imaging was performed sequentially. First, synaptophysin-mEos2 was imaged by illumination at 568 nm. Subsequently, phalloidin-ATTO 488 was imaged by illumination at 488 nm. The two spectral channels were registered using multispectral beads (dilution 1:1000, TetraSpeck, Life Technologies), which were imaged separately before the experiment, and the MultiStackReg plugin of ImageJ.

2.19 Ensemble Spectroscopy

Quantum yields were determined using a UV-VIS spectrometer (Cary 4E, Varian, Germany) and a fluorescence spectrometer (Typhoon 9400, GE Healthcare, Germany). ATTO 488 and TRITC as well as the corresponding dye-phalloidin-conjugates were diluted in either PBS or unfolding buffer (7M guanidinium chloride, 20 mM tris-HCl, 10 mM DTT, pH 7.5) down to concentrations of 2.2 – 2.9 µM (ATTO 488) and 0.5 – 0.9 µM (TRITC), respectively, and excited at 488 nm (ATTO488) or 561 nm (TRITC). At the given concentration range, the optical density (OD) of the dyes was kept below 0.05, to guarantee linearity in the absorption and emission processes. Note that the same excitation wavelengths were chosen as in single-molecule localization microscopy experiments.

3 Results

In this section two approaches are described to prepare sections from brain tissue, which can be used for making *d*STORM measurements. The first approach termed *tomo*STORM is a resin-based approach using which a series of 2D images are obtained. The 2D images are subsequently registered to form a 3D image. The second approach is a resin-free approach where a 3D *d*STORM is used to obtain the final 3D image. The second approach is preferred to the first approach due to ease of use and its ability to deal with unspecific binding. Using the second approach the distribution of synaptic proteins such as Bassoon, Piccolo, Septin 5 and voltage-gated calcium channels at the calyx of Held were investigated. In addition, results describing photoswitching properties of phalloidin-dye conjugates are described. These approaches in the end are essential to build a multicolor 3D nanoscopic map of synaptic protein architecture.

3.1 *Tomo*STORM

*Tomo*STORM is an approach where tissue is cut into a series of ultra-thin sections, which are immunostained, imaged with *d*STORM and later aligned together to construct a 3D image (Nanguneri S, et al. 2012). Using *tomo*STORM an isotropic super-resolution light microscopy data of proteins of the calyx of Held synapse is demonstrated. This is made possible by physically sectioning the sample down to 40 nm to allow for a superior resolution compared to conventional light microscopy in the z-axis and get uniform accessibility of the antibody into the tissue. The procedure for doing *tomo*STORM is as follows: a rat pup, as old as P10, is transcardially

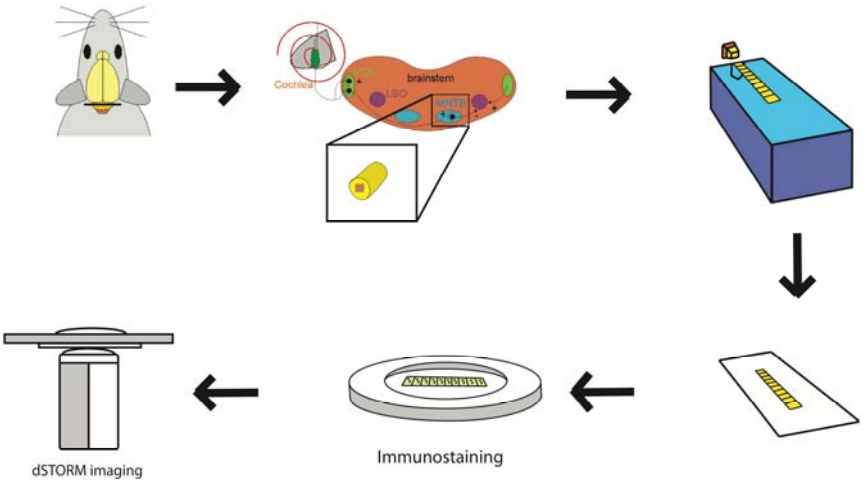

Figure 3.1: A schematic of the *tomo*STORM procedure.

perfused with 4% paraformaldehyde (Figure 3.1). The brain is dissected out and vibratome sectioned coronally. The section containing the MNTB is isolated and the MNTB is cut out. The cut out region is high pressure frozen and freeze-substituted with HM20, a lowicryl based resin, and subsequently polymerized. The resin-embedded tissue is shaped and mounted on a ultramicrotome. Using a diamond knife the shaped block is sectioned into a series of sections forming a ribbon. The ribbon is transferred to a coverslip for immunostaining. After immunostaining the section is mounted on the microscope to perform *d*STORM.

A resin called LR White was initially tested. Embedding tissue in LR White did not preserve the ultrastructure of the tissue. The *d*STORM images of plasma membrane that delineates cells looked distraughted (Figure 3.2). Therefore, the resin was changed to HM20, whose infiltration into the tissue requires ultra low temperatures (-80° C). Such conditions preserve the morphology of the tissue after resin infiltration (McDonald KL, 2009). This is verified using transmission electron microscopy of samples prepared with both LR White and HM 20 resin (Figure 3.3).

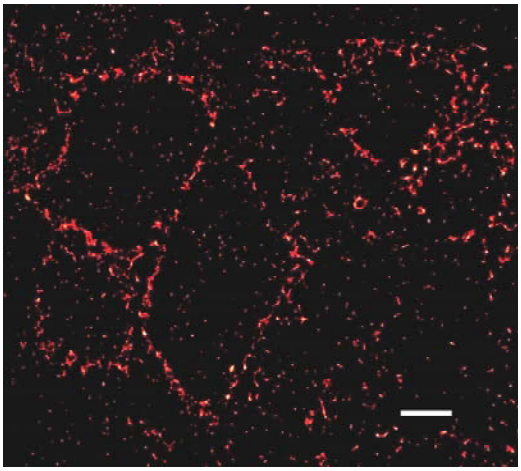

Figure 3.2: *d*STORM image of calyx of Held expressing membrane bound GFP. The GFP signal recorded with anti-GFP conjugated to Alexa 647 looks highly clumped implying that tissue morphology is distraughted. Scale: 3 µm

Because *d*STORM is a super-resolution light microscopy technique, which ideally achieves a resolution of 20 nm, it is very important that the structures that are imaged resemble those seen in the electron microscope. In other words the ultrastructure of the sample needs to be well preserved to obtain any meaningful interpretation of the *d*STORM data. Therefore, high pressure freezing was employed which was followed by freeze-substitution where the sample is gradually dehydrated with methanol and subsequently infiltrated with HM 20 resin for embedding.

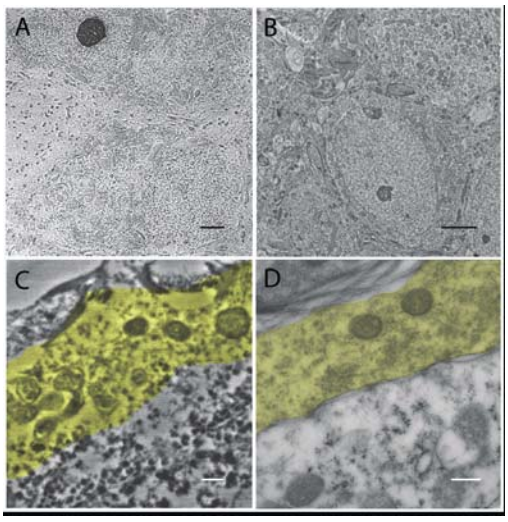

Figure 3.3: Comparison of electron micrographs of LRWhite embedded tissue of the auditory brain stem (A, C) and HM 20 embedded brain tissue (B, D). The high pressure-frozen HM 20 sections show

much better ultrastructure preservation compared to LR White embedded sections. Scale bars in A and B 2 µm, in C and D 250 nm.

A series of 53 sections were imaged. Calyces were membrane labeled with GFP and immunostained for GFP with an antibody conjugated to Alexa 647. Each section was 2 dimensional *d*STORM datum. Features such as membrane-to-membrane distance of the presynaptic compartment match those seen with electron microscope. This is proof that performing *d*STORM this way gives information about structurally well preserved biological synaptic compartments (Figure 3.4).

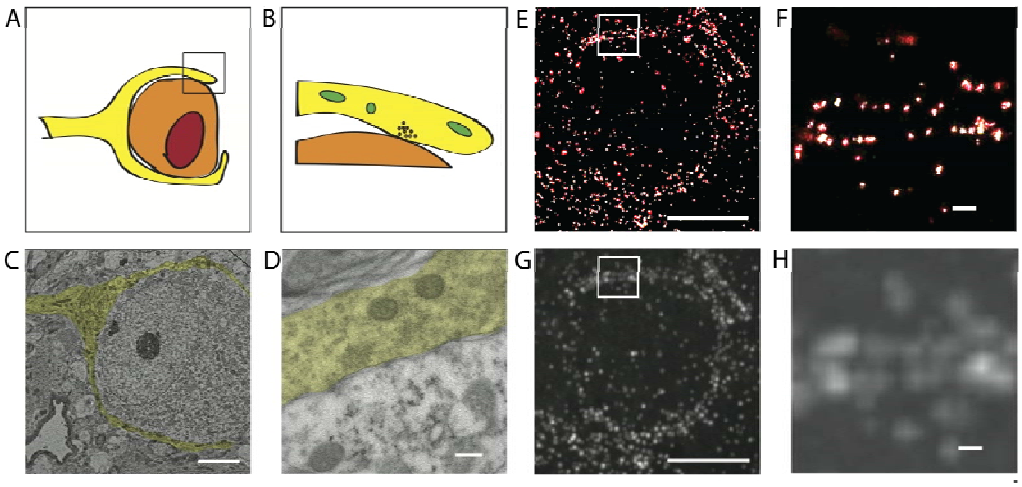

Figure 3.4: Structure of the calyx of Held on an overview scale (left panels) and on the scale of synaptic contacts (right panel). (A, B) Schematic representation, calyx (yellow), principal cell (orange), nucleus (orange). (C, D) Electron micrograph of the calyx of Held (yellow). (E, F) *d*STORM images of the calyx of Held. (G, H) Widefield images of the calyx of Held. Scale bars 5 µm (left panels), 250 nm (right panels).

The GFP distribution along the membrane is not continuous. This could arise because of two reasons: 1) the labeling efficiency of the antibody is not optimum 2) the GFP distribution in reality is very spotty owing to the fact that myristoylated GFP gets segregated into lipid rafts. Such features of lipid-raft like distribution of GFP are not seen in standard light microscope because of its poor resolution. This could be ascertained by taking 15 consecutive sections of the *d*STORM dataset and overlaying them to make a z-projection. The 15 consecutive sections correspond to a distance of 600 nm, which is the theoretical resolution along z-axis of a confocal microscope. The overlaid image has a continuous membrane structure as obtained with a confocal

microscope. Despite the presence of crude membrane outline of the calyx of Held synapse, its boundaries were outlined nevertheless and a crude 3D representation was created. The 3D representation resembles 3D calyceal structures created with EM datasets Figure 3.5.

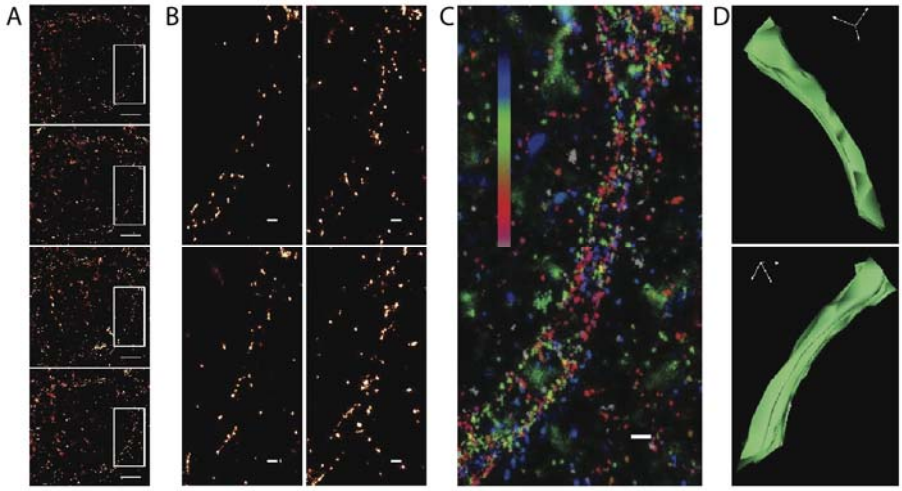

Figure 3.5: memGFP outlining the calyx membrane. (A) Four consecutive sections from a dataset of 53 sections containing segments of an entire calyx. Scale bars 2 µm. (B) Magnified views of the boxes illustrated in (A). Scale bars 250 nm. (C) Superposition of 15 consecutive aligned sections. Z-position of each section is color-coded (top: blue, bottom: purple). Scale 250 nm. (D) Two 3D views of the reconstructed segment shown in (C).

Because a system is needed where multicolor imaging could be performed the one-color imaging scheme was modified as described in the following manner: for each super-resolution image obtained a standard-resolution image was obtained. Though the super-resolution images represented different structures, the standard-resolution image, which is the reference image, remained the same. The standard-resolution image is aligned and the transformation matrix is applied to the super-resolution image so that both super-resolution images are in very good registration. After imaging the first color super-resolution image, the signal was bleached and ready to use for immunolabeling for subsequent *d*STORM measurements. The first super-resolution image obtained this way corresponded to the mitochondrial protein cytochrome C and the second super-resolution image corresponded to the membrane. The bleaching scheme is successful as there is little overlap of signal from the two super-resolution images (Figure 3.6).

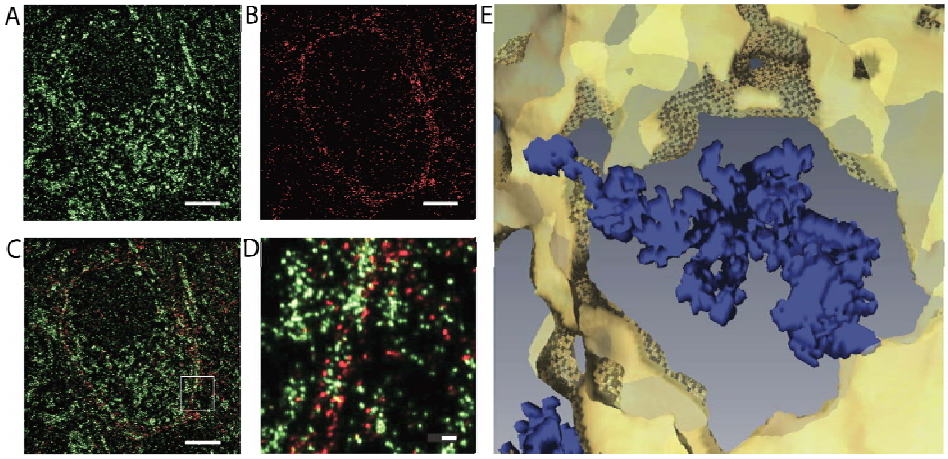

Figure 3.6: Dual color *d*STORM images of mitochondria and their localization within the calyx of Held. (A) Anti-cytochrome c oxidase stain. Nucleus spared. The soma of the principal neuron is densely populated with mitochondria. (B) Anti-GFP stain of a single section through the calyx of Held. (C) Overlay of (A) and (B). (D) 3D rendering of a mitochondrion (blue) and surrounding membrane (yellow). Scale bars are 250 nm.

The *tomo*STORM approach, which performs fluorescence light microscopy on resin embedded sections, is suitable for proteins, which are either abundantly found such as cytochrome C or over-expressed such as membrane labeled GFP. Labeling proteins which are sparsely distributed is difficult to detect because of the poor signal to noise ratio.

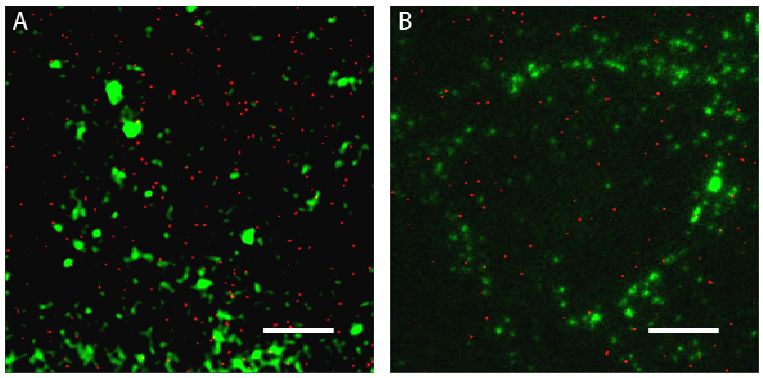

Figure 3.7: Antibody labeling of synaptic proteins on a thin section. (A) *d*STORM Bassoon (red) signal reaches the size of unspecific labeling. (B) *d*STORM PSD 95 (red) signal like Bassoon signal reaches the size of unspecific labeling. The membrane in both panels is delineated by the membrane bound GFP (green) and imaged in standard-resolution mode. Scale: 5 µm

The poor signal to noise ratio is due to unspecific labeling of the antibody. When the labeling density is high especially while labeling proteins found in great abundance the signal from unspecific labeling, which are isolated fluorescent signal, it is convenient to separate clusters (true signal) from randomly distributed isolated fluorescent events (false signal). When the true signal begins to get increasingly isolated (eg.: labeling of active zone proteins such as Bassoon or post synaptic density 95 such as PSD 95) fishing out the true signal from false signal based on the criterion mentioned above becomes difficult (Figure 3.7) .

3.2 Tokuyasu Ultracryotomy

From the past experience it is known that labeling for active zone proteins works well when performed on plain PFA fixed tissue. Therefore 4 µm thin cryosections were made and 3D *d*STORM measurements were performed on it. Thin sections are especially useful for this purpose as they remain, when placed on the coverslip, stuck perfectly flat. This property is very essential for doing *d*STORM as *d*STORM uses total internal reflection microscopy with objectives whose effective sample penetration is about 4 µm. And the sample is subsequently immunolabeled so that fluorescence microscopy could be performed. The 4 µm thick sections of the MNTB was made as follows: the region of interest containing the MNTB which was cut out is dropped into 2.3 M sucrose. Sucrose acts as a cryoprotectant. The sucrose-infiltrated pieces of tissue are dropped into a vessel containing liquid nitrogen in order to freeze the sample to solidity. A cryo-chamber is set up in the ultramicrotome. The cryo-chamber is connected to the liquid nitrogen tank and the temperature of the cryo-chamber is dropped to -40° C by introducing liquid nitrogen into it. Once the chamber is as cold as -40° C, the sample is mounted onto the sample holder in the chamber and using a cryo diamond knife 4 µm thick sections were made which were subsequently flattened and made to undergo immunostaining for super-resolution fluorescence light microscopy (Figure 3.8).

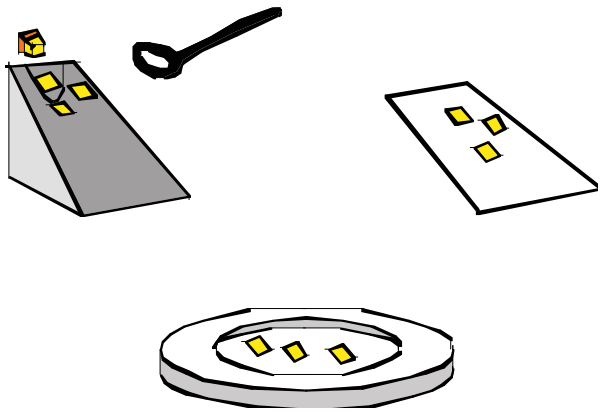

Figure 3.8: A schematic of Tokuyasu cryosectioning

Unlike in the *tomo*STORM approach, in a typical 3D *d*STORM setup, the fluorescence emission is made to go through a cylindrical lens so that an astigmatism is created based on which fluorophores' z distance could easily be discriminated. This kind of imaging offers a z-resolution of 50 nm (Huang B. et al, 2009). For instance the vesicular protein vGlut1 was imaged under 3D *d*STORM conditions and the 3D position of the fluorophores is color-coded (Figure 3.9). As can be discerned from the color-coding the vesicles occupy a highly 3 dimensional space in a volume covering 600 nm. As immunostaining for many proteins on this kind of sample preparation is feasible, the 3D relationship of active zone proteins in the calyx of Held synapse was probed.

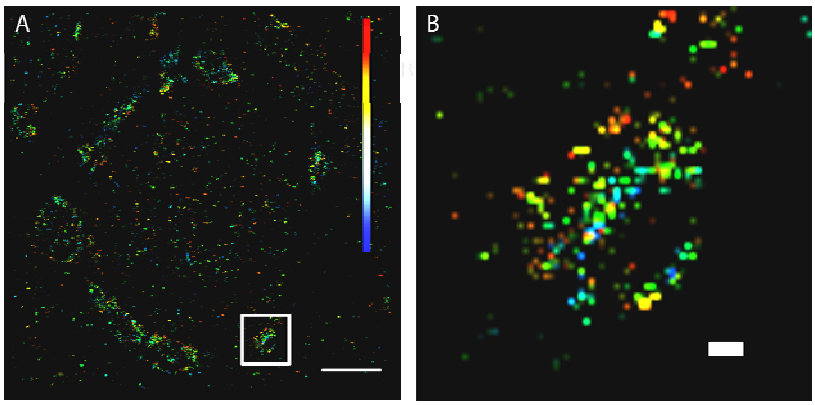

Figure 3.9: (A) 3D *d*STORM imaging of vGlut1 staining in the calyx of Held, an overview. The z-axis information is color-coded (0-600 nm). Scale: 2 µm. (B) magnified view of a compartment shows that the vesicular organization has a discrete nanostructural organization. Scale: 250 nm.

As staining of active zone proteins such as Bassoon is feasible with this method 3D *d*STORM imaging was done on Bassoon. Super-resolution image of Bassoon in the calyx of Held reveals that Bassoon is clustered. This feature is also evident in normal standard-resolution fluorescence microscopy. What is not evident in the normal standard-resolution fluorescence microscopy, however, is that magnified view of a super-resolution Bassoon cluster reveals that Bassoon is not uniformly distributed along the active zone. It has a perforated structure, which cannot be revealed with standard wide field fluorescence microscopy cannot resolve the perforations (Figure 3.10).

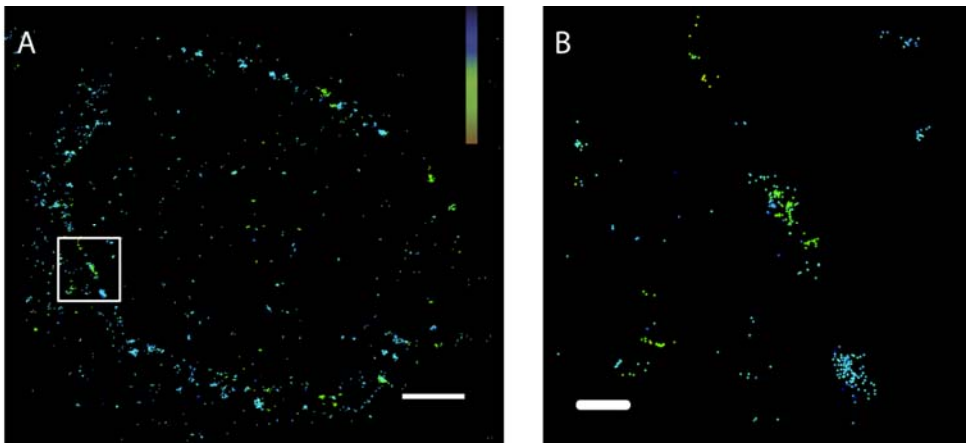

Figure 3.10: (A) 3D *d*STORM imaging of Bassoon staining in the calyx of Held, an overview. The z-axis information is color-coded (0-600 nm). Scale: 2 µm. (B) Magnified view of a compartment shows that the vesicular organization has a discrete nanostructural organization. Scale: 250 nm.

In addition, the resin free approach is suitable for photoactivated localization microscopy (PALM) (Betzig, E. et al., 2006, McKinney, SA., et al., 2009), which is in principle similar to *d*STORM but makes use of photoswitchable fluorescent proteins such as mEos2. 300 nm and 4 µm cryosections were imaged with calyces expressing membrane bound mEos2. 2D PALM of mEos2 on 300 nm thin cryosections show sharp membrane features such as the presynaptic compartment (Figure 3.11 B).

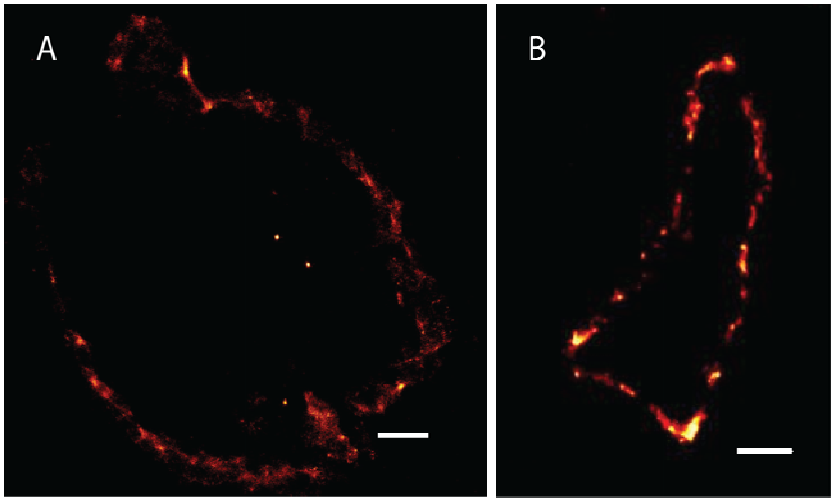

Figure 3.11: (A) 2D PALM image on a 4 µm section containing the calyx of Held labeled with mEos2. The image looks fuzzy owing to a high density of mEos2 molecules. Scale: 5 µm. (B) 2D PALM image of a compartment of calyx of Held labeled with mEos2 on a 300 nm section. Scale: 500 nm.

The sharpness is due to the fact that on a 300 nm thin section few molecules need to be photoswitched, which is a prerequisite for doing single molecule localization microscopy (SMLM) such as *d*STORM or PALM. Active zones span larger than 300 nm. As a result, fluorescence signal from antibody staining of active zones is undersampled. Therefore, 2D PALM was performed on 4 µm thick sections. 2D PALM on 4 µm thick sections covers mEos2 signal that spans an optical volume of 600 nm. However, the challenge of trying to photoswitch a larger number of molecules remained which is far from an ideal situation for *d*STORM or PALM. As a result calyceal compartments look fuzzy (Figure 3.11 A).

The large density of fluorophores also is an obstacle for doing 3D SMLM. The necessary astigmatism for 3D SMLM is destroyed owing to overlapping fluorophore signals. As a result performing 3D PALM proved to be difficult owing to poor signal to noise ratio (Figure 3.13). This could be overcome with bleaching the sample so that only a few fluorescent proteins turn on. Bleaching, however, leads to loss of signal as some of the mEos2 molecules get irreversibly bleached. Future experiments should take into consideration the expression levels of mEos2 in the membrane. For instance, decreasing virus titer can lead to a decrease in the mEos2 molecules and thus lead to a increase in the signal to noise ratio. This would then result in sharper optical sections of membrane compartment.

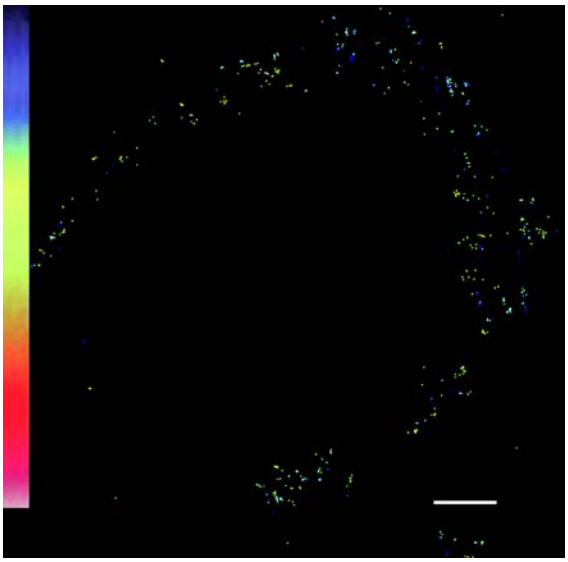

Figure 3.13: 3D PALM on a 4 µm thick section containing the calyx of Held expressing mEos2 as a membrane marker. The z-axis information is color-coded (0-600 nm). High density of mEos2 molecules required excessive bleaching for clear single molecule detection leading to a loss of signal due to irreversible photobleaching of some mEos2 molecules. Scale 3 µm.

In conclusion, antibody labeling of less abundant proteins such as the proteins of the active zone are better addressed with Tokuyasu's ultracryotomy. Moreover, as this method avoids resin, preservation of fluorescence from fluorescent proteins is possible. Therefore, this method is preferred to *tomo*STORM to make *d*STORM measurements of active zone proteins possible.

3.2.1 Bassoon and Piccolo

Bassoon and Piccolo are two proteins of the cytomatrix that play a role in clustering synaptic vesicles (Mukherjee et al. 2010). Using a diffraction-limited microscope, namely a confocal microscope, on the calyx of Held it was found that Bassoon and Piccolo form clusters whose size resembles that of the active zone and that majority of the clusters overlap. Dual color *d*STORM was performed on this to gather more information.

In order to probe the distribution of different proteins in the synaptic terminus multi-color *d*STORM were performed for more proteins. Typically, owing to the variation

in redox potential, a maximum of two dyes can be photoswitched, enabling *d*STORM imaging of two synaptic proteins. Therefore, this possibility was exploited to study the nanoscopic organization of the two active zone proteins namely Bassoon and Piccolo. Both Bassoon and Piccolo are presynaptic proteins, which are known to organize the cytomatrix of the active zone.

In agreement with the work there is overlap between the Piccolo and Bassoon clusters (Figure 3.14). As it is already ascertained that the two proteins are essential for organizing the vesicle pool in the synapse it can be concluded that the two overlapping signals are presynaptic in origin.

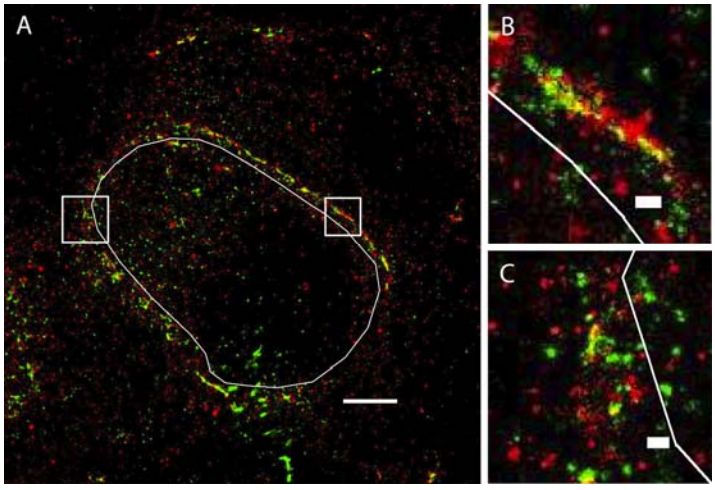

Figure 3.14: Dual color 2D *d*STORM of cytomatrix proteins Bassoon (green) and Piccolo (red). (A) Overview shows that they overlap most of the time. (B, C) Magnified views show a mixture of unitary Bassoon and Piccolo signals, and colocalized signals of Bassoon and Piccolo.

The calyx of Held synapse, owing to its unitary gigantic nature with multiple release sites, also yields itself well to image analysis. As the majority of active zones contain both Bassoon and Piccolo clusters, this information can be used to correct for misalignment between the two channels. Co-staining of Bassoon and Piccolo show highly overlapping distribution of the two presynaptic proteins. Magnified view of the clusters reveal that the two proteins also overlap within the cluster indicating that they are intermingled in the cytomatrix.

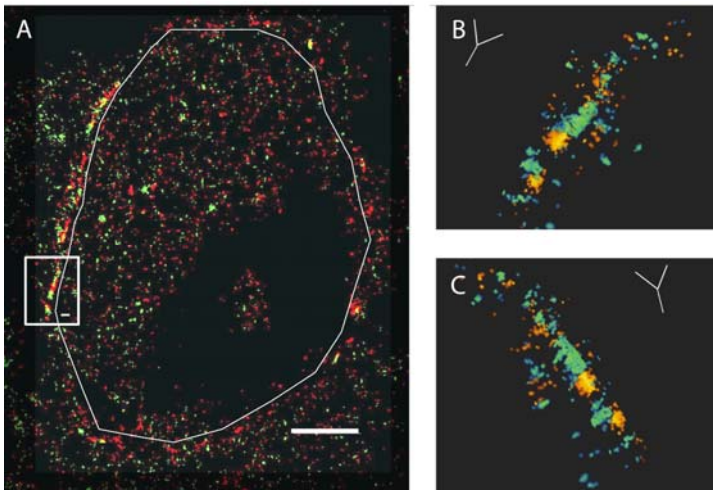

Figure 3.15: (A) Overview of dual color 2D *d*STORM of Piccolo (green) and Bassoon (red) at P7. Scale: 1 µm. (B, C) Magnified view is a 3D rendering of the inset depicting Piccolo (blue) distribution with respect to Bassoon (orange). Scale: 200 nm (see inset)

In addition to 2D dual color *d*STORM imaging, 3D dual color *d*STORM imaging of Bassoon and Piccolo distribution was performed (Figure 3.15). Information from 3D dual color *d*STORM images of Bassoon and Piccolo distribution compliments those of 2D dual color *d*STORM.

In conclusion, besides, the presence of colocalization at the standard-resolution scale, there is as well colocalization at the nanoscopic level indicating that Bassoon and Piccolo perform redundant function. In addition unitary Bassoon and Piccolo signals can also be visualized, but the significance of these signals can only be speculated. They may well arise due to molecular crowding effects that leads to exclusion of one of the antibody species from another. This makes an argument for the use of nanobodies, which have the potential of overcoming steric hindrance.

In addition, they may also arise from the fact that there are differences in molecular organization of active zones where one of the two active zone proteins may dominate. This may not necessarily lead to differences in function as the two proteins are homologous and play similar roles at the active zone

3.2.2 Septin 5

Septin 5 at the calyx of Held active zone brakes the synaptic vesicles from readily releasing. It is known to have differential effects during maturation. It is present at the release site at the onset of hearing at P7 and is completely removed by the time maturation is finished at P17. As a result, these two maturational points were used for *d*STORM analysis. To visualize the distribution of Septin 5 in the AZ, dual color *d*STORM on Septin 5 and Piccolo was performed to see what additional information, if present, can be obtained. Dual color *d*STORM images show, at P7 Septin 5 colocalizes with the active zone protein Piccolo. Not only does Septin 5 colocalize with Piccolo, but because of the super-resolution capability of *d*STORM it can be visualized that Septin 5 occupies only a fraction of the active zone. Calcium channel cluster as well has been modeled to occupy a fraction of the active zone (Meinrenken et al., 2003). Therefore, release of vesicles could happen in designated zones. As Septin 5 has been implicated in applying the necessary brakes (Yi-Mei Yang et al., 2010), it follows that Septin 5 needs to be present only where vesicle release takes place Figure 3.16.

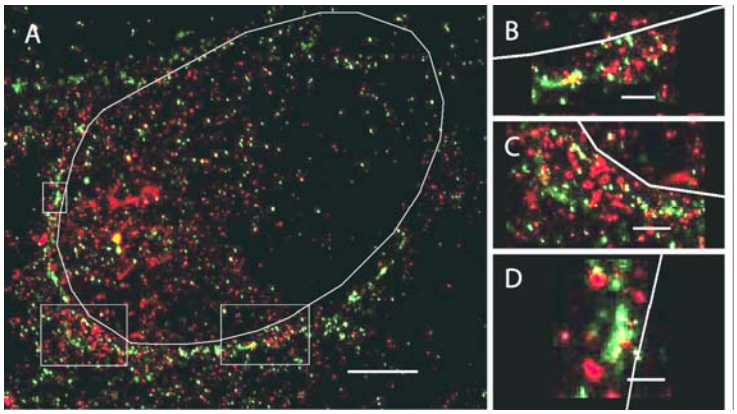

Figure 3.16: (A) Overview of dual color 2D *d*STORM of Septin 5 (red) and Piccolo (green) at P7. Scale: 1 µm. (B, C, D) Magnified view reveals that Septin 5 is highly colocalized with Piccolo at this age. Scale: 200 nm.

In P17, however, there is very little overlap between Piccolo and Septin 5 (Figure 3.17). Moreover, *d*STORM apparently shows Septin 5 still exists in the neighbourhood of the active zone although it does not seem to colocalize with it.

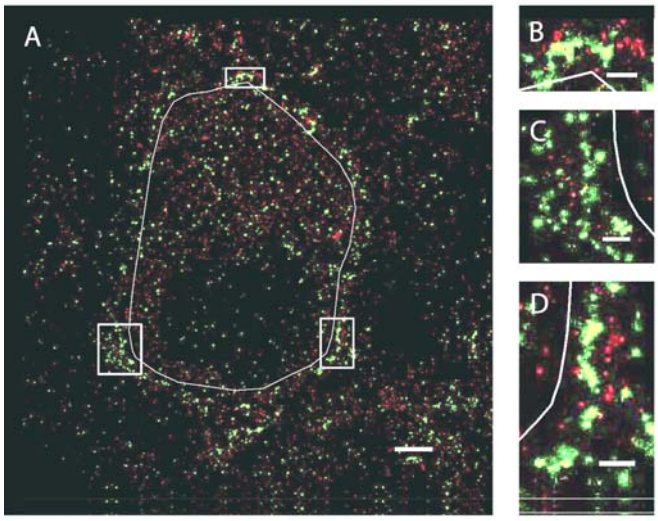

Figure 3.17: (A) Overview of dual color 2D *d*STORM of Septin 5 (red) and Piccolo (green) at P17. Scale: 1 µm. (B, C, D) Magnified view reveals that Septin 5 is not as much colocalized with Piccolo at this age as it is at P7. Scale: 200 nm.

Quantification of colocalization has been carried out for the 2 ages using Manders Colocalization Analysis (MCA). MCA is particularly used in situations where the quantity of the objects in the two images is not same. For instance, there is clearly more Septin 5 than Piccolo at the release face.

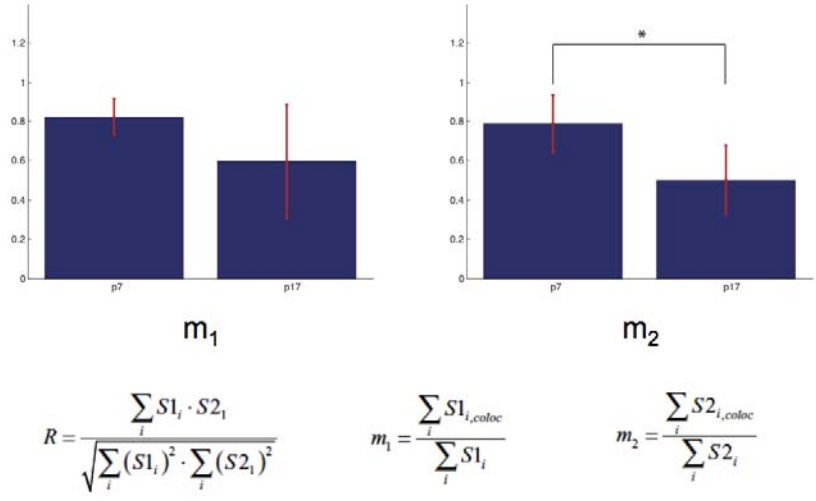

Figure 3.18: Manders colocalization analysis reveals that the amount of Piccolo colocalizing with Septin 5 at P7 and P17 is insignificant. However, the amount of Septin 5 colocalizing with piccolo at P7 and P17 is significant.

MCA gives out 2 values, namely m_1 and m_2. m_1 denotes the extent of colocalization of green (Piccolo) with red (Septin 5), while m_2 denotes the extent of colocalization of red with green (Figure 3.18). The difference in colocalization of green with red is not significant for the 2 ages meaning a large fraction of Piccolo does not colocalize with Septin 5. The difference in colocalization of red with green is significant between the 2 age groups. There is more Septin 5 colocalizing with Piccolo at P7 than at P17.

In addition, 3D dual color *d*STORM imaging of Septin 5 and Piccolo was performed. 3D images reveal that the release face, which is marked by Piccolo, is spotted with Septin 5 (Figure 3.19). This indicates that Septin 5 mediated calcium channel microdomain clusters are sparsely distributed over the release zone (Meinrenken et al 2003).

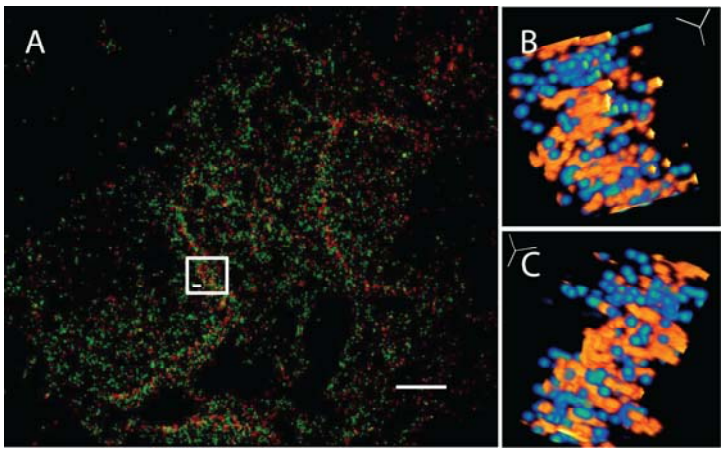

Figure 3.19: (A) Overview of dual color 2D *d*STORM of Septin 5 (green) and Piccolo (red) at P7. Scale: 1 µm. (B,C) Magnified view is a 3D rendering of the inset depicting Septin 5 (blue) distribution with respect to Piccolo (orange). Scale: 200 nm (inset).

In summary, the data obtained with *d*STORM images conform well to the published results implying that information obtained with *d*STORM provide a biologically meaningful information. Moreover, a population of active zones can be analysed from one image as large fields of view can be obtained with a light microscopy.

3.2.3 Calcium Channel Localization

Calcium channels are clustered at the active zones. These clusters are tethered in place by the active zone proteins where synaptic vesicles exocytosis happens. Due to molecular crowding accessing channels would be challenging.

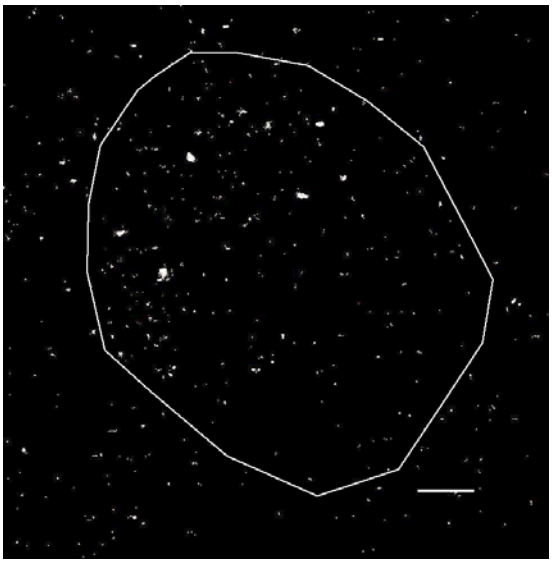

Figure 3.20: 2D *d*STORM image of P/Q type calcium channel tagged with GFP and labeled with GFP nanobody tagged with Alexa 647. Low density of true signal makes it difficult to separate true signal from false signal from unspecific nanobody labeling if any. Scale: 3 μm

GFP nanobodies owing to their small size (1-2 nm) have been used to address this problem. These nanobodies are tagged with a fluorescent dye such as Alexa 647 can be used to label GFP tagged proteins in cells. Moreover, as there are many transgenic lines, which express proteins tagged with GFP, it is now feasible to use GFP nanobodies to target these proteins for performing *d*STORM (Ries et al., 2012)

P/Q type calcium channels in the calyx of Held are clustered in a microdomain scenario, which occupy a tiny fraction of the active zone (Meinrenken et al., 2003). Though antibodies exist, labeling P/Q type calcium channels has proven extremely difficult. This could be due to molecular crowding at the active zone because nanobodies extend 1-2 nm in diameter they can especially navigate a highly crowded space (personal communication). As a result, labeling for the P/Q calcium channel tagged with GFP using GFP nanobody was performed (Figure 3.20). Fluorescence immunohistochemistry is plagued with unspecific binding of the antibody. In the case that a certain protein exists as a cluster, solitary unspecific label (false signal) can be separated from clustered label (true signal) with ease. However, the moment a true signal begins to get solitary in nature such as the case seen in calcium channel distribution, separating true signal from false signal becomes problematic. Moreover,

there is also no control to verify if the nanobody can truly overcome molecular crowding. In conclusion, *d*STORM image of P/Q type calcium channel tagged with GFP and labeled with nanobody is hard to interpret.

Labeling strategies need to be developed that can increase the signal to noise ratio. One way this could be accomplished is by an energy transfer mechanism such as FRET or PET. A donor could be placed on a protein in close proximity to the calcium channel, which contain the acceptor. This way, for instance, only the signal from the channels present in the active zone could be read out.

3.3 Alternative Photoswitches for Multicolor *d*STORM

As conventional buffer mediated *d*STORM can accommodate only two photoswitching dyes, namely Alexa 532 and Alexa 647, an attempt is made to expand this by investigating the photoswitching property of fluorophores tagged to phalloidin.

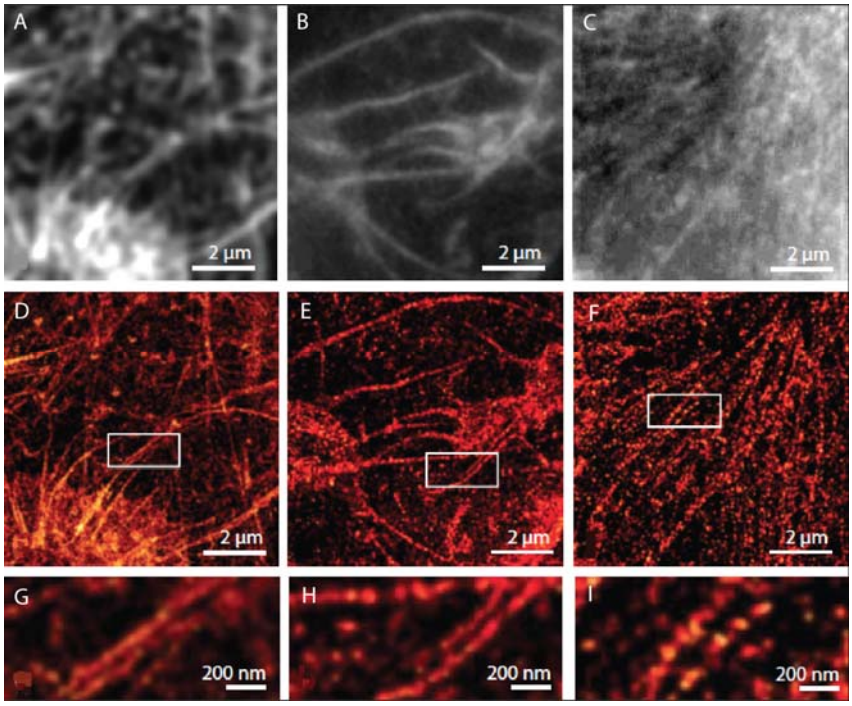

Figure 3.20. Super-resolution imaging of actin structures with various phalloidin probes. (A) – (C) Widefield images of Hela cells stained for actin with phalloidin conjugated to ATTO 488 (A), TRITC (B) and BODIPY 650 (B). (D) – (F) Super-resolution images of the same cells recorded in PBS as imaging buffer. (G) – (I) Magnified views of regions selected from (D) – (F).

As mentioned earlier, as the probe gets smaller in dimensions, quenching of fluorescence can be observed. The amino acid tryptophan when in close proximity (1-2 nm) to the fluorescent dye is known to interact with the excited state of the fluorescent dye and quench its fluorescence. Experience with imaging actin filaments labeled with phalloidin-ATTO 488 told us that phalloidin-ATTO 488 makes a good photoswitch in plain PBS. This is due to the close proximity of the conjugated dye to the quencher tryptophan, which occurs as a special case in phalloidin. This observation and selected 3 dyes that were conjugated to phalloidin namely ATTO 488, TRITC and BODIPY 650 (Figure 3.20) was exploited. The sample was imaged by increasing laser intensity. Quenching led all 3 probes photoswitch at appropriate laser intensities. Quenching can occur by static and dynamic means. Static quenching can be due to stable complex formation lasting many milliseconds while dynamic quenching is merely collisional lasting nanoseconds in timescale.

Bulk quenching, which is the sum of static and dynamic quenching that a fluorophore undergoes, can be observed by measuring the relative fluorescence quantum yields. Bulk quenching, however, cannot differentiate between static versus dynamic quenching. Fluorescence lifetime measurements, on the other hand, is sensitive only to dynamic quenching. Therefore, both these measurements were conducted while assessing for bulk quenching, a relative quantum yield of 48 % for ATTO 488 and a relative quantum yield of 27 % for TRITC was obtained. As quenching in PET is mediated by hydrophobic interactions between the molecules, addition of guanidinium chloride should restore the relative quantum yield to 100 %. This effect was confirmed. In addition, fluorescence lifetime measurements of 2.2 ns for free TRITC dye and 2.3 ns for phalloidin conjugated to TRITC was obtained implying that static quenching is the modus operandi. For ATTO 488 free dye, fluorescence lifetime of 4.1 ns was observed. When measured in presence of tryptophan a biexponential decay was observed with fluorescence lifetimes of 3.0 ns (82%) and 0.7 ns (18%). Phalloidin-ATTO 488 as well gave a biexponential decay 3.4 ns (78%) and 1.2 ns (22%).

These observations are in agreement with published results. A stable dye-tryptophan-complex is the nature of the non-fluorescent OFF-state is assumed. Therefore, the kinetics of photoswitching is governed by association and dissociation dynamics of this complex.

Photoswitching performance for SMLM depends on ON/OFF switching kinetics of the fluorophore (Sauer, M. 2013). A good quality SMLM image needs a long-lived OFF state and short-lived ON state. The ratio of kon/koff needs to be sufficiently high for SMLM. The ON and OFF times were determined and the rate constants were extracted and kon/koff ratios for the 2 dyes were determined. For ATTO 488, a kon/koff of 883 and TRITC a kon/koff of 1023 was reported (Figure A1 – A4, Appendix). The ratios are sufficiently large to allow imaging of dense structures such as cellular actin filaments. Moreover, a photon count of 822 photons for a molecule of ATTO 488 and 939 photons for a molecule of TRITC were determined. These values correspond to theoretical localization accuracy of 10 nm.

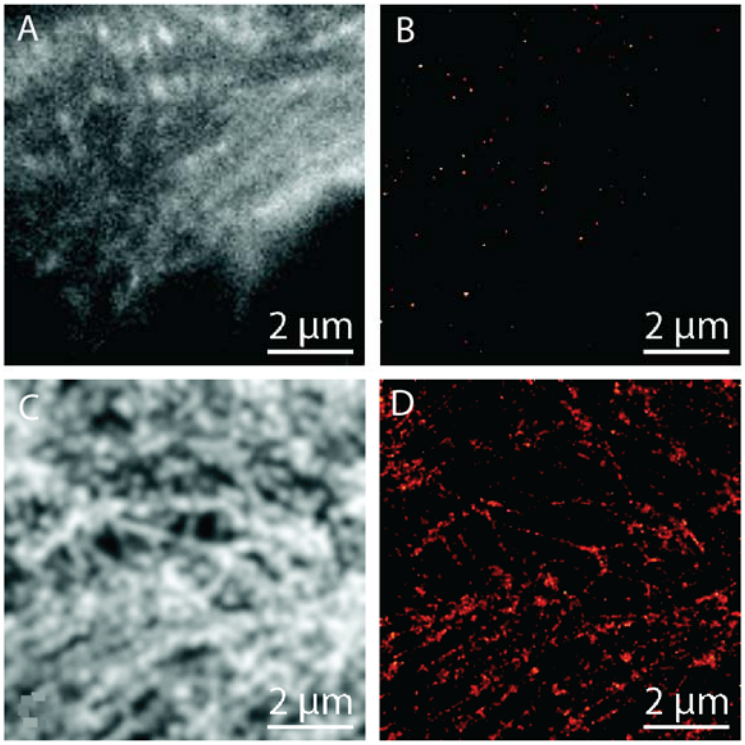

Figure 3.27: Super-resolution imaging of actin structures labelled with Alexa Fluor 647 in two different imaging buffers. (A), (C) Widefield images of Hela cells stained for actin with phalloidin-Alexa Fluor 647. (B) Super-resolution image of the cell shown in (A) in PBS as imaging buffer. (D)

Super-resolution image of the cell shown in (C) recorded in the presence of 100 mM MEA according to the *d*STORM protocol.

The redox potential of cyanine dyes does not favor reduction by tryptophan. A control experiment was performed where phalloidin-Alexa 647 was used to label filamentous actin. As expected, no photoswitching in PBS was observed. Upon addition of 100 mM of MEA, however, good switching was seen (Figure 3.27). Oxazine dyes are known to form stable dye-tryptophan complexes. As a result, phalloidin-oxazine dye conjugates are less suitable for fluorescence nanoscopy.

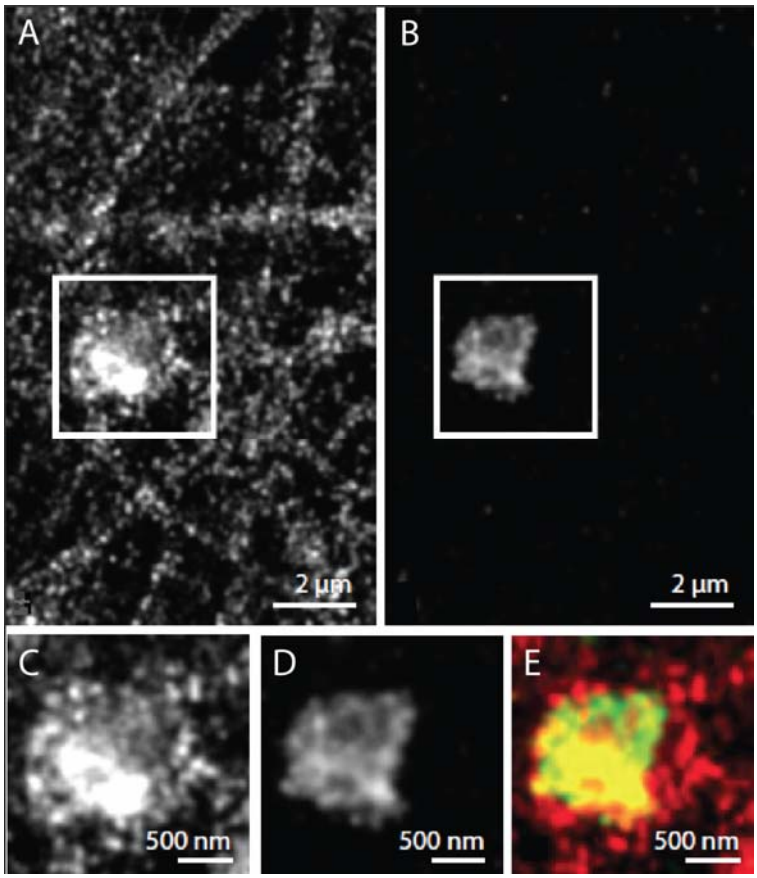

Figure 3.28. Dual-color imaging of actin and synatophysin in neuronal cells. Super-resolution images of primary cultured hippocampal neurons labelled for actin with phalloidin-ATTO 488 (A) and synaptophysin by expressing synaptophysin-mEos2 (B). (C, D) Magnified view of the boxed regions shown in (A, B). (E) Dual-color visualization of actin and synaptophysin.

Many photoswitchable proteins are quenched when imaged with MEA. Taking advantage of the capability of performing *d*STORM in PBS, two-color experiment was performed where mEos2 tagged to synaptophysin – vesicular protein and phalloidin-ATTO 488 labelling the filamentous actin was imaged. Synaptic vesicles are clustered at the active zone. The molecular mechanism ensuring clustering is under debate. F-actin is a candidate molecule. It has been reported using *d*STORM that actin forms rings in axons, which are spaced about 190 nm (Xu, K. et al., 2012). Super-resolution image shows a dense network of actin and vesicle cluster containing different densities of synaptic vesicles (Figure 3.28).

In summary, quenching-based photoswitching offers an alternative to buffer-mediated photoswitching and can be a potential tool for performing multicolor *d*STORM. The study on quenching-based photoswitching in phalloidin-fluorophore conjugates is limited to performing super-resolution microscopy on actin. Therefore, probes need to be designed in a special manner that can mimic the properties of phalloidin-fluorophore conjugates for a more general usage of quenching-based photoswitching for super-resolution light microscopy.

4 Discussion

The present work comprises developing technology to perform *d*STORM measurements on thick vibrotome sectioned brain tissue. Such as thick specimen, whose thickness is in the range to 100 to 200 µm, is not only able to attach itself to the cover-slip but also not conducible for performing *d*STORM measurements because thick specimen contributes to enormous background autofluorescence, which spoils the localization precision of *d*STORM. The cause of autofluorescence is the fixation of proteins with paraformaldehyde (PFA). PFA fixed biological matter when excited with light in the visible range lead emission of fluorescence. Therefore, a technique called *tomo*STORM was developed that entailed performing ultrathin physical sections (40 nm in thickness) of the sample. These ultrathin sections not only allowed for easy epitope accessibility and but also contributed to a gain in resolution in z-axis. The gain in z resolution arises from the fact that the thickness of the section alone determines the resolution in z-axis. The resolution along the z-axis of an optical setup under ideal conditions is 600 nm. Therefore, the gain by physical sectioning is by many orders of magnitude greater. Limitations in staining for proteins with *tomo*STORM, however, proved to be enormous. As a result, another technique was developed, which adopted Tokuyasu ultracryotomy for thin tissue sectioning (4 µm) for the use in *d*STORM. Improvement in z-resolution is accomplished by performing 3D *d*STORM microscopy as opposed to physical sectioning. As sections in this approach were resin-free antigenicity is better preserved.

4.1 *Tomo*STORM

In this study, Array Tomography (AT) was combined with *d*STORM for the study of synaptic protein organization in the calyx of Held. As described in the protocol of AT, LR White was used as the resin to perform embedding of the brain tissue. While using nanoscopic techniques such as electron microscope and *d*STORM, one needs to ensure that the ultra-structure of the tissue is well maintained to ensure the protein distribution at the synapse is as less disturbed as possible. *d*STORM images of LR White sections immunostained for the membrane bound GFP showed a distorted organization of the plasma membrane. Electron micrograph of LR White sections

confirmed that the tissue preservation is poor. Therefore, the decision was taken to use another resin called HM 20, which is equally suitable for doing immunolabeling. Unlike LR White, tissue infiltration with HM 20 requires extremely low temperature conditions. Moreover, high-pressure frozen samples are known to keep their ultrastructure well preserved devoid of damaging ice crystal formation (McDonald KL, 2009). This allowed use of high-pressure frozen samples. High-pressure frozen HM 20 sections examined with electron microscope showed well-preserved ultra-structure of the brain tissue. Therefore, HM 20 was chosen for performing *d*STORM measurements. *d*STORM images of HM 20 sections immunostained for the membrane bound GFP clearly showed the membrane leaflets bounding the synaptic compartment of the calyx of Held. The width of the synaptic compartment is similar in dimensions to what is obtained with electron microscope measurements (Figure 3.4). From these observations it is concluded that use of HM 20 embedded brain tissue under high pressure frozen condition is well suited for obtaining super-resolution images (Nanguneri et al 2012) where proteins probed are as less displaced as possible.

Using *d*STORM, single color *d*STORM images were obtained. Multicolor *d*STORM imaging was achieved by making use of a standard-resolution reference image. The widefield reference images thus obtained were aligned using an ImageJ plugin, which allows the user to save the transformation matrix. Subsequently, the transformation matrix is applied to the super-resolution image that needs to be transformed leading to a registration between the two different *d*STORM datasets. This way it is demonstrated that the presynaptic mitochondrial cytochrome C signal is confined to the two leaflets of the synaptic compartment. This process though described for two colors can be extended in principle to obtaining well-registered (numbers) multicolor dataset (lit). Therefore, with *tomo*STORM a super-resolution voxel size of 28 nm x 28 nm x 40 nm could be demonstrated.

Though the resin approach has been particularly useful in overcoming the limitations in the z-resolution, it is nevertheless not devoid of nonspecific labeling of the antibody. As long as a protein, which is found in great abundance, is labeled, clustering of true signal makes the discrimination between true versus false immunostaining signal possible. As the abundance of the proteins such as those

present in the active zone starts to decrease, it becomes increasingly hard to discriminate between true versus false signal, as the density of true signal becomes the same as that of the false signal.

From prior experience, labeling of active zone proteins works well in nonresin embedded tissue, which is not physically sectioned. In addition, resin infiltration requires dehydrating conditions, which denatures proteins. Denaturation of fluorescent proteins such as GFP, mEos2 leads to loss of fluorescence. Therefore, the step was taken to avoid resin and find an alternative way to improve resolution in the z-axis.

4.2 Tokuyasu's Cryosectioning Approach

Overcoming limitations with *tomo*STORM required an alternative approach, which avoided resin. The alternative approach should have the benefit of labeling for proteins found in less abundance, have minimum autofluorescence and the sample needs to stay adhered to the coverslip. Therefore, the fixed brain sample was cryoprotected in sucrose and frozen it in liquid nitrogen to cut 1-4 μm thick samples under a temperature of -40° C using a cryo-diamond knife. Avoiding resin in this manner runs the risk of poor z-resolution. This is addressed by using a cylindrical lens in the emission pathway to discriminate the positions of single molecules along the z-axis with a resolution of 50 nm which is comparable to that obtained by physical sectioning the sample. This approach is termed 3D *d*STORM (Huang B. et al., 2008), which has a voxel size of 20 nm x 20 nm x 50 nm.

As a proof of principle, ultra-cryosections thus obtained were labeled for various synaptic proteins found in the calyx of Held such as Bassoon, Piccolo, vGlut1 and Septin 5. Single color 3D *d*STORM was successfully performed on the vGlut1 and bassoon distribution in the calyx. Bassoon at nanoscopic level has a donut shaped topology. In addition, avoiding denaturing resin condition allows one to use photoswitchable fluorescent proteins such as mEos2 for performing single molecule localization experiments. Use of mEos2 on thick samples, however, is problematic because an abundance of mEos2 leads to enormous background fluorescence from

mEos2 present in the out of focus zone. As a result acquiring single molecule imaging of such an mEos2 sample would entail bleaching mEos2 molecules not only present in the focal volume but also those present in the out of focus region. Such a bleaching scheme would leave very few functional mEos2 molecules in the focal volume thereby leading to a highly discontinuous structure (Figure 3.13). There are two possible solutions to overcome the problem of abundance of mEos2 in the sample. One is to use ultrathin cryosections (100 nm - 300 nm) and the other is to reduce the expression levels of mEos2 in the sample. A 300 nm ultrathin section containing mEos2 has been successfully imaged. Membrane features are discontinous, which fits well in comparison to sections obtained from *tomo*STORM method. As active zones span in diameter greater than 300 nm, working with such thin sections for active zone protein labeling leads to a high under sampling of the active zone. Future work needs to focus on reducing the expression levels of mEos2 so that working with thick samples does not become prohibitive.

4.3 Bassoon and Piccolo

Bassoon and Piccolo are two active zone proteins that compose the cytomatrix of the active zone and play a role in the clustering of vesicles (Mukherjee et al. 2009). In the calyx of Held, Bassoon and Piccolo are organized so that there is a significant overlap of the two proteins as confirmed by confocal imaging (Dondzillo A, et al., 2010). As the two proteins are homologous these two proteins perform redundant function at the active zone of clustering the vesicles.

Dual color 3D *d*STORM analysis of the two proteins has revealed a similar overlap of the two proteins not only at the macroscopic level but also at the nanoscopic level. In addition, there exists at the nanoscopic level within a given active zone regions which are occupied by only Bassoon and devoid of Piccolo and vice versa. The functional relevance of this may not be very significant as the two proteins have highly similar function causing a redundancy of their function in the active zone. A multiplexing of antibody staining for additional proteins maybe needed to unravel other molecular partners of Bassoon and Piccolo to explain if there is a difference in the manner in which these two proteins cluster at the nanoscopic level.

4.4 Septin 5 at the Active Zone

The calyx of Held transforms from a microdomain configuration at the onset of hearing to a nanodomain configuration at the age of P17 marking the completion of maturation. Septin 5 a filamentous protein is known to retard vesicle release via its association with SNARE complex. Septin 5 knock-out mice at P7 show phenotype similar to P17. Therefore, lack of Septin 5 pushes the synaptic vesicles closer to the release plate. As a model it is shown that the Septin 5 is found in between the vesicle and the calcium channel functioning to keep the vesicle a certain distance apart from the calcium channels (Yi-Mei Yang et al., 2010). Dual color *d*STORM was performed to see the extent of colocalization between Septin 5 and Piccolo, an active zone marker at the two ages. Dual color *d*STORM showed that at P7 the release face of the active zone is dotted by Septin 5. At P17, however, Septin 5 is increasingly found not at the release face but in the neighbourhood of the release face. In addition 3D dual color *d*STORM of P7 show that Septin 5 dots the release face of the active zone. The implication of this could be that as Septin 5 is probably needed to keep the vesicles and calcium channels apart, Septin 5 could in essence be contacting the calcium channels (Yi-Mei Yang et al., 2010) and in doing so causing them to cluster (Meinrenken et al., 2003).

4.5 Voltage-Gated Calcium Channel

Calcium channel labeling with conventional antibody has been particularly challenging due to molecular crowding of proteins at the active zone (personal communication). Therefore, making use of P/Q type calcium channel tagged to GFP, the calcium channel distribution was probed with GFP nanobodies. Because calcium channels are not as densely clustered as Bassoon, the challenge was to fish the true signal from the unspecifically labeled signal. This is the same problem as that encountered with labeling for less abundant proteins on resin embedded thin sections. The density of the true signal is close to the density of unspecific labeling. Future work should focus on developing smaller tags such as SNAP-tags that could be conjugated to the calcium channels. This way the dye molecule would specifically bind to where the tag is located. Alternatively, voltage-gated channels in general have

been better accessed when approached from the extracellular side of the membrane (Lorincz and Nusser, 2010). Perhaps, tissue-processing approaches need to be developed that retain all the components of a given cell and destroy all neighbouring components that way epitope accessibility from outside a cell is possible.

4.6 Alternative Photoswitching Strategies for Multicolor *d*STORM

Fluorophores such as ATTO 488, TRITC and BODIPY 650 when conjugated to phalloidin show photoswitching capability in PBS. This form of photoswitching is mediated by tryptophan-induced quenching. Conventional way of performing *d*STORM experiments requires the use of reducing buffer environment. As each dye has its unique buffer recipe for photoswitching, there is a need to use a compromise buffer to enable two or more dyes to photoswitch. Such a buffer condition is not ideal for any one dye. As phalloidin-dye conjugates photoswitch in plain PBS, they offer an alternative approach to perform *d*STORM experiments. There is, however, a caveat. Phalloidin probes are limited to doing *d*STORM measurements on actin filaments. Therefore, in order to exploit this form of photoswitching one needs to rationally design probes that mimic phalloidin. This would entail finding a to place a quencher within a distance of 1-2 nm of the dye. Besides the amino acid tryptophan, amino acid histidine and nucleic acid guanosine are also known to quench dyes. Recombinant proteins such as nanobodies carry a histidine tag, which helps in their purification using nickel column. Aptamers are probes, which are purely based on nucleic acids. Therefore, conjugating dyes to nanobodies and aptamers should form a potential avenue for developing quenching-based photoswitching probes.

4.7 Outlook

In this study, we have made an attempt to use the diffraction-unlimited light microscopy (*d*STORM) to look at the distribution of proteins at the calyx of Held synapse. Two tissue-processing approaches have been presented namely *tomo*STORM and Tokuyasu's ultracryotomy. *tomo*STORM can only be used for proteins which exist in great abundance, those that are either over-expressed like membrane bound GFP or endogenous protein as cytochrome C. In a recent approach

thin section light microscopy has been combined with isotopic imaging to characterize the turn over of proteins. The future of *tomo*STORM depends on how efficiently the experimenter can deal with unspecific labeling. On the other hand Tokuyasu's ultracryosections gets away with thin sections as it benefits in z-resolution by using 3D *d*STORM. Tokuyasu's approach is limited to only dual color *d*STORM images. This is due to the fact that in *d*STORM only two dyes can be photoswitched and multiplexing by stripping antibodies is difficult as it requires harsh conditions that may be damaging to the tissue. However, it is superior to *tomo*STORM as it can better characterize the less abundantly present active zone proteins. The future of Tokuyasu's approach depends on implementing new concepts of doing single molecule localization microscopy. One approach called DNA-PAINT has multiplexing capacity and therefore is well suited to be combined with Tokuyasu's method to look at a population of proteins (Jungmann R, et al., 2014).

5 Abbreviations

2D	2 Dimensional
3D	3 Dimensional
AMPA	α-Amino-3-hydroxy-5-methyl-4-isoxazolepropionic acid receptor
ATTO	Name of the dye produced by ATTO-Tec, Germany
AVCN	Anterior Ventral Cochlear Nucleus
AZ	Active Zone
BODIPY	Boron-dipyrromethene
CAZ	Cytomatrix of Active Zone
CNS	Central Nervous System
*d*STORM	*direct* Stochastic Optical Reconstruction Microscopy
EGTA	Ethylene Glycol Tetra Acetic Acid
EM	Electron Microscope
EPSC	Excitatory Post Synaptic Current
GBC	Globular Bushy Cells
GFP	Green Fluorescent Protein
GluA4	Glutamate Receptor type 4
HM20	Lowicryl HM20 is a acrylate-and methacrylate based embedding media
Kon	Rate at which a fluorophore turns ON
Koff	Rate at which a fluorophore turns OFF
memGFP	membrane bound GFP
MCA	Manders Colocalization Analysis
MNTB	Medial Nuclear Trapezoid Body
NMDA	N-Methyl-D-aspartic acid receptor
PALM	Photoactivated Localization Microscopy
PBS	Phosphate Buffer Saline
PFA	Paraformaldehyde
PET	Photon-induced Electron Tranfer

PSD	Post Synaptic Density
PSF	Point Spread Function
SMLM	Single Molecule Localization Microscopy
SNAP-tag	a technology, where a 20 kDa mutant of the DNA repair protein O^6-alkylguanine-DNA alkyltransferase that reacts specifically and rapidly with benzylguanine (BG) derivatives
STED	Stimulated Emission Depletion
SV	Synaptic Vesicle
TRITC	Tetramethylrhodamine B isothiocyanate
tSNARE	trans-soluble *N*-ethylmaleimide-sensitive-factor attachment receptor
*tomo*STORM	Tomographic Stochastic Optical Reconstruction Microscopy
VGCC	Voltage-gated calcium channels
vGlut1	Vesicular glutamate receptor type 1

6 References

Ackley, B.D., Harrington, R.J., Hudson, M.L., Williams, L., Kenyon, C.J., Chisholm, A.D., and Jin, Y. (2005). The two isoforms of the Caenorhabditis elegans leukocyte-common antigen related receptor tyrosine phosphatase PTP-3 function independently in axon guidance and synapse formation. *J. Neurosci.* 25, 7517–7528.

Adam V, Moeyaert B, David CC, Mizuno H, Lelimousin M, Dedecker P, Ando R, Miyawaki A, Michiels J, Engelborghs Y, Hofkens J. 2011. Rational design of photoconvertible and biphotochromic fluorescent proteins for advanced microscopy applications. *Chem Biol* 18:1241–1251.

Altrock WD, tom Dieck S, Sokolov M, Meyer AC, Sigler A, Brakebusch C, Fassler R, Richter K, Boeckers TM, Potschka H, Brandt C, Loscher W, Grimberg D, Dresbach T, Hempelmann A, Hassan H, Balschun D, Frey JU, Brandstatter JH, Garner CC, Rosenmund C, Gundelfinger ED (2003) Functional inactivation of a fraction of excitatory synapses in mice deficient for the active zone protein bassoon. *Neuron* 37:787–800

Barral, Y., and Kinoshita, M. (2008). Structural insights shed light onto septin assemblies and function. *Curr. Opin. Cell Biol*. 20, 12–18.

Basu, J., Shen, N., Dulubova, I., Lu, J., Guan, R., Guryev, O., Grishin, N.V., Rosenmund, C., and Rizo, J. (2005). A minimal domain responsible for Munc13 activity. *Nat. Struct. Mol. Biol*. 12, 1017–1018.

Bates, M., Blosser, T.R. & Zhuang, X. *Phys. Rev. Lett.* **94**, 108101 (2005).

Bates M, Huang B, Dempsey GT, Zhuang X. 2007. Multicolor super-resolution imaging with photoswitchable fluorescent probes. *Science* 317:1749–53

Bates M, Dempsey GT, Chen KH, Zhuang X (2012) Multicolor superresolution fluorescence imaging via multi-parameter fluorophore detection. *Chemphyschem* 13: 99–107.

Beites, C.L., Campbell, K.A., and Trimble, W.S. (2005). The septin Sept5/ CDCrel-1 competes with alpha-SNAP for binding to the SNARE complex. *Biochem. J*. 385, 347–353.

Betzig, E., A. Lewis, A. Harootunian, M. Isaacson, and E. Kratschmer (1986). "Near Field Scanning Optical Microscopy (NSOM)". *Biophys. J.* **49**: 269.

Betzig E, Patterson GH, Sougrat R, Lindwasser OW, Olenych S, Bonifacino JS, Davidson MW, Lippincott-Schwartz J, Hess HF. (2006). Imaging intracellular fluorescent proteins at nanometer resolution. *Science* 313:1642–1645.

Bonazzi M, Spano S, Turacchio G, Cericola C, Valente C, Colanzi A, Kweon HS, Hsu VW, Polishchuck EV, Polishchuck RS, Sallese M, Pulvirenti T, Corda D,

Luini A (2005) CtBP3/BARS drives membrane fission in dynamin-independent transport pathways. *Nat Cell Biol* 7:570–580

Bloom and Aghajanian 1968. Fine structural and cytochemical analysis of the staining of synaptic junctions with phosphotungstic acid. *J Ultrastruct Res.* Mar; 22(5):361-75.

Borst JGG, Soria van Hoeve J 2012. The calyx of held synapse: from model synapse to auditory relay. *Annu Rev Physiol*. 2012; 74:199-224

Borst JGG, Helmchen F, Sakmann B. 1995. Pre- and postsynaptic whole-cell recordings in the medial nucleus of the trapezoid body of the rat. *J. Physiol.* 489:825–40

Brakemann T, Stiel AC, Weber G, Andresen M, Testa I, Grotjohann T, Leutenegger M, Plessmann U, Urlaub H, Eggeling C, Wahl MC, Hell SW, Jakobs S. 2011. A reversibly photoswitchable GFP-like protein with fluorescence excitation decoupled from switching. *Nat Biotechnol* 29:942–947.

Bubeck D, Filman DJ, Kuzmin M, Fuller SD, Hogle JM (2008) Post-imaging fiducial markers aid in the orientation determination of complexes with mixed or unknown symmetry. *J Struct Biol* 162: 480–490.

Bucurenciu I, Kulik A, Schwaller B, Frotscher M, Jonas P (2008) Nanodomain coupling between Ca2+ channels and Ca2+ sensors promotes fast and efficient transmitter release at a cortical GABAergic synapse. *Neuron* 57: 536–545.

Cases-Langhoff C, Voss B, Garner AM, Appeltauer U, Takei K, Kindler S, Veh RW, De Camilli P, Gundelfinger ED, Garner CC (1996) Piccolo, a novel 420 kDa protein associated with the presynaptic cytomatrix. *Eur J Cell Biol* 69:214–223

Castillo, P.E., Janz, R., Südhof, T.C., Tzounopoulos, T., Malenka, R.C., and Nicoll, R.A. (1997). Rab3A is essential for mossy fibre long-term potentiation in the hippocampus. *Nature* 388, 590–593.

Chao J, Ram S, Ward ES, Ober RJ (2009) A comparative study of high resolution microscopy imaging modalities using a three-dimensional resolution measure. *Opt Express* 17: 24377–24402.

Chen H, Ahsan SS, Santiago-Berrios MB, Abruna HD, Webb WW. 2010. Mechanisms of quenching of Alexa fluorophores by natural amino acids. *J Am Chem Soc* 132:7244–7245.

Choquet, D. Fast AMPAR trafficking for a high-frequency synaptic transmission. *Eur. J. Neurosci.* 32, 250–260 (2010).

Christoph J. Meinrenken, J. Gerard G. Borst and Bert Sakmann (2003) Local routes revisited: the space and time dependence of the Ca2+ signal for phasic transmitter release at the rat calyx of Held. *J. Physiology*

Cingolani LA, Goda Y. (2008) Actin in action: The interplay between the actin cytoskeleton and synaptic efficacy. *Nat Rev Neurosci* 9: 344–356.

Dai, Y., Taru, H., Deken, S.L., Grill, B., Ackley, B., Nonet, M.L., and Jin, Y. (2006). SYD-2 Liprin-a organizes presynaptic active zone formation through ELKS. *Nat. Neurosci*. 9, 1479–1487.

Dani, A., Huang, B., Bergan, J., Dulac, C. & Zhuang, X. (2010).Superresolution imaging of chemical synapses in the brain. *Neuron* 68, 843–856

Davydova D, Marini C, King C, Klueva J, Bischof F, Romorini S, Montenegro-Venegas C, Heine M, Schneider R, Schröder MS, Altrock WD, Henneberger C, Rusakov DA, Gundelfinger ED, Fejtova A.Bassoon specifically controls presynaptic P/Q-type Ca(2+) channels via RIM-binding protein. *Neuron*. 2014 Apr 2;82(1):181-94. doi: 10.1016/j.neuron.2014.02.012.

Dempsey GT, Bates M, Kowtoniuk WE, Liu DR, Tsien RY, Zhuang X. (2009). Photoswitching mechanism of cyanine dyes. *J Am Chem Soc* 131:18192–18193.

Dempsey GT, Vaughan JC, Chen KH, Bates M, Zhuang X. 2011. Evaluation of fluorophores for optimal performance in localization-based super-resolution imaging. *Nature Methods* 1027(8).

Deng, L., Kaeser, P.S., Xu, W., and Südhof, T.C. (2011). RIM proteins activate vesicle priming by reversing autoinhibitory homodimerization of Munc13. *Neuron* 69, 317–331.

Dick O, tom Dieck S, Altrock WD, Ammermuller J, Weiler R, Garner CC, Gundelfinger ED, Brandstatter JH (2003) The presynaptic active zone protein bassoon is essential for photoreceptor ribbon synapse formation in the retina. *Neuron* 37:775–786

Dondzillo A, Sätzler K, Horstmann H, Altrock WD, Gundelfinger ED, et al. (2010) Targeted three-dimensional immunohistochemistry reveals localization of presynaptic proteins Bassoon and Piccolo in the rat calyx of Held before and after the onset of hearing. *J Comp Neurol* 518: 1008–1029.

Doose S, Neuweiler H, Sauer M. (2005). A close look at fluorescence quenching of organic dyes by tryptophan. *Chemphyschemistry* 6: 2277–2285.

Dresbach T, Hempelmann A, Spilker C, Tom Dieck S, Altrock WD, Zuschratter W, Garner CC, Gundelfinger ED. 2003. Functional regions of the presynaptic cytomatrix protein bassoon: Significance for synaptic targeting and cytomatrix anchoring. *Mol Cell Neurosci* 23:279–291.

Dulubova I, Yamaguchi T, Min SW, Gao Y, Südhof TC, Rizo J. 2002. How Tlg2p/syntaxin16 “snares” Vps45. *EMBO J* 21: 3620–3631.

Dulubova, I., Lou, X., Lu, J., Huryeva, I., Alam, A., Schneggenburger, R., Südhof, T.C., and Rizo, J. (2005). A Munc13/RIM/Rab3 tripartite complex: from priming to plasticity? *EMBO J*. 24, 2839–2850.

Endesfelder U, Malkusch S, Flottmann B, Mondry J, Liguzinski P, Verveer PJ, Heilemann M. 2011. Chemically induced photoswitching of fluorescent probes – A general concept for super-resolution microscopy. *Molecules* 16:3106–3118.

Frank T, Rutherford MA, Strenzke N, Neef A, Pangršič T, Khimich D, Fejtova A, Gundelfinger ED, Liberman MC, Harke B, Bryan KE, Lee A, Egner A, Riedel D, Moser T. (2010). Bassoon and the synaptic ribbon organize Ca2+ channels and vesicles to add release sites and promote refilling. *Neuron* 68, 724–738

Fedchyshyn, M.J., and Wang, L.Y. (2005). Developmental transformation of the release modality at the calyx of Held synapse. *J. Neurosci*. 25, 4131–4140.

Fenster SD, Chung WJ, Zhai R, Cases-Langhoff C, Voss B, Garner AM, Kaempf U, Kindler S, Gundelfinger ED, Garner CC (2000) Piccolo, a presynaptic zinc finger protein structurally related to Bassoon. *Neuron* 25:203–214

Fenster SD, Kessels MM, Qualmann B, Chung WJ, Nash J, Gundelfinger ED, Garner CC (2003) Interactions between Piccolo and the actin/dynamin-binding protein Abp1 link vesicle endocytosis to presynaptic active zones. *J Biol Chem* 278:20268–20277

Fernández-Busnadiego R, Asano S, Oprisoreanu AM, Sakata E, Doengi M, Kochovski Z, Zürner M, Stein V, Schoch S, Baumeister W, Lucić V. (2013) Cryo-electron tomography reveals a critical role of RIM1α in synaptic vesicle tethering. *J Cell Biol*. 2013 May 27; 201(5):725-40

Forsythe ID. 1994. Direct patch recording from identified presynaptic terminals mediating glutamatergic EPSCs in the rat CNS, in vitro. *J. Physiol.* 479:381–87

Fouquet, W. *et al.* (2009). Maturation of active zone assembly by *Drosophila* Bruchpilot. *J. Cell Biol.* 186, 129–145

Fujimoto K, Shibasaki T, Yokoi N, Kashima Y, Matsumoto M, Sasaki T, Tajima N, Iwanaga T, Seino S (2002) Piccolo, a Ca2+ sensor in pancreatic beta-cells. Involvement of cAMP-GEFII. Rim2. Piccolo complex in cAMP-dependent exocytosis. *J Biol Chem* 277:50497–50502

Furstenberg A, Heilemann M. 2013. Single-molecule localization microscopy – Near-molecular spatial resolution in light microscopy with photoswitchable fluorophores. *Phys Chem Chem Phys* 15: 14919–14930.

Garcia J, Gerber SH, Sugita S, Sudhof TC, Rizo J (2004) A conformational switch in the Piccolo C2A domain regulated by alternative splicing. *Nat Struct Mol Biol* 11:45–53

Gelles, J., Schnapp, B.J. & Sheetz, M.P. (1988) Tracking kinesin-driven movements with nanometre-scale precision. *Nature* 331, 450–453.

Gracheva, E.O., Hadwiger, G., Nonet, M.L., and Richmond, J.E. (2008). Direct interactions between C. elegans RAB-3 and Rim provide a mechanism to target vesicles to the presynaptic density. *Neurosci. Lett*. 444, 137–142.

Groh A, de Kock CPJ, Wimmer VC, Sakmann B, Kuner T. (2008). Driver or coincidence detector: modal switch of a corticothalamic giant synapse controlled by spontaneous activity and short-term depression. *J Neurosci*. 28:9652–9663.

Grotjohann T, Testa I, leutenegger M, Bock H, Urban NT, Lavoie-Cardinal F, Willig KI, Eggeling C, Jakobs S, Hell SW. 2011. Diffraction-unlimited all-optical imaging and writing with a photochromic GFP. *Nature* 478:204–208.

Guinan JJ Jr, LiRY-S. 1990. Signal processing in brainstem auditory neuronswhich receive giant endings (calyces of Held) in the medial nucleus of the trapezoid body of the cat. *Hear. Res.* 49:321–34

Gustafsson MG. 2000. Surpassing the lateral resolution limit by a factor of two using structured illumination microscopy. *J Microsc* 198:82–87.

Hallermann S, Fejtova A, Schmidt H, Weyhersmüller A, Silver RA, Gundelfinger ED, Eilers J. Bassoon speeds vesicle reloading at a central excitatory synapse. *Neuron*. 2010 Nov 18; 68(4):710-23. doi: 10.1016/j.neuron.2010.10.026.

Han, Y., Kaeser, P.S., Südhof, T.C., and Schneggenburger, R. (2011). RIM determines Ca2+ channel density and vesicle docking at the presynaptic active zone. *Neuron* 69, 304–316.

Harris KM, Perry E, Bourne J, Feinberg M, Ostroff L, et al. (2006) Uniform serial sectioning for transmission electron microscopy. *J Neurosci* 26:12101–12103.

Hata Y, Slaughter CA, Südhof TC. 1993. Synaptic vesicle fusion complex contains unc-18 homologue bound to syntaxin. *Nature* 366: 347–351.

Hayashi T, McMahon H, Yamasaki S, Binz T, Hata Y, Südhof TC, Niemann H. 1994. Synaptic vesicle membrane fusion complex: Action of clostridial neurotoxins on assembly. *EMBO J* 13: 5051–5061.

Heilemann M, Margeat E, Kasper R, Sauer M, Tinnefeld P (2005) Carbocyanine dyes as efficient reversible single-molecule optical switch. *Journal of the American Chemical Society* 127: 3801–3806.

Heilemann M, van de Linde S, Schuttpelz M, Kasper R, Seefeldt B, et al. (2008) Subdiffraction-resolution fluorescence imaging with conventional fluorescent probes. *Angew Chem Int Ed Engl* 47: 6172–6176.

Heilemann M (2010) Fluorescence microscopy beyond the diffraction limit. *J Biotechnol* 149: 243–251.

Hell SW (2009) Microscopy and its focal switch. *Nat Methods* 6: 24–32.

Hell SW (2007). Far-Field Optical Nanoscopy. *Science*

Hell SW, Wichmann J. 1994. Breaking the diffraction resolution limit by stimulated emission: Stimulated-emission-depletion fluorescence microscopy. *Opt Lett* 19:780–782.

Hell SW, M. Kroug, *Appl. Phys. B* 60, 495 (1995).

Hess ST, Girirajan TP, Mason MD. 2006. Ultra-high resolution imaging by fluorescence photoactivation localization microscopy. *Biophys J* 91:4258–4272.

Hidalgo Carcedo C, Bonazzi M, Spano S, Turacchio G, Colanzi A, Luini A, Corda D (2004) Mitotic Golgi partitioning is driven by the membrane-fissioning protein CtBP3/BARS. *Science* 305:93–96

Hirokawa, N., Sobue, K., Kanda, K., Harada, A., and Yorifuji, H. (1989). The cytoskeletal architecture of the presynaptic terminal and molecular structure of synapsin 1. *J. Cell Biol.* 108, 111–126.

Huang B, Jones SA, Brandenburg B, Zhuang X (2008) Whole-cell 3D STORM reveals interactions between cellular structures with nanometer-scale resolution. *Nat Methods* 5: 1047–1052.

Huang, B., Babcock, H. & Zhuang, X. (2010). Breaking the diffraction barrier: super-resolution imaging of cells. *Cell* 143, 1047–1058.

Huang, Y.Y., Zakharenko, S.S., Schoch, S., Kaeser, P.S., Janz, R., Südhof, T.C., Siegelbaum, S.A., and Kandel, E.R. (2005). Genetic evidence for a protein-kinase-A-mediated presynaptic component in NMDA-receptordependent forms of long-term synaptic potentiation. *Proc. Natl. Acad. Sci. USA* 102, 9365–9370.

Ihara, M., Tomimoto, H., Kitayama, H., Morioka, Y., Akiguchi, I., Shibasaki, H., Noda, M., and Kinoshita, M. (2003). Association of the cytoskeletal GTP binding protein Sept4/H5 with cytoplasmic inclusions found in Parkinson's disease and other synucleinopathies. *J. Biol. Chem*. 278, 24095–24102.

Jean-Baptiste M, Morest DK. (1975). Transneuronal changes of synaptic endings and nuclear chromatin in the trapezoid body following cochlear ablations in cats. *J. Comp. Neurol.* 162:111–34

Jungmann R, Avendaño MS, Woehrstein JB, Dai M, Shih WM, Yin P. (2014) Multiplexed 3D cellular super-resolution imaging with DNA-PAINT and Exchange-PAINT. *Nat Methods.* 2014 Mar;11(3):313-8.

Kaeser, P.S., Deng, L., Wang, Y., Dulubova, I., Liu, X., Rizo, J., and Südhof, T.C. (2011). RIM proteins tether Ca2+ channels to presynaptic active zones via a direct PDZ-domain interaction. *Cell* 144, 282–295.

Kamiyama D, Huang B. 2012. Development in the STORM. *Dev Cell* 23:1103–1110.

Klehs K, Christoph Spahn, Ulrike Endesfelder, Steven F. Lee, Alexandre Fürstenberg, and Mike Heilemann 2014. Increasing the Brightness of Cyanine Fluorophores for Single-Molecule and Superresolution Imaging. *ChemPhysChem*

Kim S, Ko J, Shin H, Lee JR, Lim C, Han JH, Altrock WD, Garner CC, Gundelfinger ED, Premont RT, Kaang BK, Kim E (2003) The GIT family of proteins forms multimers and associates with the presynaptic cytomatrix protein Piccolo. *J Biol Chem* 278:6291–6300

Keppler A, Gendreizig S, Gronemeyer T, Pick H, Vogel H, et al. (2003) A general method for the covalent labeling of fusion proteins with small molecules in vivo. *Nat Biotechnol* 21: 86–89.

Khimich D, Nouvian R, Pujol R, tom Dieck S, Egner A, Gundelfinger ED, Moser T (2005) Hair cell synaptic ribbons are essential for synchronous auditory signalling. *Nature* 434:889–894

Koushika, S.P., Richmond, J.E., Hadwiger, G., Weimer, R.M., Jorgensen, E.M., and Nonet, M.L. (2001). A post-docking role for active zone protein Rim. *Nat. Neurosci.* 4, 997–1005.

Lando D, Endesfelder U, Berger H, Subramanian L, Dunne PD, Mccoll J, Klenerman D, Carr AM, Sauer M, Allshire RC, Heilemann M, Laue ED. 2012. Quantitative single-molecule microscopy reveals that CENP-A(Cnp1) deposition occurs during G2 in fission yeast. *Open Biol* 2:120078.

Lakadamyali M, Babcock H, Bates M, Zhuang X, Lichtman J (2012) 3D multicolor super-resolution imaging offers improved accuracy in neuron tracing. *PLoS One* 7: e30826.

Link E, Edelmann L, Chow JH, Binz T, Yamasaki S, Eisel U, Baumert M, Südhof TC, Niemann H, Jahn R. 1992. Tetanus toxin action: Inhibition of neurotransmitter release linked to synaptobrevin poteolysis. *Biochem Biophys Res Commun* 189: 1017–1023.

Lu, J., Machius, M., Dulubova, I., Dai, H., Südhof, T.C., Tomchick, D.R., and Rizo, J. (2006). Structural basis for a Munc13-1 homodimer to Munc13-1/ RIM heterodimer switch. *PLoS Biol.* 4, e192.

Lu-Yang Wang (2007) Synapses: Coupling of Presynaptic Voltage-gated Ca^{2+} Channels to Vesicular Release of Neurotransmitter

Medalia O, Weber I, Frangakis AS, Nicastro D, Gerisch G, Baumeister W. Macromolecular architecture in eukaryotic cells visualized by cryoelectron tomography. *Science.* 2002 Nov 8; 298 (5596):1209-13.

Micheva KD, Smith SJ (2007) Array tomography: a new tool for imaging the molecular architecture and ultrastructure of neural circuits. *Neuron* 55: 25–36.

Malecki M, Small JV (1987) Immunocytochemistry of Contractile and Cytoskeletal Proteins in Smooth-Muscle – Lowicryl, Lr White, and Polyvinylalcohol Compared. *Protoplasma* 139: 160–169.

Mark MD, Maejima T, Kuckelsberg D, Yoo JW, Hyde RA, Shah V, Gutierrez D, Moreno RL, Kruse W, Noebels JL, Herlitze S (2011) Delayed postnatal loss of P/Q-type calcium channels recapitulates the absence epilepsy, dyskinesia, and ataxia phenotypes of genomic Cacna1a mutations. *J Neurosci.* 2011 Mar 16; 31(11):4311-26

McDonald KL. (2009) A review of high-pressure freezing preparation techniques for correlative light and electron microscopy of the same cells and tissues. *J Microsc.* 2009 Sep;235(3):273-81.

McKinney SA, Murphy CS, Hazelwood KL, Davidson MW, Looger LL. (2009). A bright and photostable photoconvertible fluorescent protein. *Nature Methods.* 2009 Feb;6(2):131-3.

Meinrenken CJ, Borst JG, Sakmann B (2002) Calcium secretion coupling at calyx of held governed by nonuniform channel-vesicle topography. *J Neurosci* 22: 1648–1667.

Micheva KD, Busse B, Weiler NC, O'Rourke N, Smith SJ (2010) Single-synapse analysis of a diverse synapse population: proteomic imaging methods and markers. *Neuron* 68: 639–653.

Mukherjee K, Yang X, Gerber SH, Kwon HB, Ho A, Castillo PE, Liu X, Südhof TC. (2010) Piccolo and bassoon maintain synaptic vesicle clustering without directly participating in vesicle exocytosis. *Proc Natl Acad Sci U S A.* Apr 6;107(14):6504-9.

Muranyi W, Malkusch S, Müller B, Heilemann M, Kräusslich HG. (2013) Super-resolution microscopy reveals specific recruitment of HIV-1 envelope proteins to viral assembly sites dependent on the envelope C-terminal tail. *PLoS Pathog.* 2013 Feb;9(2):e1003198.

Muyldermans, S. (2013). "Nanobodies: Natural Single-Domain Antibodies". *Annual Review of Biochemistry* **82**: 775–797.

Nanguneri S., Flottmann B., Horstmann H., Heilemann M., Kuner T. (2012) Three-Dimensional, Tomographic Super-Resolution Fluorescence Imaging of

Serially Sectioned Thick Samples. *PLoS ONE*

Nanguneri S., Flottmann B., Herrmannsdörfer F., Kuner T., and Heilemann M. (2014). Single-Molecule Super-Resolution Imaging by Tryptophan-Quenching-Induced Photoswitching of Phalloidin-Fluorophore Conjugates

Nägerl, U.V., Willig, K.I., Hein, B., Hell, S.W. & Bonhoeffer, T. (2008).Live-cell imaging of dendritic spines by STED microscopy. *Proc. Natl. Acad. Sci. USA* 105, 18982–18987

Neuweiler H, Johnson CM, Fersht AR. 2009. Direct observation of ultrafast folding and denatured state dynamics in single protein molecules. *Proc Natl Acad Sci U S A* 106:18569–18574.

Opazo F, Matthew L, Michelle B, Christina S, Claudia G, Teja W G, Andrew D E and S O Rizzoli 2012. Aptamers as potential tools for superresolution microscopy. *Nature Methods*

Pavani SR, Thompson MA, Biteen JS, Lord SJ, Liu N, et al. (2009) Three dimensional, single-molecule fluorescence imaging beyond the diffraction limit by using a double-helix point spread function. *Proc Natl Acad Sci U S A* 106: 2995–2999.

Phillips GR, Huang JK, Wang Y, Tanaka H, Shapiro L, Zhang W, Shan WS, Arndt K, Frank M, Gordon RE, Gawinowicz MA, Zhao Y, Colman DR (2001) The presynaptic particle web: ultrastructure, composition, dissolution, and reconstitution. *Neuron* 32:63–77

Punge A, Rizzoli SO, Jahn R, Wildanger JD, Meyer L, et al. (2008) 3D reconstruction of high-resolution STED microscope images. *Microscopy Research and Technique* 71: 644–650.

Ram S, Prabhat P, Ward ES, Ober RJ (2009) Improved single particle localization accuracy with dual objective multifocal plane microscopy. *Opt Express* 17: 6881–6898.

Ries, J.; Kaplan, C.; Platonova, E.; Eghlidi, H.; Ewers, H. (2012). "A simple, versatile method for GFP-based super-resolution microscopy via nanobodies". *Nature Methods* **9** (6): 582–584.

Rothbauer U, Zolghadr K, Tillib S, Nowak D, Schermelleh L, Gahl A, Backmann N, Conrath K, Muyldermans S, Cardoso MC, Leonhardt H. Targeting and tracing antigens in live cells with fluorescent nanobodies. *Nat Methods*. (2006) Nov;3(11):887-9.

Rust MJ, Bates M, Zhuang X. (2006). Sub-diffraction-limit imaging by stochastic optical reconstruction microscopy (STORM). *Nat Methods* 3:793–795.

Sauer M. (2013). Localization microscopy coming of age: from concepts to biological impact. *J Cell Sci.*;126 (Pt 16):3505-13. doi: 10.1242/jcs.123612. Review.

Sätzler K, Sohl LF, Bollmann JH, Borst JG, Frotscher M, et al. (2002) Three-dimensional reconstruction of a calyx of Held and its postsynaptic principal neuron in the medial nucleus of the trapezoid body. *J Neurosci* 22: 10567–10579.

Schermelleh L, Heintzmann R, Leonhardt H (2010) A guide to super-resolution fluorescence microscopy. *J Cell Biol* 190: 165–175.

Schneggenburger R, Forsythe ID (2006) The calyx of Held. *Cell Tissue Res* 326: 311–337.

Schwenger DB, Kuner T (2010) Acute genetic perturbation of exocyst function in the rat calyx of Held impedes structural maturation, but spares synaptic transmission. *Eur J Neurosci* 32: 974–984.

Schiavo G, Benfenati F, Poulain B, Rossetto O, Polverino de Laureto P, DasGupta BR, Montecucco C. 1992. Tetanus and botulinum-B neurotoxins block neurotransmitter release by proteolytic cleavage of synaptobrevin. *Nature* 359: 832–835.

Schmitz F, Konigstorfer A, Sudhof TC (2000) RIBEYE, a component of synaptic ribbons: a protein's journey through evolution provides insight into synaptic ribbon function. *Neuron* 28:857–872

Schmidt R, Wurm CA, Punge A, Egner A, Jakobs S, et al. (2009) Mitochondrial cristae revealed with focused light. *Nano Lett* 9: 2508–2510.

Schoch, S., Castillo, P.E., Jo, T., Mukherjee, K., Geppert, M., Wang, Y., Schmitz, F., Malenka, R.C., and Südhof, T.C. (2002). RIM1a forms a protein scaffold for regulating neurotransmitter release at the active zone. *Nature* 415, 321–326.

Schoch S, Gundelfinger ED. Molecular organization of the presynaptic active zone. *Cell Tissue Res.* (2006) Nov;326(2):379-91. Epub 2006 Jul 25. Review.

Shtengel G, Galbraith JA, Galbraith CG, Lippincott-Schwartz J, Gillette JM, et al. (2009) Interferometric fluorescent super-resolution microscopy resolves 3D cellular ultrastructure. *Proc Natl Acad Sci U S A* 106: 3125–3130.

Schwenger DB, Kuner T. (2010) Acute genetic perturbation of exocyst function in the rat calyx of Held impedes structural maturation, but spares synaptic transmission. *Eur J Neurosci.* Sep;32(6):974-84.

Söllner T, Bennett MK, Whiteheart SW, Scheller RH, Rothman JE. (1993). A protein assembly-disassembly pathway in vitro thatmay correspond to sequential steps of synaptic vesicle docking, activation, and fusion. *Cell* 75: 409–418.

Stevens, D.R., Wu, Z.X., Matti, U., Junge, H.J., Schirra, C., Becherer, U., Wojcik, S.M., Brose, N., and Rettig, J. (2005). Identification of the minimal protein domain required for priming activity of Munc13-1. *Curr. Biol.* 15, 2243–2248.

Suzuki, G., Harper, K.M., Hiramoto, T., Sawamura, T., Lee, M., Kang, G., Tanigaki, K., Buell, M., Geyer, M.A., Trimble, W.S., et al. (2009). Sept5 deficiency exerts pleiotropic influence on affective behaviors and cognitive functions in mice. *Hum. Mol. Genet.* 18, 1652–1660.

Südhof, T. C. and Rizo, J. (2011). Synaptic Vesicle Exocytosis. *CSH*

Südhof TC. 2012. The presynaptic active zone. *Neuron* 75:11–25.

Takao-Rikitsu E, Mochida S, Inoue E, Deguchi-Tawarada M, Inoue M, Ohtsuka T, Takai Y (2004) Physical and functional interaction of the active zone proteins, CAST, RIM1, and Bassoon, in neurotransmitter release. *J Cell Biol* 164:30311

Taschenberger H, Leao RM, Rowland KC, Spirou GA, von Gersdorff H (2002) Optimizing synaptic architecture and efficiency for high-frequency transmission. *Neuron* 36: 1127–1143.

Thompson AM, Schofield BR. 2000. Afferent projections of the superior olivary complex. *Microsc. Res. Tech.* 51:330–54

Thompson AM, Lew MD, Moerner WE. 2012. Extending microscopic resolution with single-molecule imaging and active control. *Annu Rev Biophys* 41:321–342.

Tokuyasu KT, Singer SJ. 1976 Improved procedures for immunoferritin labeling of ultrathin frozen sections. *J Cell Biol.*;71(3):894-906.

tom Dieck, S., Sanmartı´-Vila, L., Langnaese, K., Richter, K., Kindler, S., Soyke, A., Wex, H., Smalla, K.H., Kämpf, U., Fränzer, J.T., et al. (1998). Bassoon, a novel zinc-finger CAG/glutamine-repeat protein selectively localized at the active zone of presynaptic nerve terminals. *J. Cell Biol.* 142, 499–509.

tom Dieck S, Altrock WD, Kessels MM, Qualmann B, Regus H, Brauner D, Fejtova A, Bracko O, Gundelfinger ED, Brandstatter JH (2005) Molecular dissection of the photoreceptor ribbon synapse: physical interaction of Bassoon and RIBEYE is essential for the assembly of the ribbon complex. *J Cell Biol* 168:825–836

Tse FW, Tse A, Hille B, Horstmann H, Almers W (1997) Local Ca2+ release from internal stores controls exocytosis in pituitary gonadotrophs. *Neuron* 18:121–132.

Urban, N.T., Willig, K.I., Hell, S.W. & Nagerl, U.V. (2011). STED nanoscopy of actin dynamics in synapses deep inside living brain slices. *Biophys. J.* 101, 1277– 1284.

Vaiana AC, Neuweiler H, Schulz A, Wolfrum J, Sauer M, Smith JC. 2003. Fluorescence quenching of dyes by tryptophan: Interactions at atomic detail from combination of experiment and computer simulation. *J Am Chem Soc* 125:14564–14572.

van de Linde S, Wolter S, Heilemann M, Sauer M. 2010. The effect of photoswitching kinetics and labeling densities on super-resolution fluorescence imaging. *J Biotechnol* 149:260–266

van de Linde S, Krstic I, Prisner T, Doose S, Heilemann M, Sauer M. 2011a. Photoinduced formation of reversible dye radicals and their impact on super-resolution imaging. *Photochem Photobiol Sci* 10: 499–506.

van de Linde S, Loschberger A, Klein T, Heidbreder M, Wolter S, Heilemann M, Sauer M. 2011b. Direct stochastic optical reconstruction microscopy with standard fluorescent probes. *Nat Protoc* 6:991–1009.

van den Bogaart G, Meyenberg K, Risselada HJ, Amin H, Willig KI, Hubrich BE, Dier M, Hell SW, Grubmüller H, Diederichsen U, Jahn R. Membrane protein sequestering by ionic protein-lipid interactions. (2011) *Nature* 479, 552–555

von Gersdorff H, Borst JG (2002) Short-term plasticity at the calyx of held. *Nat Rev Neurosci* 3: 53–64.

Yamaguchi T, Dulubova I, Min SW, Chen X, Rizo J, Südhof TC. 2002. Sly1 binds to Golgi and ER syntaxins via a conserved N-terminal peptide motif. *Developmental Cell* 2:295–305.

Yi-Mei Yang, Michael J. Fedchyshyn, Giovanbattista Grande, Jamila Aitoubah, Christopher W. Tsang, Hong Xie, Cameron A. Ackerley, William S. Trimble, and Lu-Yang Wang (2010). Septins Regulate Developmental Switching from Microdomain to Nanodomain Coupling of Ca^{2+} Influx to Neurotransmitter Release at a Central Synapse

Yildiz A, Forkey JN, McKinney SA, Ha T, Goldman YE, Selvin PR. Myosin V walks hand-over-hand: single fluorophore imaging with 1.5-nm localization. *Science*, 2061–2065 (2003).

Wagh, D.A., Rasse, T.M., Asan, E., Hofbauer, A., Schwenkert, I., Dürrbeck, H., Buchner, S., Dabauvalle, M.C., Schmidt, M., Qin, G., et al. (2006). Bruchpilot, a protein with homology to ELKS/CAST, is required for structural integrity and function of synaptic active zones in Drosophila. *Neuron* 49, 833–844.

Wang X, Kibschull M, Laue MM, Lichte B, Petrasch-Parwez E, Kilimann MW (1999) Aczonin, a 550-kD putative scaffolding protein of presynaptic active zones, shares homology regions with Rim and Bassoon and binds profilin. *J Cell Biol* 147:151–162

Watanabe S, Punge A, Hollopeter G, Willig KI, Hobson RJ, et al. (2011) Protein localization in electron micrographs using fluorescence nanoscopy. *Nat Methods* 8: 80–84.

Waites CL, Leal-Ortiz SA, Okerlund N, Dalke H, Fejtova A, Altrock WD, Gundelfinger ED, Garner CC. Bassoon and Piccolo maintain synapse integrity

by regulating protein ubiquitination and degradation. *EMBO J.* 2013 Apr 3;32(7):954-69. doi: 10.1038/emboj.2013.27.

Wilson DW,Wilcox CA, Flynn GC, Chen E, Kuang WJ,Henzel WJ, Block MR, Ullrich A, Rothman JE. 1989. A fusion protein required for vesicle-mediated transport in both mammalian cells and yeast. *Nature* 339: 355–359.

Wimmer VC, Nevian T, Kuner T (2004) Targeted in vivo expression of proteins in the calyx of Held. *Pflugers Arch* 449: 319–333.

Weirich, C.S., Erzberger, J.P., and Barral, Y. (2008). The septin family of GTPases: architecture and dynamics. *Nat. Rev. Mol. Cell Biol.* 9, 478–489.

Wolter S, Schuttpelz M, Tscherepanow M, S VDL, Heilemann M, et al. (2010) Real-time computation of subdiffraction-resolution fluorescence images. *J Microsc* 237: 12–22.

Xu, K., Babcock, H.P. & Zhuang, X.(2012). Dual-objective STORM reveals three dimensional filament organization in the actin cytoskeleton. *Nat. Methods* 9, 185–188

Xu K, Zhong G, Zhuang X. 2013. Actin, spectrin, and associated proteins form a periodic cytoskeletal structure in axons. *Science* 339:452–456.

Zhen, M., and Jin, Y. (1999). The liprin protein SYD-2 regulates the differentiation of presynaptic termini in C. elegans. *Nature* 401, 371–375.

7 Own Publications

Nanguneri S., Flottmann B., Horstmann H., Heilemann M., Kuner T. (2012) Three-Dimensional, Tomographic Super-Resolution Fluorescence Imaging of Serially Sectioned Thick Samples. *PLoS ONE,* 7(5): e38098. doi: 10.1371/journal.pone.0038098.

Nanguneri S., Flottmann B., Herrmannsdörfer F., Kuner T., and Heilemann M. (2014). Single-Molecule Super-Resolution Imaging by Tryptophan-Quenching-Induced Photoswitching of Phalloidin-Fluorophore Conjugates. *Microscopy Research and Technique,* 510-6. doi: 10.1002/jemt.22349.

8 Appendix

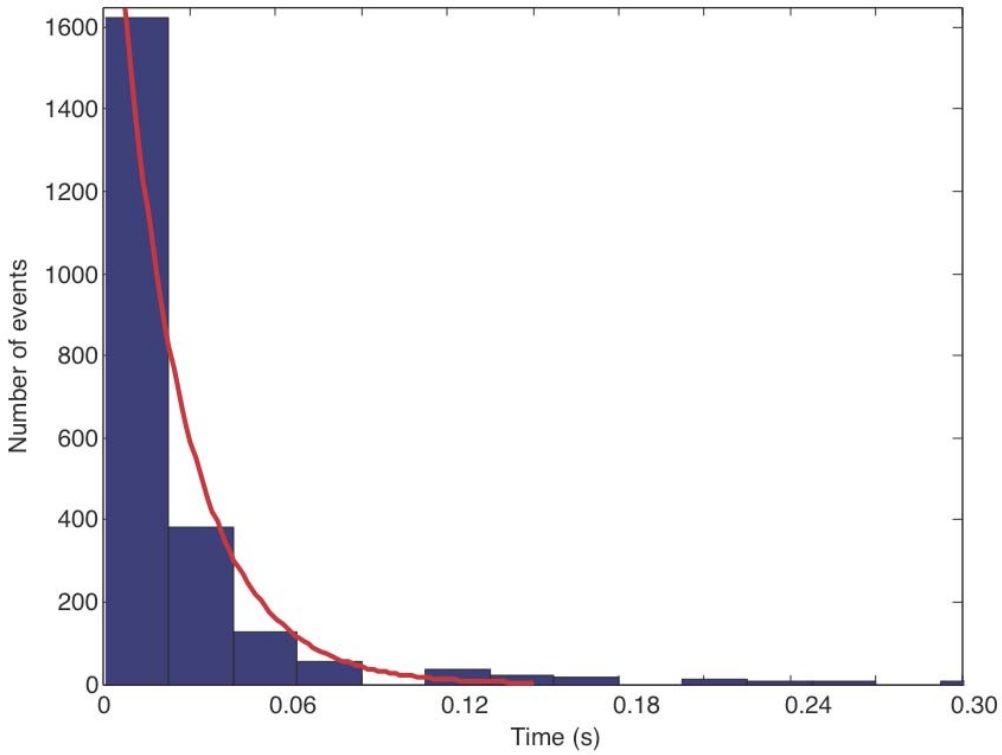

Figure A1: Estimation of time phalloidin-ATTO 488 was in 'on' state. The histogram depicts the distribution of time intervals during which the fluorophore is in 'on' state per blinking event. The x-axis stands for time in seconds and the y-axis stands for the occurrences of 'on' state intervals. It has been fitted to a mono-exponential function of the form $y=\exp(-x/\tau)$ to derive the characteristic rate constant $k_{off} = 1/\tau_{on} = 61.8\ s^{-1}$.

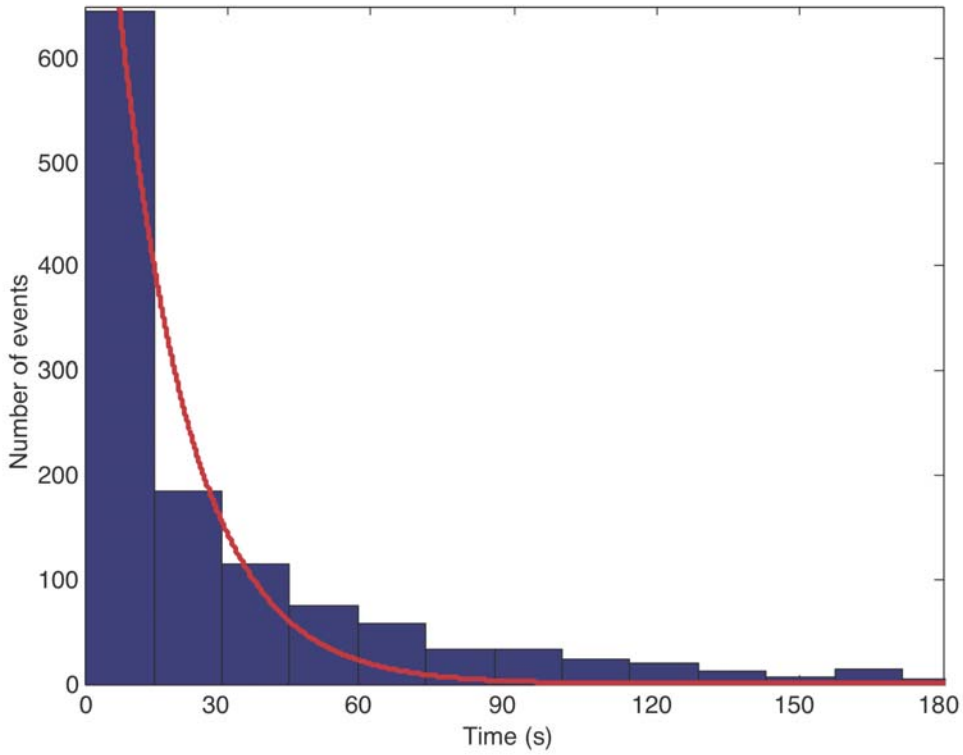

Figure A2: Estimation of time phalloidin-ATTO 488 was in 'off' state. The histogram depicts the distribution of time intervals during which the fluorophore is in 'off' state between two blinking events. The x-axis stands for time in seconds and the y-axis stands for the occurrences of 'off' state intervals. It has been fitted to a mono-exponential function of the form $y=\exp(-x/\tau)$ to derive the characteristic rate constant $k_{on} = 1/\tau_{off} = 0.07\ s^{-1}$.

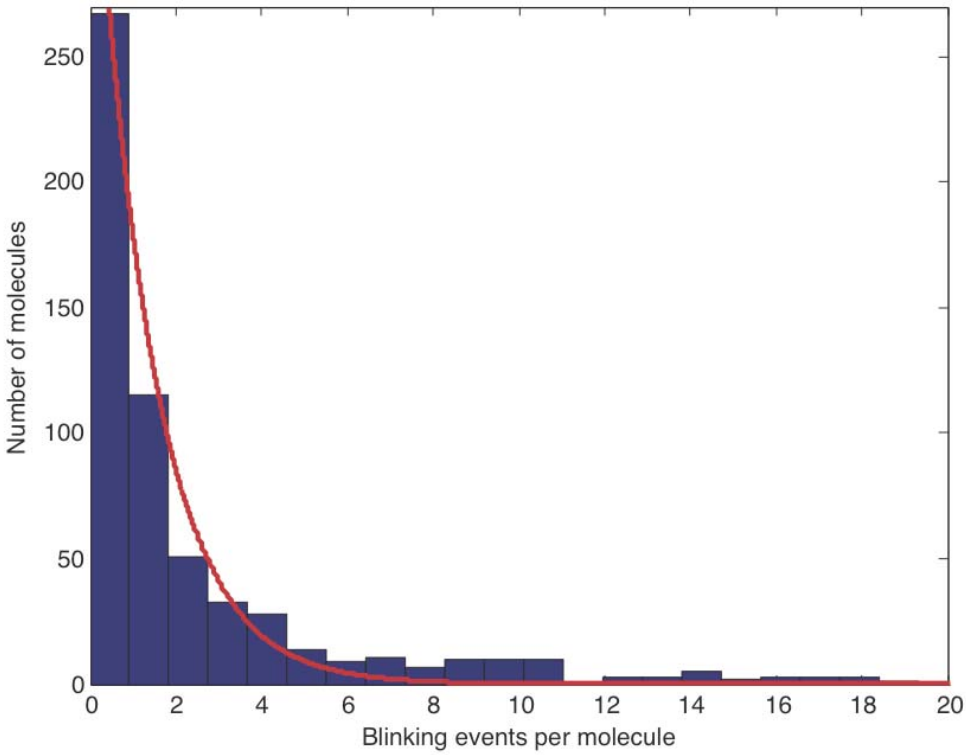

Figure A3: Histogram of phalloidin-ATTO 488 molecules undergoing blinking. The x-axis stands for the number of blinking events per molecule and the y-axis stands for the number of molecules. The experiment lasted 10000 frames with frame duration of 30 ms. The curve was fitted to a mono-exponential $y=\exp(-x/\tau)$ and gives a characteristic $\tau = 1.21$ blinking events per molecule.

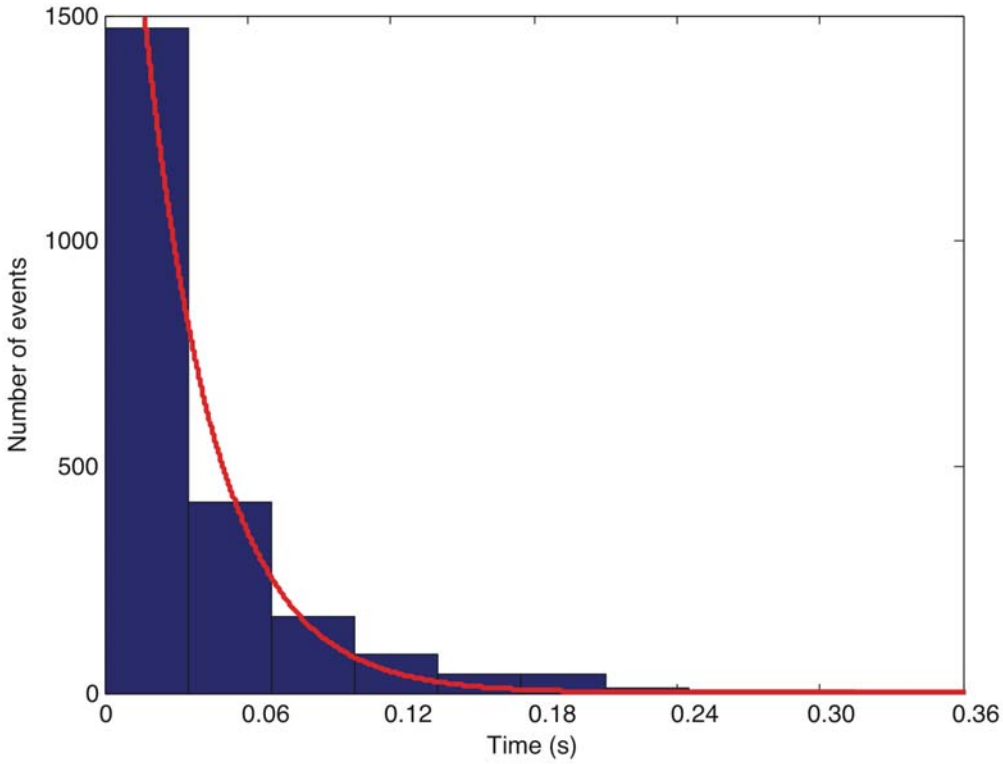

Figure A4: Estimation of time phalloidin-TRITC was in 'on' state. The histogram depicts the distribution of time intervals during which the fluorophore is in 'on' state per blinking event. The x-axis stands for time in seconds and the y-axis stands for the occurrences of 'on' state intervals. It has been fitted to a mono-exponential of the form $y=\exp(-x/\tau)$ function to derive the characteristic rate constant $k_{off} = 1/\tau_{on} = 33.43\ s^{-1}$.

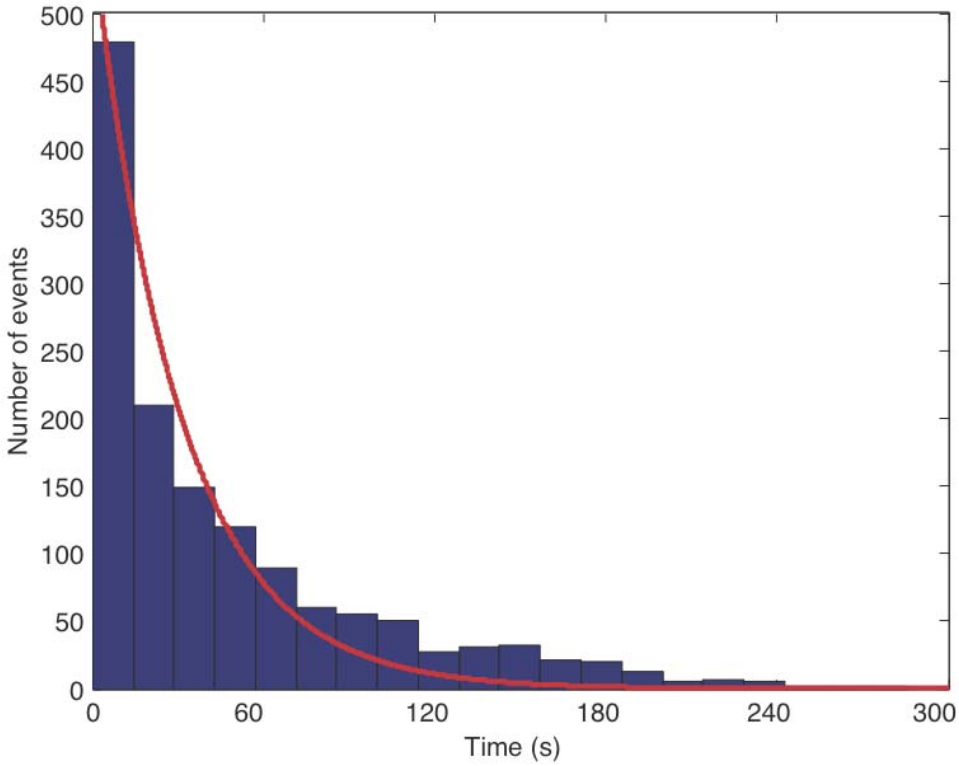

Figure A5: Estimation of time phalloidin-TRITC was in 'off' state. The histogram depicts the distribution of time intervals during which the fluorophore is in 'off' state between two blinking events. The x-axis stands for time in seconds and the y-axis depicts the occurrences of 'off' state intervals. It has been fitted to a mono-exponential function of the form $y=\exp(-x/\tau)$ to derive the characteristic rate constant $k_{on} = 1/\tau_{off} = 0.0327\ s^{-1}$.

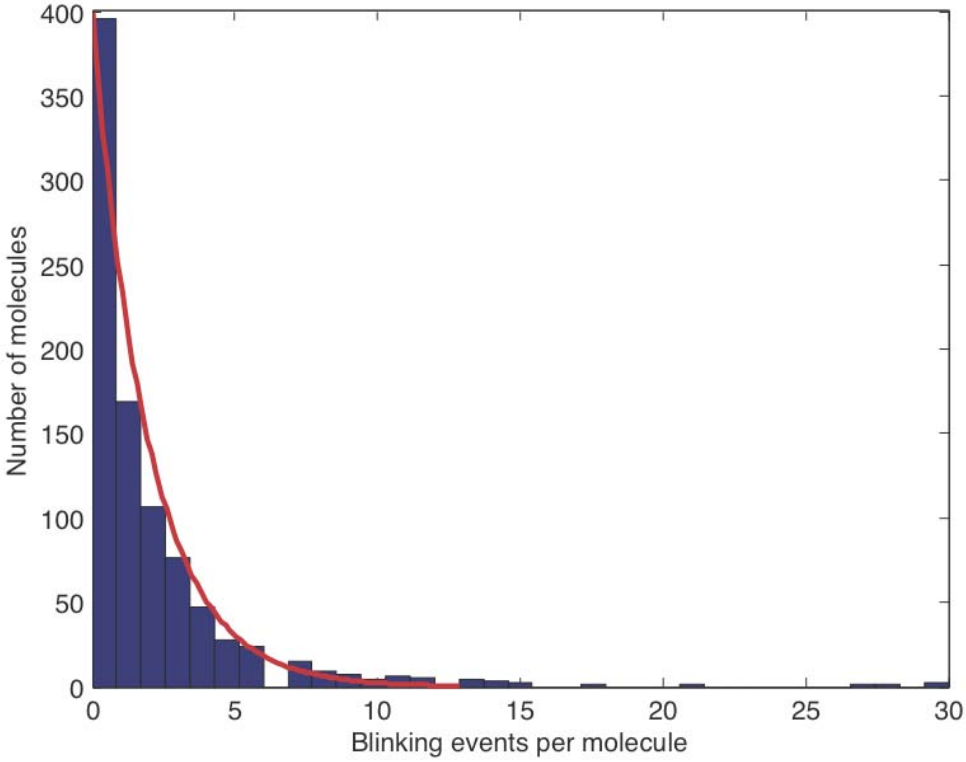

Figure A6: Histogram of phalloidin-TRITC molecules undergoing blinking. The x-axis stands for the number of blinking events per molecule and the y-axis stands for the number of molecules. The experiment lasted 10000 frames with frame duration of 30 ms. The curve was fitted to a mono-exponential of the form $y=\exp(-x/\tau)$ and gives a characteristic $\tau = 1.35$ blinking events per molecule.